ON THE FRONTAL ABLATION OF ALASKA TIDEWATER GLACIERS

By

Robert Whitfield McNabb

RECOMMENDED:

Dr. Edward Bueler

Dr. Roman Motyka

Dr. Erin Pettit

Dr. Martin Truffer

Dr. Regine Hock
Advisory Committee Chair

Dr. Sarah Fowell
Chair, Department of Geology and Geophysics

APPROVED:

Dr. Paul Layer
Dean, College of Natural Science and Mathematics

Dr. John Eichelberger
Dean of the Graduate School

Date

ON THE FRONTAL ABLATION OF ALASKA TIDEWATER GLACIERS

A

DISSERTATION

Presented to the Faculty

of the University of Alaska Fairbanks

in Partial Fulfillment of the Requirements

for the Degree of

DOCTOR OF PHILOSOPHY

By

Robert Whitfield McNabb, B.A.

Fairbanks, Alaska

August 2013

Abstract

Sea level rise is a major problem that society will face in the coming century. One of the largest unknown components of sea level rise is frontal ablation (the sum of mass loss through calving and subaqueous melting) from glaciers and ice sheets. Using estimates of ice thickness, rates of glacier length change, and glacier velocities, we present a record of frontal ablation over the period 1985-2012 for 20 Alaska tidewater glaciers. We also present a new method for estimating ice thickness by solving the continuity equation between adjacent flowlines. Because of the wealth of data available, we apply this method to Columbia Glacier, Alaska. The mean ice thickness and volume of Columbia Glacier were approximately halved over the period 1957-2007, from 281 m to 143 m, and from 294 km^3 to 134 km^3, respectively. Using bedrock slope and considering how waves of thickness change propagate through the glacier, we conclude that the rapid portion of this tidewater glacier's retreat is likely nearing an end. We present a 64 year record of length change for 50 Alaska tidewater glaciers, over the period 1948-2012. Most (31) glaciers retreated over the period. Examination of the onset of glacier retreats indicates a correlation between high summer sea surface temperature and the triggering of retreat. Finally, we present a 27 year record of surface velocity for 20 Alaska tidewater glaciers derived from Landsat imagery. Surface velocities vary by as much as 80% throughout the year, indicating that using measurements from one time of year may bias estimates of frontal ablation. The total mean rate of frontal ablation for these 20 glaciers over the period 1985-2012 is 16.2 ± 6.5 Gt a^{-1}. Extending this to the remaining 30 Alaska tidewater glaciers yields an estimate of frontal ablation of 18.3 ± 7.3 Gt a^{-1}, approximately 50% of the climatic mass balance of the region. This indicates the important, non-negligible role frontal ablation can play in regional mass balance, even where tidewater glaciers cover a small fraction of the total area.

Table of Contents

Page

Page

List of Figures

Page

Page

List of Tables

Page

Acknowledgements

I arrived in Fairbanks in August 2008 after driving from Kalamazoo with my longtime friend Alex. It was a trip that we had been talking about taking since the fifth grade, and we were glad to finally have the opportunity, and the excuse, to make the drive. Despite the grand nature of the adventure, it was of course only the beginning, as the intervening years have proven. I had visited Fairbanks twice before, first in the Summer of 2007 as a Research Experience for Undergraduates Intern, and again in Spring 2008 as a prospective graduate student. My summer in Fairbanks was spent on the 7th floor of the Elvey building, studying Space Physics. It was then that I made the determination to switch my area of study towards something that might allow me to "work" outside at some point. Enter glaciology as a perfect fit.

I did not meet my advisor, Regine Hock, until several weeks after I arrived in Fairbanks with Alex. She had been gone in the Spring when I visited, and was again away when I arrived. I suppose a smarter person might have taken the hint. In all seriousness, it's been an absolute pleasure working with Regine for lo these four and a half years. She has allowed me the freedom to explore my own ideas, and my experience has been all the richer for it. She has even forgiven me the many times that I have shown that mass balance is largely unimportant, at least when we're discussing tidewater glaciers in rapid retreat, such as Columbia Glacier.

My other committee members have been no less helpful during my time in Fairbanks. Martin Truffer, Erin Pettit, Ed Bueler, and Roman Motyka have all provided the necessary guidance to make my education as good as it could be. Whether in the classroom, seminars, or just keeping an open door to answer any dumb questions I might have, they have been as supportive as a student could ask. Roman is the only member of my committee from whom I have not taken a proper class; I have, however, had the pleasure of learning from him in the field, which might as well be a classroom for a glaciologist.

So many other colleagues in Fairbanks have provided me with guidance and help along the way. Chris Larsen, Anthony Arendt, and Mark Fahnestock have been kind enough to entertain my questions and ideas, as well as share data and advice when necessary. Will Harrison and Carl Benson have shared their thoughts, ideas, hockey talk, and allowed me to pick their minds about ideas that haven't necessarily panned out - yet. Whenever I have needed advice or help from other members of the glaciers lab, they have responded with open doors and smiles. Shad O'Neel, though not in Fairbanks, gave me the necessary kick

in the backside to start focusing on one particular idea, a lesson that I have tried my best to remember while finishing this thesis.

My first published paper, reproduced here as Chapter 2, would not have been possible without all of my co-authors. Several of them I have named already, but I must sincerely thank Al Rasmussen, Tad Pfeffer, Yushin Ahn, Matthias Braun, Twit Conway, Ben Smith, Ian Joughin, and Sam Herreid. It is because of their help, their work, and their willingness to share data, that this paper was possible.

So much of my education has come at the helpful hands of my fellow graduate students, and I apologize in advance if I fail to mention everyone. Joe Kennedy, Peter Peterson, Ronni Grapenthin, Tim Bartholomaus, Marijke Habermann, Barbara Trüssel, Dave Podrasky, Joanna Young, Cody Beedlow, Christian Kienholz, Summer Miller, Carl Andersen, Helena Buurman, Chris Bruton, Annie Worden, Owen Neill, Laura Leblanc, Jason Amundson, and Valentina Radić were all kind enough to answer my questions, hear my crazy ideas (and not laugh too hard), listen to my gripes, offer advice, drink coffee, offer a beer when needed, and in general, provide me with the necessary support to come through my education relatively unscathed. I would of course be remiss if I didn't mention my fellow members of the 2010 Summer School in McCarthy. Knowing that you all will be at a conference or a workshop gives me something more to look forward to.

Finally, my family. Ashleigh has been as supportive as one could ask in this endeavor, even following me to Fairbanks. She has always been willing to listen to me babble on about glaciers and all of the cool things that I have worked on. Even if half of what I was saying was crazy and made no sense, she has had the kindness and grace to pretend that it did. I am so glad that my parents and brother were able to visit Alaska this past summer, to finally see what all the fuss was about. As my parents were leaving Anchorage at the end of their trip, they wanted me to know that they finally got why I loved this place so much. I know that I may have to leave this place sometime soon, but I can only hope that if I do, it won't be for long.

This work, in all of its glory, has been funded in part by NSF grant EAR-0943742, NASA grant NNX11AF41G, and a UAF Center for Global Change Student Research Grant with funds from the Cooperative Institute for Alaska Research.

Chapter 1
Introduction

1.1 Background

Sea level rise is potentially one of the largest problems facing society in the coming century (IPCC, 2007; AMAP, 2011), and accurate predictions of sea level rise are important for planning purposes. There are two main components of sea level rise, steric (changes due to thermal expansion and salinity changes), and eustatic (volume change by addition of more water). At present, glaciers, ice sheets, and ice caps are responsible for approximately two thirds of the total sea level change (Shepherd and others, 2012; Gardner and others, 2013). Glacier ice contributes to eustatic sea level change through two main processes: runoff from surface and basal melt, and frontal ablation. Much is known about the contribution of surface runoff from melt to sea level rise, while comparatively little is known about the contribution of frontal ablation and basal melt to sea level rise (IPCC, 2007; Pfeffer and others, 2008; AMAP, 2011; Radić and Hock, 2011).

Frontal ablation is, as the name suggests, the ablation (or mass loss) from the glacier front (or terminus). In the case of tidewater glaciers, frontal ablation is primarily the sum of the mass lost through calving and the mass lost through melt below the waterline. It is an efficient mechanism for mass loss from the world's ocean-terminating glaciers and ice sheets, accounting for a majority of the ice loss from the ice sheets (Benn and others, 2007b; Rignot and others, 2008, 2011); the latest Intergovernmental Panel on Climate Change (IPCC) report cites the lack of knowledge of the mechanism of frontal ablation as one of the key factors limiting our accurate prediction of future sea level rise (IPCC, 2007).

Many studies have attempted to define an overarching "calving law," though due to the complex nature of ice-ocean interactions, no such law presently exists (Amundson and Truffer, 2010; Borstad and others, 2012). The earliest attempts at a calving law focused on the water depth at the calving front (Brown and others, 1982; Pelto and Warren, 1991), but these relationships were shown to break down for glaciers in rapid retreat (Van der Veen, 1996). The next group of studies focused on the height of the calving front above flotation (Van der Veen, 1996; Vieli and others, 2001); this formulation failed to provide for floating ice shelves and tongues. More recently, crevasse depth (Benn and others, 2007a) and strain rate near the calving front (Alley and others, 2008; Amundson and Truffer, 2010) have been proposed as controlling mechanisms, while statistical studies of the calving face have also been employed with success (Bassis, 2011).

Because it has long been assumed that calving is the dominant process of frontal ablation, most studies neglect submarine melting at the calving face (Vieli and others, 2002). Some studies have begun to focus on the role that submarine melt plays in terms of frontal ablation, however. In a study at LeConte Glacier, Alaska, Motyka and others (2003) found that the melt rate below the waterline was roughly equal to the mechanical calving velocity, reaching levels of 10 m d^{-1}. Another study found that an influx of warm ocean water likely led to the disintegration of the floating tongue at Jakobshavn Isbræ, Greenland, leading to that outlet glacier's speed-up and retreat (Holland and others, 2008; Motyka and others, 2011). More recently, efforts at quantifying submarine melt at other outlet glaciers in Greenland (Rignot and others, 2010, 2012) have continued to implicate the ocean as a major factor in tidewater glacier mass balance, with melt rates sometimes exceeding 0.5 m d^{-1} (Motyka and others, 2011).

In general, calving fronts operate independently of climate (Mercer, 1961; Mann, 1986; Meier and Post, 1987; Post and others, 2011), and asynchronous advance or retreat between distinct tidewater glaciers in a region is common (e.g., Hubbard Glacier, Alaska, which has been advancing while other glaciers in Alaska are retreating; Barclay and others, 2001; Ritchie and others, 2008). This asynchronicity, as well as the unstable nature of tidewater retreat (Pfeffer, 2007), implies that extrapolating past trends of tidewater glacier behavior into future climate is difficult at best (Post and others, 2011). There is, however, growing evidence from Greenland that the regional behavior of tidewater glaciers can tend to follow climatic conditions such as increases in ocean temperature (Holland and others, 2008; Moon and Joughin, 2008; Murray and others, 2010; Howat and Eddy, 2012), although the duration of this synchronous behavior may in fact be short-lived (Moon and others, 2012).

Despite the difficulties inherent in observing regional-scale glacier behavior, as well as extrapolating the behavior of some small set of glaciers to the regional-scale, some regional estimates of frontal ablation do exist. Many of these studies focus on the ice sheets (Rignot and others, 2008, 2011), while several focus on glaciers and ice caps outside of the ice sheets (Hagen and others, 2003; Burgess and others, 2005; Błaszczyk and others, 2009; Gardner and others, 2011). Many of these studies use only one or two measurements per year to calculate their estimates of frontal ablation. It is well known that glacier velocity (and hence, length change and frontal ablation, e.g. Moon and Joughin, 2008; Cuffey and Paterson, 2010) is highly variable on both a seasonal and interannual basis - indicating that care must be taken when drawing conclusions about velocity or discharge from a small set

of velocity measurements. Use of studies which focus on short (sub-decadal) time scales for drawing conclusions about future glacier change is questionable, if not impossible.

Glaciers in Alaska (and surrounding areas in British Columbia and the Yukon Territory; hereafter "Alaska" glaciers) cover nearly $89,000$ km^2 of area (Gardner and others, 2013), with over 50 current and former tidewater glaciers representing roughly 15% of that area (Viens, 1995; Kienholz and others, 2012). Many recent studies have estimated the mass balance of either all, or large sets of, Alaska glaciers, either through airborne laser altimetry (Arendt and others, 2002, 2006; Johnson and others, 2013), digital elevation model (DEM) differencing (Larsen and others, 2007; Berthier and others, 2010), satellite gravimetry (Luthcke and others, 2008, 2013), or mass balance modeling (Hock and others, 2009; Marzeion and others, 2012; Radić and others, 2013). While these studies estimate past mass balance or attempt to project future mass balance of Alaska glaciers, they do not provide estimates of either past or future frontal ablation from Alaska tidewater glaciers. In fact, most projections ignore frontal ablation entirely, and only project rates of surface mass balance.

1.2 Objectives

The ultimate goal of this study is to further our knowledge of tidewater glaciers and frontal ablation, providing a basis from which to estimate future rates of frontal ablation, and ultimately, sea level rise. To achieve this goal, we lay out the following objectives:

1. to produce a regional-scale estimate of frontal ablation for Alaska, over the time period 1985-2012.

2. to characterize the long-term front variations of tidewater glaciers in Alaska on both seasonal and interannual timescales, and examine spatial and temporal patterns;

3. to develop a method for estimating ice thickness and bed topography of tidewater glaciers;

Because an accurate estimate of ice thickness is an important and necessary component of any estimate of frontal ablation, as well as any ice flow model, we propose a method to estimate the ice thickness distribution of a glacier, given only information from the surface of the glacier. This method, and its application to Columbia Glacier, is contained in Chapter 2. Our resulting map of ice thickness (and inferred bed topography) enables us

to calculate total ice volume, and lends insight into spatial patterns of volume change, the current stability of the glacier, and the potential for drawing analogues to other glacier retreats in Alaska and other regions. This Chapter has been published in the Journal of Glaciology as McNabb and others (2012).

In Chapter 3, we use the rich archive of Landsat satellite images, as well as US Geological Survey topographic maps and aerial mapping photos, to outline tidewater glacier termini for 50 Alaska glaciers over the period 1948-2012, a collection of over $10,000$ terminus outlines. With these outlines, we calculate length changes for each of these glaciers, enabling us to analyze spatial and temporal patterns of length change on a regional level. We compare the length change record to local and regional climate, in order to investigate the potential impact that climate has on regional patterns of tidewater glacier behavior.

In Chapter 4, we use that same archive of Landsat images to calculate surface velocity fields for a subset of 20 glaciers. Using the length change record from Chapter 3, along with estimates of ice thickness from Huss and Farinotti (2012), we use these surface velocities to estimate rates of frontal ablation for those 20 glaciers. We use a simple relationship relating area to frontal ablation in order to scale our estimate to the remaining 30 glaciers in the region.

Finally, Chapter 5 summarizes the key findings of this thesis and provides an outlook for future studies of frontal ablation in Alaska and elsewhere.

1.3 References

Alley, R. B., H. J. Horgan, I. Joughin, K. M. Cuffey, T. K. Dupont, B. R. Parizek, S. Anandakrishnan and J. Bassis, 2008. A simple law for ice-shelf calving, *Science*, **322**(5906), 1344, doi:10.1126/science.1162543.

AMAP, 2011. Snow, Water, Ice and Permafrost in the Arctic (SWIPA): Climate Change and the Cryosphere, Arctic Monitoring and Assessment Programme (AMAP), Oslo, Norway.

Amundson, J. M. and M. Truffer, 2010. A unifying framework for iceberg calving models, *J. Glaciol.*, **56**(199), 822–830.

Arendt, A., K. Echelmeyer, W. Harrison, C. Lingle and B. Valentine, 2002. Rapid wastage of Alaska glaciers and their contribution to rising sea level, *Science*, **297**(5580), 382–386.

Arendt, A., K. Echelmeyer, W. Harrison, C. Lingle, S. Zirnheld, V. Valentine, B. Ritchie and M. Druckenmiller, 2006. Updated estimates of glacier volume changes in the western Chugach Mountains, Alaska, and a comparison of regional extrapolation methods, *J. Geophys. Res.*, **111**(F03019).

Barclay, D., P. Calkin and G. Wiles, 2001. Holocene history of Hubbard Glacier in Yakutat Bay and Russell Fiord, southern Alaska, *Geol. Soc. of Am. Bull.*, **113**, 388–402.

Bassis, J. N., 2011. The statistical physics of iceberg calving and the emergence of universal calving laws, *J. Glaciol.*, **57**(201), 3–16.

Benn, D. I., N. R.J. Hulton and R. H. Mottram, 2007a. 'Calving laws', 'sliding laws' and the stability of tidewater glaciers, *Ann. Glaciol.*, **46**, 123–130.

Benn, D. I., C. R. Warren and R. H. Mottram, 2007b. Calving processes and the dynamics of calving glaciers, *Earth Sci. Rev.*, **82**, 143–179.

Berthier, E., E. Schiefer, G. K. C. Clarke, B. Menounos and F. Rémy, 2010. Contribution of Alaskan glaciers to sea-level rise derived from satellite imagery, *Nature Geosci.*, **3**, 92–95.

Błaszczyk, M., J. A. Jania and J. O. Hagen, 2009. Tidewater Glaciers of Svalbard: Recent changes and estimates of calving fluxes, *Polish Polar Res.*, **30**(2), 85–142.

Borstad, C. P., A. Khazendar, E. Larour, M. Morlighem, E. Rignot, M. P. Schodlok and H. Seroussi, 2012. A damage mechanics assessment of the Larsen B ice shelf prior to collapse: Toward a physically-based calving law, *Geophys. Res. Lett.*, **39**(L18502), doi:10.1029/2012GL053317.

Brown, C. S., M.F. Meier and A. Post, 1982. Calving speed of Alaska tidewater glaciers, with application to Columbia Glacier, *USGS Prof. Pap.*, **1258-C**.

Burgess, D., M. J. Sharp, D. W. F. Mair, J. Dowdeswell and T. J. Benham, 2005. Flow dynamics and iceberg calving rates of Devon Ice Cap, Nunavut, Canada, *J. Glaciol*, **51**(173), 219–230.

Cuffey, K. M. and W. S. B. Paterson, 2010. The physics of glaciers, Butterworth-Heinemann, fourth ed.

Gardner, A. S., G. Moholdt, B. Wouters, G. J. Wolken, D. O. Burgess, M. J. Sharp, J. G. Cogley, C. Braun and C. Labine, 2011. Sharply increased mass loss from glaciers and ice caps in the Canadian Arctic Archipelago, *Nature*, **473**, 357–360.

Gardner, A. S., G. Moholdt, J. G. Cogley, A. A. Arendt, J. Wahr, E. Berthier, R. Hock, W. T. Pfeffer, G. Kaser, S. R. M. Ligtenberg, T. Bolch, M. J. Sharp, J. O. Hagen, M. van den Broeke and F. Paul, 2013. A consensus estimate of glacier contributions to sea level rise: 2003-2009, *Science*, **340**, doi:10.1126/science1234532.

Hagen, J. O., K. Melvold, F. Pinglot and J. A. Dowdeswell, 2003. On the net mass balance of the glaciers and ice caps in Svalbard, Norwegian Arctic, *Arct., Antarct., and Alp. Res.*, **35**(2), 264–270.

Hock, R., M. de Woul, V. Radić and M. Dyurgerov, 2009. Mountain glaciers and ice caps around Antarctica make a large sea-level rise contribution, *Geophys. Res. Lett.*, **36**(L07501), doi:10.1029/2008GL037020.

Holland, D. M., R. H. Thomas, B. De Young, M. H. Ribergaard and B. Lyberth, 2008. Acceleration of Jakobshavn Isbræ triggered by warm subsurface ocean waters, *Nature Geosci.*, **1**, 659–664, doi:10.1038/ngeo316.

Howat, I. and A. Eddy, 2012. Multi-decadal retreat of Greenland's marine-terminating glaciers, *J. Glaciol.*, **57**(203), 389–396.

Huss, M. and D. Farinotti, 2012. Distributed ice thickness and volume of all glaciers around the globe, *J. Geophys. Res.*.

IPCC, 2007. Climate Change 2007: The Physical Science Basis: Contribution of Working Group I to the Fourth Assessment Report of the Intergovernmental Panel on Climate Change, Cambridge University Press, [S. Solomon and D. Qin and M. Manning and Z. Chen and M. Marquis and K. B. Averyt and M. Tignor and H. L. Miller (eds.)].

Johnson, A. J., C. F. Larsen, N. Murphy, A. A. Arendt and S. L. Zirnheld, 2013. Mass balance in the Glacier Bay area of Alaska, USA, and British Columbia, Canada, 1995-2011, using airborne laser altimetry, *J. Glaciol.*, **59**(216), doi:10.3189/2013JoG12J101.

Kienholz, C., S. J. Herreid, J. H. Rich, A. A. Arendt and R. M. Hock, 2012. A new inventory of all Alaska glaciers, Abstract C21C-0604 presented at 2012 Fall Meeting, AGU, San Francisco, Calif., 3-7 Dec.

Larsen, C. F., R. J. Motyka, A. A. Arendt, K. A. Echelmeyer and P. E. Geissler, 2007. Glacier changes in southeast Alaska and northwest British Columbia and contribution to sea level rise, *J. Geophys. Res.*, **112**(F01007).

Luthcke, S. B., A. A. Arendt, D. D. Rowlands, J. J. McCarthy and C. F. Larsen, 2008. Recent glacier mass changes in the Gulf of Alaska region from GRACE mascon solutions, *J. Glaciol.*, **54**(188), 767–777.

Luthcke, S. B., T. Sabaka, B. Loomis, A. Arendt, J. McCarthy and J. Camp, 2013. Antarctica, Greenland and Gulf of Alaska land ice evolution from an iterated GRACE global mascon solution, *J. Glaciol.*, **59**(216), doi:10.3189/2013JoG12J147.

Mann, D. H., 1986. Reliability of a fjord glacier's fluctuations for paleoclimatic reconstructions, *Quat. Res.*, **25**, 10–24.

Marzeion, B., A. H. Jarosch and M. Hofer, 2012. Past and future sea-level change from the surface mass balance of glaciers, *The Cryos.*, **6**, 1295–1322.

McNabb, R., R. Hock, S. O'Neel, L. A. Rasmussen, Y. Ahn, M. Braun, H. Conway, S. Herreid, I. Joughin, W. T. Pfeffer, B. E. Smith and M. Truffer, 2012. Using Surface Velocities to Calculate Ice Thickness and Bed Topography: A Case Study at Columbia Glacier, Alaska, *J. Glaciol.*, **58**(212).

Meier, M. F. and A. Post, 1987. Fast tidewater glaciers, *J. Geophys. Res.*, **92**(B9), 9051–9058.

Mercer, J. H., 1961. The response of fjord glaciers to changes in the firn limit, *J. Glaciol.*, **3**, 850–858.

Moon, T. and I. Joughin, 2008. Changes in ice front position on Greenland's outlet glaciers from 1992 to 2007, *J. Geophys. Res.*, **113**(F02022), doi:10.1029/2007JF000927.

Moon, T., I. Joughin, B. Smith and I. Howat, 2012. 21st-century evolution of Greenland outlet glacier velocities, *Science*, **336**, 576–578, 10.1126/science.1219985.

Motyka, R. J., L. Hunter, K. Echelmeyer and C. Connor, 2003. Submarine melting at the terminus of a temperate tidewater glacier, Leconte Glacier, Alaska, *Ann. Glaciol.*, **36**, 57–65.

Motyka, R. J., M. Fahnestock, M. Truffer, J. Mortensen and S. Rysgaard, 2011. Submarine melting of the 1985 Jakobshavn Isbræ floating tongue and the triggering of the current retreat, *J. Geophys. Res.*, **116**(F1), doi:10.1029/2009JF001632.

Murray, T., K. Scharrer, T. D. James, S. R. Dye, E. Hanna, A. D. Booth, N. Selmes, A. Luckman, A. L. C. Hughes, S. Cook and P. Huybrechts, 2010. Ocean regulation hypothesis for glacier dynamics in southeast Greenland and implications for ice sheet mass changes, *J. Geophys. Res.*, **115**(F03026), doi:10.1029/2009JF001522.

Pelto, M. S. and C.R. Warren, 1991. Relationship between tidewater glacier calving velocity and water depth at the calving front, *Ann. Glaciol.*, **15**, 115–118.

Pfeffer, W. T., 2007. A simple mechanism for irreversible tidewater glacier retreat, *J. Geophys. Res.*, **112**(F03S2), doi:10.1029/2006JF000590.

Pfeffer, W. T., J. T. Harper and S. O'Neel, 2008. Kinematic Constraints on Glacier Contributions to 21st-Century Sea-Level Rise, *Science*, **321**, 1340–1343.

Post, A., S. O'Neel, R. J. Motyka and G. Streveler, 2011. A complex relationship between calving glaciers and climate, *EOS Trans.*, **92**(37), 305–306.

Radić, V. and R. Hock, 2011. Regionally differentiated contribution of mountain glaciers and ice caps to future sea-level rise, *Nat. Geosci.*, **4**, 91–94, doi:10.1038/NGEO1052.

Radić, V., A. Bliss, A. C. Beedlow, R. Hock, E. Miles and J. G. Cogley, 2013. Regional and global projections of twenty-first century glacier mass changes in responce to climate scenarios from global climate models, *Clim. Dyn.*, doi:10.1007/s00382-013-1719-7.

Rignot, E., J. E. Box, E. Burgess and E. Hanna, 2008. Mass balance of the Greenland ice sheet from 1958 to 2007, *Geophys. Res. Lett.*, **35**(L20502), doi:10.1029/2008GL035417.

Rignot, E., M. Koppes and I. Velicogna, 2010. Rapid submarine melting of the calving faces of West Greenland glaciers, *Nature Geosci.*, **3**, 187–191.

Rignot, E., I. Velicogna, M. R. van den Broeke, A. Monaghan and J. T. Lenaerts, 2011. Acceleration of the contribution of the Greenland and Antarctic ice sheets to sea level rise, *Geophys. Res. Lett.*, **38**(L05503), doi:10.1029/2011GL046583.

Rignot, E., I. Fenty, D. Menemenlis and Y. Xu, 2012. Spreading of warm ocean waters around Greenland as a possible cause for glacier acceleration, *Ann. Glaciol.*, **53**(60), 257–266.

Ritchie, J., C. Lingle, R. Motyka and M. Truffer, 2008. Seasonal fluctuations in the advance of a tidewater glacier and potential causes: Hubbard Glacier, Alaska, USA, *J. Glaciol.*, **54**(186), 401–411.

Shepherd, A. and 46 others, 2012. A reconciled estimate of ice-sheet mass balance, *Science*, **338**, 1183–1189, doi:10.1126/science.1228102.

Van der Veen, C. J., 1996. Tidewater calving, *J. Glaciol.*, **42**(141), 375–385.

Vieli, A., M. Funk and H. Blatter, 2001. Flow dynamics of tidewater glaciers: a numerical modelling approach, *J. Glaciol.*, **47**(159), 595–606.

Vieli, A., J. Jania and L. Kolondra, 2002. The retreat of a tidewater glacier: observations and model calculations on Hansbreen, Spitsbergen, *J. Glaciol.*, **48**(163), 592–600.

Viens, R. J., 1995. Dynamics and Mass Balance of Temperate Tidewater Calving Glaciers of Southern Alaska, (Master's thesis, Univ. of Washington).

Chapter 2
Using Surface Velocities to Calculate Ice Thickness and Bed Topography: A Case Study at Columbia Glacier, Alaska[1]

2.1 Abstract

Information about glacier volume and ice thickness distribution is essential for many glaciological applications, but direct measurements of ice thickness can be difficult and costly. We present a new method that calculates ice thickness via an estimate of ice flux. We solve the familiar continuity equation between adjacent flowlines, which decreases the computational time required compared to a solution on the whole grid. We test the method on Columbia Glacier, a large tidewater glacier in Alaska, and compare calculated and measured ice thicknesses with favorable results. This shows the potential of this method for estimating ice thickness distribution of glaciers for which only surface data are available. We find that both the mean thickness and volume of Columbia Glacier were approximately halved over the period 1957-2007, from 281 m to 143 m, and from 294 km^3 to 134 km^3, respectively. Using bedrock slope and considering how waves of thickness change propagate through the glacier, we conduct a brief analysis of the instability of Columbia Glacier, which leads us to conclude that the rapid portion of the retreat may be nearing an end.

2.2 Introduction

Knowledge of glacier volume and ice thickness distribution are essential for hydrological applications, ice flow modeling, assessing the impact of climate change on glaciers, and sea level rise predictions, among other applications. Direct measurements of ice thickness at a point (e.g., from a borehole) or along a track (e.g., using radio-echo sounding or seismic methods) are time consuming and expensive. Direct measurements of total ice volume generally require many such points or tracks. In addition, errors in interpolation or extrapolation from along track measurements of ice thicknesses can introduce large anomalies in calculated ice-flux divergence, if the interpolation technique used does not conserve mass or ice flux (Seroussi and others, 2011). A mass-conserving method for interpolating ice thickness has been developed by Morlighem and others (2011). Techniques using radar tomography and interferometry have recently been developed, but they have mostly been applied to portions of the Greenland Ice Sheet with flat surfaces, and their performance

[1]Published as McNabb, R., R. Hock, S. O'Neel, L. A. Rasmussen, Y. Ahn, M. Braun, H. Conway, S. Herreid, I. Joughin, W. T. Pfeffer, B. E. Smith and M. Truffer, 2012. Using Surface Velocities to Calculate Ice Thickness and Bed Topography: A Case Study at Columbia Glacier, Alaska, *J. Glaciol.*, **58**(212).

and applicability to outlet and tidewater glaciers is not yet known (Paden and others, 2010).

Previous studies have focused on calculating ice volume and ice thickness distribution of glaciers without direct measurement. One of the simplest methods is volume-area scaling (e.g., Bahr and others, 1997; Radić and others, 2008). These methods are easily implemented, requiring information about glacier area and parameterization of the shape of the bed topography. In general, the shape of the bed of individual glaciers is not well known, but the method has proven useful for characterizing regional ice volumes (Radić and Hock, 2010).

Other studies have inferred ice thickness distribution through direct evaluation of the mass continuity equation (e.g., Rasmussen, 1988; Morlighem and others, 2011), while others use a simplification of the equation to overcome data gaps (e.g., Fastook and others, 1995; Warner and Budd, 2000; Farinotti and others, 2009b), or through applications of the shallow-ice approximation (e.g., Li and others, 2011). More recently, a method has been proposed which uses neural networks along with simplifications of the mass continuity equation to estimate the bed topography and ice volumes of entire regions, where little more than surface topography might be known (Clarke and others, 2009).

Here we propose a new method for calculating ice thickness, by evaluating the mass continuity equation between adjacent flowlines, rather than through a local solution or on a large grid. With velocity fields that cover some portion of a glacier, a digital elevation model (DEM) of the glacier surface, rates of surface mass balance and thinning, and knowledge of the ice thickness at the boundary of the domain of interest, it is possible to calculate the ice thickness distribution of the glacier over the region covered by the velocity field used. Because no assumption is made about the ice flux through the terminus of the glacier, this method is directly applicable to both land and marine/lake terminating glaciers.

We apply this method to Columbia Glacier, a large tidewater glacier in Alaska. We investigate the sensitivity of the calculated ice thicknesses to flowline separation and input variables, and produce a new, high-resolution gridded bed topography map for Columbia Glacier. We then use this bed topography map to calculate ice thickness, evaluating the success of this computation through direct comparison with radar profiles of ice thickness. Using this, we calculate total ice volume in 2007 and 1957. Finally, we examine spatial patterns of volume change at Columbia Glacier, the stability of the current tidewater extent,

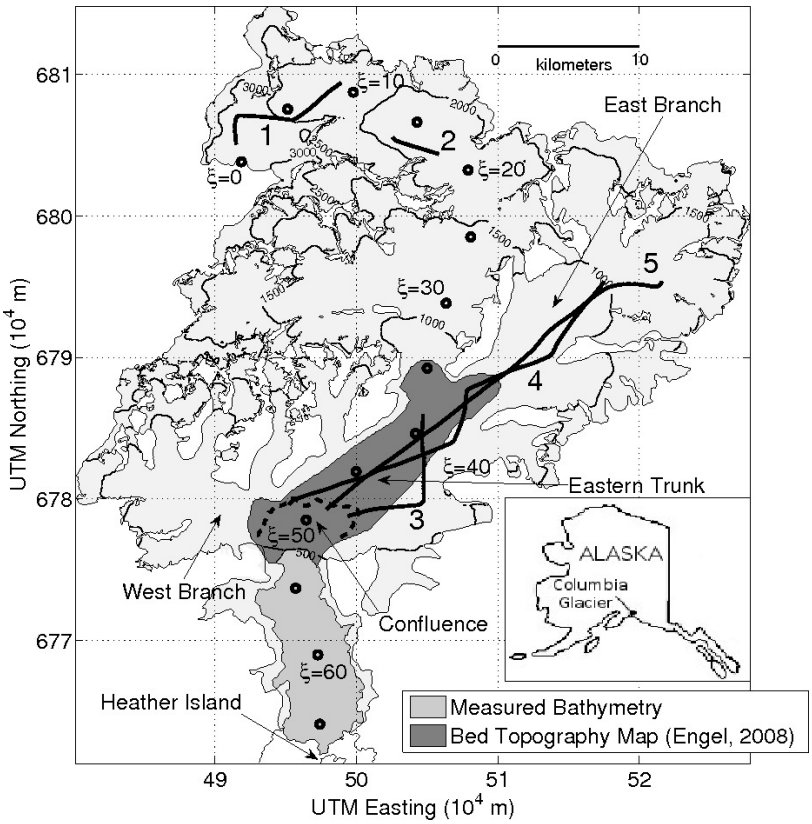

Figure 2.1. Columbia Glacier, showing 1957 glacier extent in gray. Contour lines indicate 1957 surface elevations. Open circles indicate distance, ξ, from the head of the glacier following the central flowline defined by Meier and others (1985). Extent of measured bathymetry is shown, as well as extent of bed topography map by Engel (2008). Thick black lines indicate location of radar tracks, numbered 1-5. Location of terminus in June 2011 is shown as a dashed line.

and potential analogues to Columbia Glacier with both Glacier Bay and Icy Bay, Alaska.

2.3 Columbia Glacier

Columbia Glacier (Fig. 2.1) is a large tidewater glacier, approximately 30 km to the west of Valdez, Alaska. At present (2011), the glacier has a surface area of approximately 910 km^2, ranging from sea level to 3700 m above sea level (a.s.l.). The glacier reached its most recent extended position ca. 1850, terminating near the northern edge of Heather Island (Calkin and others, 2001). Around 1980, the glacier began a rapid retreat that continues through the present (e.g., Meier and Post, 1987; O'Neel and others, 2005; Pfeffer, 2007; Walter and others, 2010; Rasmussen and others, 2011). Since then, the glacier has retreated over 23

km. During the course of the retreat, ice speeds near the terminus have exceeded 25 m d^{-1} (O'Neel and others, 2005). Since 1976, the glacier has been monitored by the United States Geological Survey (USGS), as well as the University of Colorado at Boulder (CU-Boulder) with aerial photogrammetry, and since 2004 with time lapse photogrammetry (e.g., Krimmel, 2001; O'Neel and others, 2005; Walter and others, 2010). It is the single largest contributor of Alaska glaciers to sea level rise, accounting for roughly 6% of the total regional contribution over the period 1962-2006 (Berthier and others, 2010). In the periods 1957-2007 and 2007-2011, the glacier lost approximately 132 km^2 ($\sim$12%) and 20 km^2 of area, respectively. Columbia is the best studied example of tidewater glacier retreat in the world. Ice flow, ice discharge, and Columbia's tidewater retreat are all extensively documented, providing rich insight into the underlying processes that modulate tidewater glacier behavior and stability.

2.4 Datasets

For the proposed method, the required input data are glacier surface topography in the form of a digital elevation model (DEM), surface velocities, surface mass balance rates, rates of ice surface elevation change, and ice thickness at the boundary of the domain of interest. The method is validated using known ice thicknesses and bed elevations. A summary of available datasets is shown in Table 2.1. A centerline coordinate system ξ, where $\xi = 0$ km at the head of the glacier, was proposed by Meier and others (1985), and is used here to present centerline data.

2.4.1 Map Data and Digital Elevation Models

Full glacier coverage DEMs are available for 1957 and 2007. The 1957 DEM is a digitized United States Geological Survey (USGS) 1:63,360 topographic map, with an associated glacier outline. The 2007 DEM is generated using a SPOT (Satellite Pour l'Observation de la Terre) panchromatic image acquired on September 22, 2007, and has a spatial resolution of 40 m (Korona and others, 2009).

The 2007 Columbia Glacier outline was manually digitized from the same SPOT panchromatic image as the 2007 DEM. Additionally, two Landsat images acquired on September 13, 2006 and July 3, 2009 were used to digitize the glacier outline where it was obscured by cloud cover or snow in the SPOT image. A watershed algorithm was used to find the Columbia Glacier flow basin using the 1957 DEM (Kienholz, 2010). This was then

Table 2.1. Overview of datasets, available for Columbia Glacier, used in this study. Number in parentheses indicates number of datasets available during given time period. Datasets without citation are unpublished.

Dataset Contents	Date	Glacier Coverage	Citation
Surface Velocity	1984-1985	partial (4)	Krimmel (2001)
	2005-2006	partial (2)	
	2009-2010	partial (2)	
	2011	full (6)	
Digital Elevation Model	1957	full	USGS Topographic Map
	1980	partial	Krimmel (2001)
	1984-1985	partial (4)	Krimmel (2001)
	2005-2006	partial (2)	
	2009-2010	partial (2)	
	2007	full	Korona and others (2009)
Bathymetry	2005	partial	Noll (2005)
Radar	2010	partial	
Surface Mass Balance	1948-2007	partial	Rasmussen and others (2011)
	1978	partial	Mayo and others (1979)
	2010	partial	O'Neel (2012)
Landsat TM/ETM+	1985-2011	full (82)	
Glacier Outline	1957	full	USGS Topographic Map
	2007	full	
	2011	terminus only	

manually corrected to represent 2007 flow divides, using the 2007 DEM. Terminus position for 2007 was mapped to correspond to the 2007 DEM.

Smaller spatial coverage DEMs, determined using photogrammetric techniques, are associated with each surface velocity dataset, and are available yearly for the periods 1976-2001 (Krimmel, 2001) and 2004-2010. The majority of these DEMs are limited to the Eastern trunk of the glacier and the former terminus area (the current proglacial fjord), covering approximately 265 km^2, or 30% of the glacierized area in 1957.

2.4.2 Fjord Bathymetry and Glacier Bed Elevation

High resolution bathymetric data are available in the large proglacial fjord that has opened up since the onset of retreat, up to the location of the 2004 terminus (Noll, 2005). Bathymetric data were collected in 2005 by the NOAA ship *Rainier* using multibeam sonar. These data cover 6% of the 1957 glacier extent (Fig. 2.1), and have a reported accuracy of 7% of water depth.

A partial bed topography map, covering 16% of the 1957 glacier extent, is also available above the location of the 2004 terminus, but has limited accuracy (Engel, 2008). In addition, the coverage of this map is limited to the lower part of the eastern trunk of the glacier, a substantial portion of which has since calved off. The upstream limit of this map is approximately 35 km from the head of the glacier, and 13 km from the June 2011 terminus. This bed topography map was produced using the mass continuity equation, surface velocity fields, and surface elevation change data derived from centerline altitude profiles. Engel (2008) also makes the assumption that surface mass balance is zero over the period of retreat. Details of the method used to produce this topography map can be found in O'Neel and others (2005) and Engel (2008).

2.4.3 Ice Thickness

Ice thickness data were collected on April 22, 2010, from a de Havilland Otter airplane towing an impulse radar with 2 MHz center-frequency antennas, in a configuration similar to that used in 2006 to sound Bering and Malaspina glaciers (Conway and others, 2009). Waveforms were geolocated using GPS onboard the airplane. Ice thickness at each location was estimated from the difference in two-way travel time from the surface to the bed, assuming a wave speed in ice of 170 m μs^{-1}. The resolution (1/4 wavelength) when using

a 2 MHz antenna is approximately 20 m in ice. Uncertainty in the estimate of ice thickness comes from uncertainty in the wave speed (about 2 m μs^{-1}, which corresponds to 1.2% of the ice thickness, or 7.2 m for 600 m thick ice), and from picking the travel time to the surface and to the bed. This uncertainty when picking the two-way travel time of the maximum reflection amplitude with our 2 MHz system is about 0.1 μs^{-1}, which corresponds to 8.5 m. The uncertainty would increase in the presence of side reflectors, which can introduce ambiguity in bed pick positions. Assuming these uncertainties are not correlated, the combined uncertainty for 600 m thick ice is $\sim$ 14 m. This uncertainty is comparable in magnitude to differences in estimates of thickness at cross-over points between tracks, which typically agree to better than 10 m. Ice thickness data are available through the Advanced Cooperative Arctic Data and Information Service portal under "Collaborative Research IPY: Dynamic Controls on Tidewater Glacier Retreat" (University Corporation for Atmospheric Research, 2012).

2.4.4 Surface Mass Balance

Estimates of the vertical profile of annual surface mass balance during 1948-2007 were made by Rasmussen and others (2011) using upper-air temperatures and winds. Their model was calibrated with 67 mass balance measurements made mainly in 1977 and 1978. It assumes that both precipitation and the positive degree-day factor are constant with altitude. Accumulation increases with altitude, however, because both precipitation and the fraction of precipitation falling as snow increases. Ablation decreases with altitude because the number of positive degree days decreases. The model does not explicitly consider radiation or redistribution of fallen snow. Reported root mean square error is 1.0 m water equivalent (w.e.) a^{-1}, with coefficient of determination r^2 = 0.88 (Bevington, 1969). Mean values over the period range from -6.7 m w.e. a^{-1} at 100 m a.s.l. to 5.4 m w.e. a^{-1} at 3700 m. a.s.l., and the mean equilibrium line altitude is 940 m a.s.l. over the period. Over the period 1948–1981, the modeled surface mass balance of the entire glacier is positive ($\sim$0.8 km^3 w.e. a^{-1}). The modeled surface mass balance remains positive through 1995 ($\sim$1.2 km^3 w.e. a^{-1}), and then turns negative after 1995 (~ -0.4 km^3 w.e. a^{-1}).

2.4.5 Surface Velocities

Surface velocity fields covering part of the glacier have been calculated over the periods 1976-2001 (Krimmel, 2001; O'Neel and others, 2005) and 2004-2010 using aerial photogrammetry. Krimmel (2001) presents a record of 121 flights made between 1957 and 2001 that are unevenly spaced in time. Manual feature tracking is used to determine average velocity fields between successive pairs of images, as well as mean surface topography between successive pairs of images. Spacing between image pairs ranges from 10 to 138 days. Time of year for flights typically falls into two ranges, January-March and July-October. To maintain consistency with the full-coverage DEMs, only velocity sets from mid-July onward are considered, resulting in a set of 29 flight pairs.

For flights made since 2004, photogrammetric analysis is done using automated feature tracking, allowing for a much denser spatial coverage (Ahn and Howat, 2011). Densities of velocity measurements range from approximately one measurement for every 20 grid cells, to nearly one measurement per 100 m $\times$ 100 m grid cell.

Full glacier coverage velocity fields for 2011 were determined with standard feature and speckle-tracking techniques (Strozzi and others, 2002; Joughin, 2002) applied to TerraSAR-X synthetic aperture radar data. Formal errors, based on the statistics of the matches, are computed and are generally small (1 to 10 m a^{-1}). There may be velocity errors of less than about 3% due to error in the DEM-derived slopes used to correct for vertical motion (Joughin and others, 1996).

2.5 Method

The method used here is based on principles first described in Rasmussen (1988), and also described in O'Neel and others (2005). We solve for ice thickness between adjacent flowlines, in order to avoid the consideration of cross-flow gradients. We choose this method of evaluating the continuity equation because its implementation is relatively simple.

First, consider a cell (of area S), through the lateral boundaries of which there is no flow (Fig. 2.2). In practice, this could be two adjacent flowlines, an ice catchment basin such as those employed by Farinotti and others (2009b), or an entire glacier. If the latter two examples are used, care must be taken with the spatially-averaged surface velocities and ice thicknesses, as discussed below.

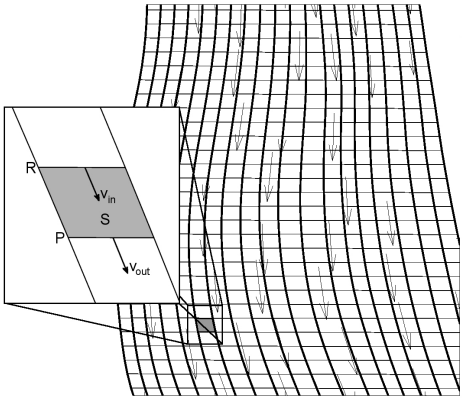

Figure 2.2. Schematic illustration of glacier surface. Black arrows indicate flow vectors, thick black lines indicate flowlines, and black lines transverse to flow are boundaries of cells. Inset: map view of a cell, with area S, through the lateral boundaries of which there is no flow. R and P designate the upstream and downstream boundaries of the cell, respectively. $v_{\text{in}}, v_{\text{out}}$ indicate the ice velocity at the upstream and downstream boundaries of the cell, respectively.

Assuming a constant ice density, the mass conservation equation is given by

$$\frac{\partial H}{\partial t} = \dot{b} - \nabla \cdot \vec{q}, \tag{2.1}$$

where H is the ice thickness, $\nabla \cdot \vec{q}$ is the ice flux divergence and $\dot{b}$ is the climatic-basal mass balance rate (i.e., the sum of the surface, internal, and basal mass balances; Cogley and others, 2011). In general, and at Columbia Glacier in particular, the climatic-basal balance rate is dominated by the surface mass balance rate $\dot{b}_{\text{sfc}}$, and so we replace $\dot{b}$ with $\dot{b}_{\text{sfc}}$ from here.

Using Gauss' Theorem, re-arranging and then integrating Equation (2.1) over the surface area S of any cell, we obtain the following:

$$q_{\text{in}} - q_{\text{out}} = \int_S \left(\dot{b}_{\text{sfc}} - \frac{\partial H}{\partial t} \right) \, dS, \tag{2.2}$$

where $q_{\text{in}}, q_{\text{out}}$ are the ice fluxes through the upstream and downstream boundaries (R and P, Fig. 2.2) of the cell, respectively. Next, we consider the fact that the integral of the velocity profile over the ice thickness H is:

$$\frac{1}{H} \int_H v(z) \, dz = \gamma v_{\text{sfc}}, \tag{2.3}$$

where $\gamma \in [0.8, 1]$ is a factor relating the surface velocity v_{sfc} with the depth-averaged velocity (Cuffey and Paterson, 2010).

Along R, we have the following (the result for P is similar; here, x is defined along the boundary P or R):

$$q_{\text{in}} = \int_0^{W_R} \gamma v_{\text{sfc}}(x) H(x)\, dx = \gamma W_R \overline{Hv}_{\text{sfc}}, \tag{2.4}$$

where v_{sfc} is measured normal to R, and W_R is the length of the boundary R. For simplicity, we assume γ is spatially and temporally constant. This is not necessarily the case, but sensitivity experiments (see section "Sensitivity Analysis") indicate that changing values of γ have little impact on the calculated ice thickness in this study.

We now desire to solve Equation (2.4) for $\bar{H}$. From the Mean Value Theorem, we know that there exists $x_0 \in [0, W_R]$ such that the following is true:

$$\int_0^{W_R} \gamma v_{\text{sfc}} H\, dx = \gamma v_{\text{sfc}}(x_0) H(x_0) W_R. \tag{2.5}$$

What we then seek is the spatial scale on which both H and v_{sfc} are approximately constant, so that any variation in H or v_{sfc} is small, and therefore $H(x_0)v_{\text{sfc}}(x_0) = \overline{Hv}_{\text{sfc}}$. Clearly, this is not the case when the cell covers most or all of the glacier width, and so care must be taken if the cell covers a substantial portion of the glacier width. An analysis of the sensitivity of the calculated ice thickness to initial separation distance of adjacent flowlines follows.

On a scale where H and v_{sfc} are approximately constant, $\overline{Hv}_{\text{sfc}}$ is approximated by Hv_{sfc}, and we can combine Equations (2.2) and (2.4) to solve for H at the upstream boundary, R, given the ice flux q_{out} at the upstream boundary P:

$$H = \frac{q_{\text{out}} + \int_S \left(\dot{b}_{\text{sfc}} - \frac{\partial H}{\partial t} \right) dS}{\gamma W_R v_{\text{sfc}}}. \tag{2.6}$$

We can also solve for H at the downstream boundary, starting at the upstream boundary of the glacier. The direction of computation (up or down glacier) will depend on the data availability. This results in a calculation of the ice thickness at many cross-sections between a pair of adjacent flowlines; with many such pairs of flowlines, we can extend the calculation to cover the entire region of interest.

To solve Equation (2.6), we need the following information: values of surface mass balance $\dot{b}_{\text{sfc}}$, values of surface elevation change $\partial H/\partial t$, a surface velocity field, and an estimate of the ice thickness at the boundary of the domain of interest. Values of $\dot{b}_{\text{sfc}}$ can be interpolated from measurements, or obtained from model outputs. Considerable thought has been put into the differences between rates of surface elevation change derived from profiles versus those derived from DEM differencing (e.g., Arendt and others, 2002; Larsen

and others, 2007). Thinning rates derived from profiles can be used, but may not be representative of the margins of the glacier (Berthier and others, 2010). The surface velocity field can be derived from various sources such as photogrammetry or radar based measurements, but it must cover the region of the glacier over which we wish to calculate ice thickness. If the available velocity fields cover the entire glacier, the fact that $H \to 0$ at the boundary of the glacier is a sufficient initial estimate of the ice thickness at the boundary of the domain of interst; otherwise, some prior knowledge of the ice thickness is necessary. The next section details the datasets used for this study, and how they are used to solve Equation (2.6).

2.6 Application to Columbia Glacier

With the fjord bathymetry and surface DEMs, we have ice thicknesses for years where Columbia Glacier extended into the proglacial fjord, and thus have ice thicknesses at the downstream boundary of the flowlines. Because of the glacier's continued retreat since bathymetry measurements were last taken in 2005, the full coverage velocity maps in 2011 do not overlap with the region of measured bed topography. To calculate the bed topography using the 2011 velocity fields, we must first calculate the bed topography in the region between the proglacial fjord and the current glacier ("Confluence", Fig. 2.1). The velocity maps from the mid-2000s are then used to calculate the bed topography well upstream of the region of the 2011 terminus, and the remainder of the bed topography is calculated using the 2011 velocity fields.

We selected velocity fields from 1984, 1985, 2005, 2006, and 2009, based on measurement density and time of year (Table 2.1). Each velocity field is associated with a DEM and a modeled profile of surface mass balance. Thinning rates for each of these datasets are calculated by differencing two subsequent DEMs.

We calculated ice thicknesses upstream from the region where bathymetry is known (Fig. 2.1) in the following manner. To avoid interpolating velocities in the region near the calving front, we selected upstream and downstream boundaries for the flowlines; these boundaries are never within 3 km of the calving front for any particular velocity field. Flowlines are calculated using MATLAB's built-in `stream2` function (MATLAB ©1984–2013 Mathworks, Inc.), and are re-calculated for each velocity field. The resulting flowline vertices define cell boundaries for the thickness calculation. It should be noted that these cell boundaries do not have constant area or dimension: their size changes according to

the flow field (Fig. 2.2). At the downstream edge of this flow band, we calculated ice thickness using the known surface elevation and the bathymetry. We then calculated the ice thickness at the upstream boundary of each cell, according to Equation (2.6), using both rates of surface mass balance and rates of surface elevation change.

Before retreat began at Columbia Glacier, the majority ($> 90\%$) of the ice motion was calculated to be sliding (Rasmussen, 1988), and this has held throughout the retreat. Assuming Glen's flow law with exponent $n = 3$ and 90% of the motion due to sliding gives $\gamma = 0.98$ (Cuffey and Paterson, 2010). Based on this, and the results of the sensitivity test in the next section, we set $\gamma = 1$, which corresponds to the case where vertical shear is negligible or absent. We also set the initial flowline spacing to 250 m, as this allows for faster calculation.

We repeated the calculation of H over each of the available partial velocity fields sets to provide redundancy in the calculation, and calculated bed elevation by subtracting the ice thickness from the surface elevation. We then gridded the calculated bed elevations to a 100 meter grid by taking the arithmetic mean of calculated values that fall within each grid cell. On average, the spread between individual values for a grid cell is $\sim$ 13m, which is well within the uncertainties associated with the input data. This gridded topography provides a map of bed elevation that covers the region of the confluence, as well as part of the west branch, and the eastern trunk (Fig. 2.1).

This incomplete bed topography map is then used as input with the 2011 velocity fields, and the bed topography calculation is thereby extended to the entire glacier extent. Because a full-coverage surface DEM of Columbia Glacier that matches with the 2011 TerraSAR-X velocity fields is not presently available, we use previous full-coverage DEMs to estimate surface elevations in areas not covered by the 2010 partial DEM as follows. First, thinning rates between 1957 and 2007 are calculated using the two full-coverage DEMs. A full coverage map of relative thinning rates, A, is produced by dividing the map of these thinning rates by their mean value over the same area covered by the 2010 DEM. Next, annual thinning rates between 2007 and 2010 are calculated, using the 2010 DEM, and are assumed to be valid for 2011. The mean of these values is calculated, and the final surface elevation map is calculated:

$$Z_{2011} = Z_{2007} + \frac{4}{3}\overline{Z_{2010} - Z_{2007}} * A, \tag{2.7}$$

where Z is the surface elevation for the subscripted year, $\overline{Z_{2010} - Z_{2007}}$ is the mean value of

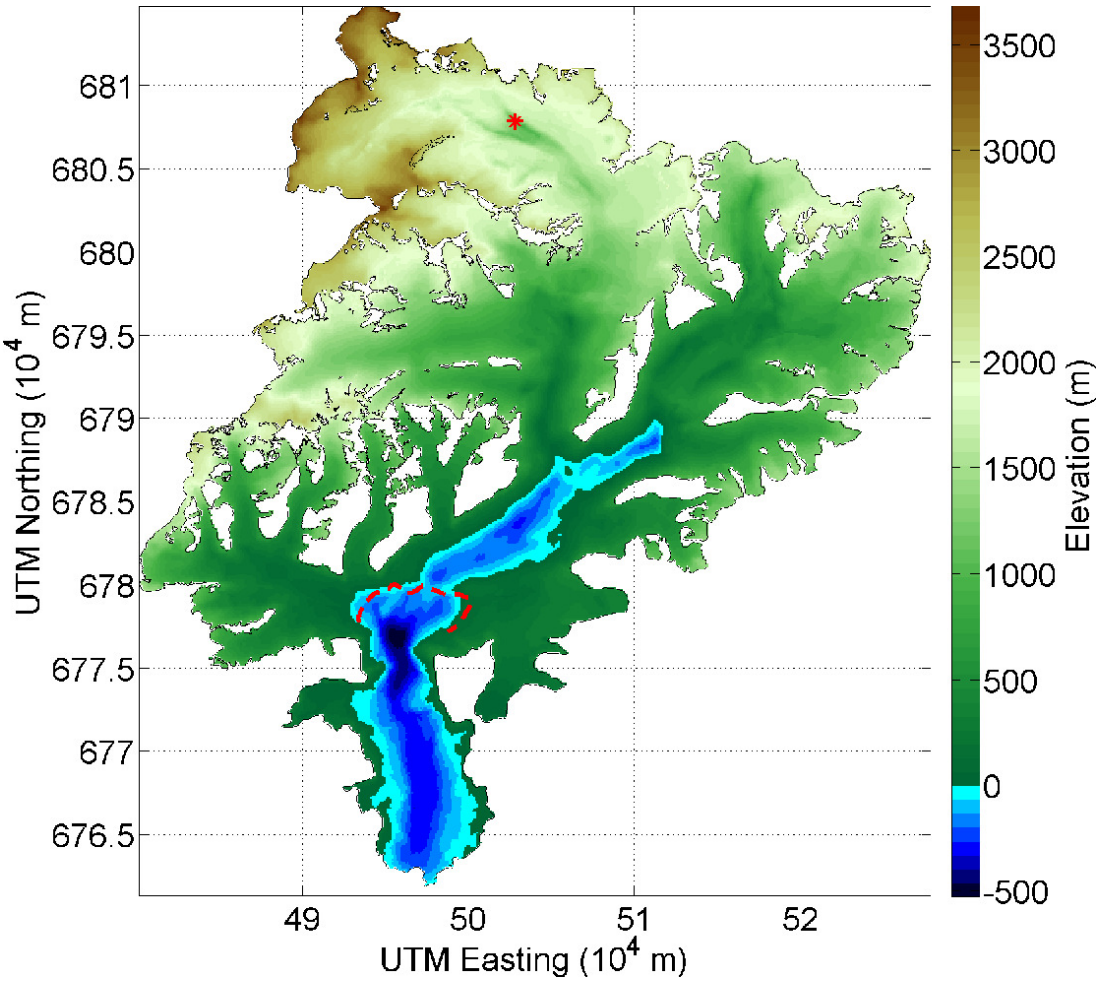

Figure 2.3. Calculated bed topography map for Columbia Glacier, 1957 extent. May 2011 terminus location shown as a red dashed line. Location of thickest ice in both 1957 and 2007 is shown as a red star.

the 2007-2010 thinning rates evaluated over the 2010 domain, and A is the ratio between the 1957-2007 thinning rates and the spatial mean. This estimation can add a considerable amount of uncertainty into the ice thickness calculation, and this is discussed with the uncertainty and error analysis.

2.7 Results

General information about the calculated topography map is given in Table 2.2, and the final topography map itself is shown in Figure 2.3. Bed topography data are available as supplemental material to this paper.

Table 2.2. General results for the new bed topography map. S indicates glacier map area, V total ice volume, V below s.l. is volume of ice that is below sea level, $H_{\max}$ is maximum ice thickness, $\overline{H}$ is mean ice thickness ($\pm$ one std. dev.), H_{med} is median ice thickness, and z_{bed} is bed elevation.

Year	S	V	V below s.l.	$H_{\max}$	$\overline{H}$	H_{med}	Max. z_{bed}	Min. z_{bed}
	km^2	km^3 ice eq.	km^3 ice eq.	m	m	m	m	m
1957	1067	294	17	1040	280 ± 215	225	3670	-525
2007	935	134	7	1005	145 ± 140	100	-	-504
2011	915	N/A	4	N/A	N/A	N/A	-	-282

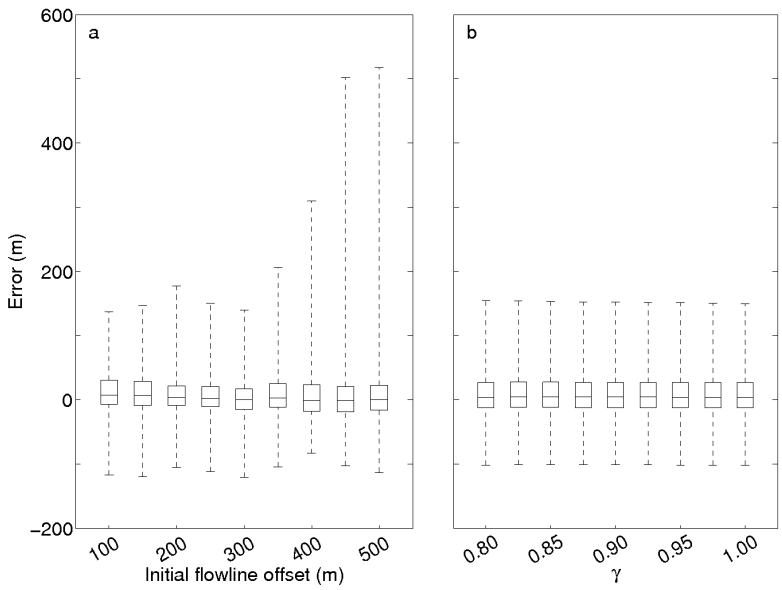

Figure 2.4. Results of analysis of calculated ice thickness sensitivity to changes in (a) initial flowline offset, and (b) γ (Equations 2.3-2.6). Error is defined as the difference between measured and calculated ice thicknesses.

2.7.1 Sensitivity Analysis

We conduct analysis of the sensitivity of calculated ice thickness to the main components of the model: initial flowline separation (i.e., the starting flowband width), γ, surface mass balance rates, rates of surface elevation change, and the velocity direction, using the four velocity fields from 1984 and 1985. The sensitivity analysis is limited to the area downstream of the 2004 terminus (i.e., where the bathymetry is known), as the density of bed topography measurements there allows for a more complete comparison of ice thicknesses. The soft-rock geology that characterizes the Chugach Range (e.g., Wilson and others, 1998) garners expectations of rapid erosion, with the implication that bathymetric measurements do not perfectly represent the glacier bed when ice was present. Whether these expected high rates of erosion directly result in sedimentation in the fjord is not known; for simplicity, we assume that the measured bathymetry represents the glacier bed.

First, we investigate the effect of changing initial separation of flowlines on calculated ice thickness. Because the most dense velocity fields (derived from TerraSAR-X) are available in a 100 meter grid, this is taken as a lower limit for the flowline separation. Initial flowline separation is then varied, in 50 meter increments, up to 500 meters. Results are

Table 2.3. Results of analysis of calculated ice thickness sensitivity to changes in surface mass balance ($\dot{b}_{\text{sfc}}$), surface elevation change ($\partial H/\partial t$), and velocity vector direction (α), over the domain covered by measured bathymetry (Fig. 2.1). Here, error is defined as the difference between measured and calculated ice thickness. Mean error is reported as arithmetic mean $\pm$ one standard deviation.

Variable	Δ	Max. error	Mean error	RMSE
		m	m	m
$\dot{b}_{\text{sfc}}$ (m a^{-1})	+1.0	145	7 ± 42	30
	+0.5	148	7 ± 43	31
	0	150	8 ± 43	31
	-0.5	153	9 ± 43	32
	-1.0	156	9 ± 43	33
$\partial H/\partial t$ (m a^{-1})	-2.0	141	6 ± 42	32
	-1.0	144	7 ± 42	31
	0	150	8 ± 43	31
	+1.0	156	9 ± 44	31
	+2.0	161	10 ± 44	31
α(deg)	0.5	152	8 ± 43	31
	1.0	161	8 ± 43	31
	2.0	187	8 ± 43	32
	5.0	323	9 ± 44	32
	10.0	305	9 ± 44	32

shown in Figure 2.4a. Overall, flowline separation shows very little effect on either mean absolute difference or root mean square error (RMSE). As flowline separation increases beyond 300 m, however, maximum error increases significantly, suggesting that the limit where $H(x_0)v_{\text{sfc}}(x_0) \approx \overline{Hv}_{\text{sfc}}$ is flowline separations of around 300 m.

Second, we investigate the sensitivity of the calculated bed topography to values of γ by varying γ from 0.8 to 1 (Fig. 2.4b). RMSE for the given values of γ are all within a 1.5 m range, indicating that values of γ are not as important as the initial flowline separation. For a typical grid cell in this region (covered by the bathymetry data, Fig. 2.1), typical values are about -0.5 m w.e. a^{-1} for $\dot{b}_{\text{sfc}}$, 4.5 m w.e. a^{-1} for $\partial H/\partial t$, and 2×10^8 m^3 a^{-1} for q_{in} and q_{out}. Given this, calculated ice thicknesses are on the order of 500 m; for this value, varying γ from 0.8 to 1.0 changes the calculated ice thickness by less than 1 m.

Further analysis of Equation (2.6) shows that even away from the fast-flowing portion of the glacier, changes in γ introduce changes in ice thickness that are much smaller than the uncertainties associated with the components of Equation (2.6).

Third and fourth, we investigate the effect of varying surface mass balance rates $\dot{b}_{\text{sfc}}$ by increasing and decreasing $\dot{b}_{\text{sfc}}$ by 0.5 and 1.0 m a^{-1}, and by increasing and decreasing values of $\partial H/\partial t$ by 1.0 and 2.0 m a^{-1}. Results are summarized in Table 2.3. Very little change in error is observed. Again, given typical values of components of Equation (2.6), values of $\dot{b}_{\text{sfc}}$ and $\partial H/\partial t$ are typically one to four orders of magnitude less than ice velocities, and ice fluxes are typically several orders of magnitude larger than the terms in the right hand side of Equation (2.2). This is a reflection of the fact that for tidewater glaciers in rapid retreat like Columbia Glacier, climatic balances are dwarfed by dynamic changes (Meier and Post, 1987; Pfeffer, 2007), at least on the lower region of the glacier.

Finally, we investigate the effect of perturbing the input velocity fields. To this end, we perturb the angle of the velocity vectors using a uniform random distribution on the interval $[-\Delta\alpha, \Delta\alpha]$, where $\Delta\alpha$ is measured in degrees. We use the values of $0.5, 1, 2, 5$, and 10 for $\Delta\alpha$. Results are summarized in Table 2.3. For large ($> 5^\circ$) values of $\Delta\alpha$, maximum error increases significantly (by a factor of 2 over unperturbed values), but mean error and RMSE remain relatively unchanged. Most likely, this is due to the random nature of the perturbations - with equal numbers of positive and negative changes, we would expect the overall effect on the mean to be small.

2.7.2 Uncertainty and Error Analysis

Because full coverage DEMs are not available for the same time as full coverage surface velocity maps, surface elevations must be estimated using the existing full and partial coverage DEMs, as shown by Equation (2.7). To estimate the uncertainty introduced by this method, we calculate a full-coverage DEM for 2010, and compare the estimated surface elevations to the measured surface elevations. The resulting RMSE in surface elevations is 26.6 m.

For the full and partial coverage DEMs, we estimate uncertainties by comparing elevations in non-glacierized areas, resulting in an estimated vertical position error of 2 m. With a mean time separation of one year between successive DEMs, this results in an uncertainty of 2.8 m a^{-1} in calculated rates of surface elevation change.

For velocity datasets derived from non-digital photogrammetry (dates before 2004),

Krimmel (2001) estimates an uncertainty in displacement of 4 m between successive images. Given a typical time separation between successive images of 0.115 a, this translates to an uncertainty in velocity of approximately 35 m a^{-1}.

For velocity datasets derived from digital photogrammetry (2004-2010), uncertainties arise from point identification on photographs and interpolation of irregularly spaced data to grid nodes. We use the following equation to estimate the uncertainty (in m a^{-1}) in velocities derived from aerial photographs:

$$E_{\text{vel}} = 365\frac{C\Delta x}{\Delta t}, \tag{2.8}$$

where C is uncertainty in image registration and feature tracking in pixels (p), Δx is the image resolution in m p^{-1}, and Δt is the time separation between successive images in days. Using typical values of $1-2$ p for C, 2 m p^{-1} for Δx, and 40 d for Δt, we estimate an uncertainty of $18-36$ m a^{-1} in velocity values. Given this, we use the upper bound on the uncertainty (36 m a^{-1}), to encompass both digital and non-digital datasets.

We estimate the uncertainty introduced by interpolating irregularly spaced velocities to grid nodes by calculating the standard deviation of the difference between interpolated and uninterpolated values at the same point. The resulting interpolation error is approximately 13 m a^{-1}.

As reported by Rasmussen and others (2011), the RMSE in values of $\dot{b}_{\text{sfc}}$ used is 1.0 m w.e. a^{-1}. The total uncertainty in calculated ice thickness, assuming that each of the estimated uncertainties (DEM, thinning rates, velocity, and $\dot{b}_{\text{sfc}}$) are independent and quadratically additive, is 46.7 m.

This treatment is for random uncertainty only, and does not address systematic error. To ensure that systematic errors are not present in values of $\dot{b}_{\text{sfc}}$ and $\partial H/\partial t$, we check the value of $\dot{b}_{\text{sfc}} - \partial H/\partial t$, integrated over the 2007 glacier domain, obtaining a value of 6.5 km^3 a^{-1}. This is comparable with estimates of calving fluxes for Columbia Glacier (O'Neel and others, 2005; O'Neel, 2012), lending confidence that the errors in measurement are not systematic.

2.7.3 Ice Thickness and Bed Topography

We calculate ice thickness distribution for the glacier for the two years in which we have full coverage DEMs, 1957 and 2007 (Fig. 2.5). Over that period, the mean thickness ($\pm$ one standard deviation) of the glacier is nearly halved, from 280 ± 215 m in 1957 to 145 ± 140 m

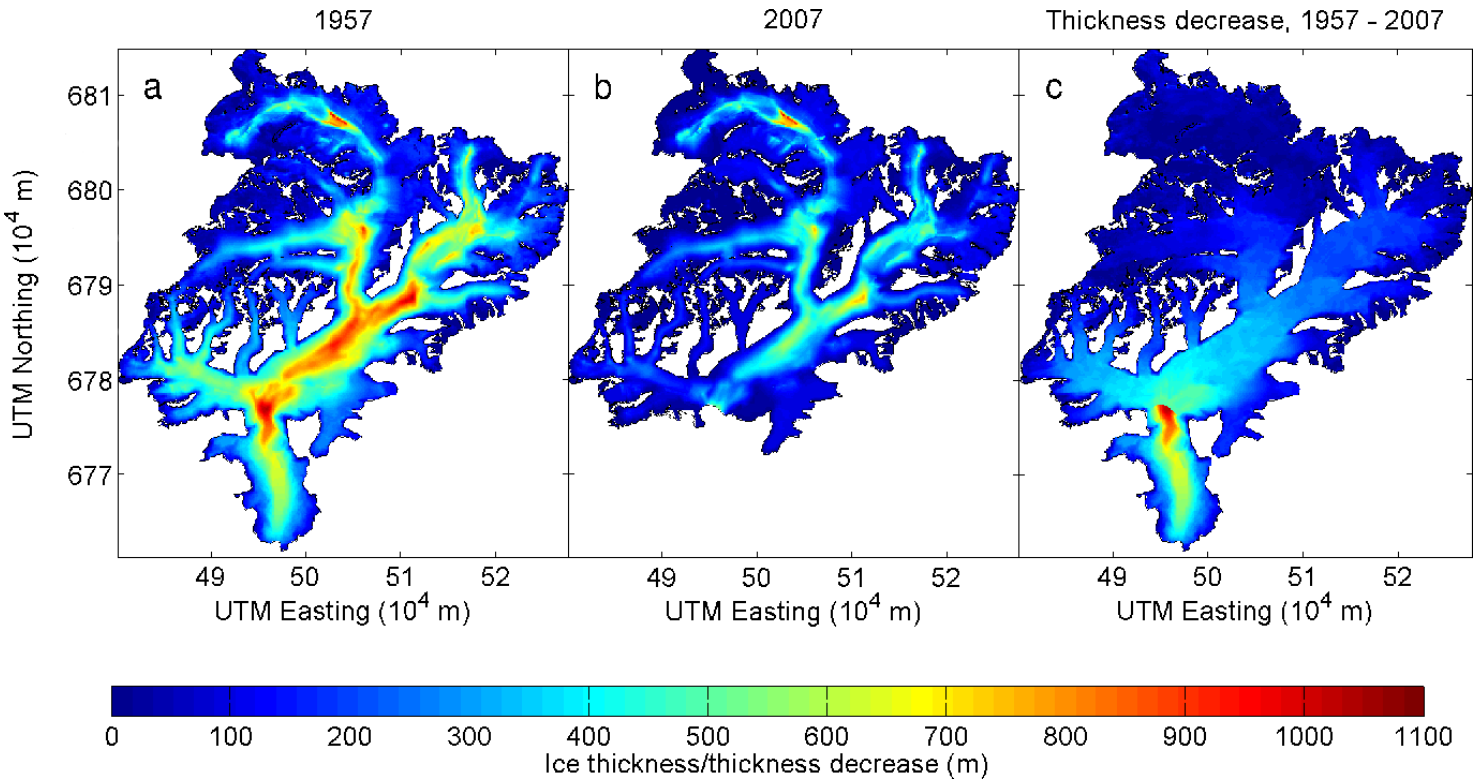

Figure 2.5. Calculated ice thickness map (a) 1957 and (b) 2007, and (c) thickness decrease 1957-2007 for Columbia Glacier.

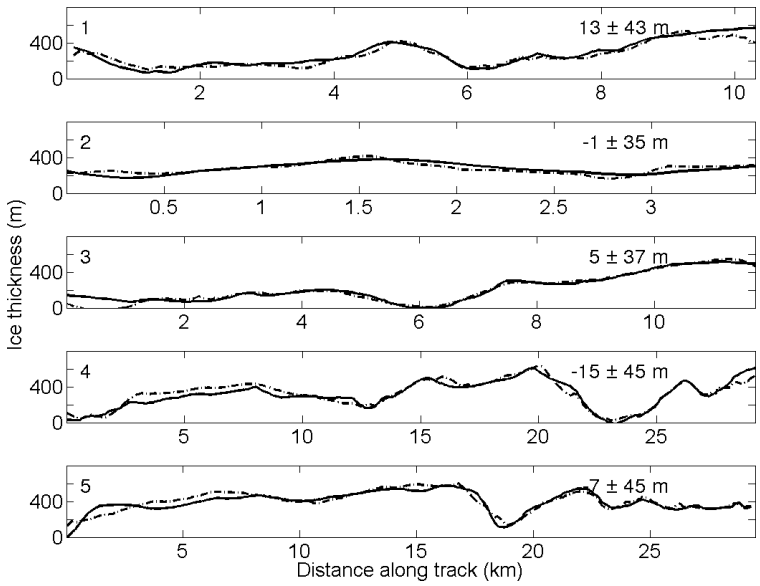

Figure 2.6. Comparison of calculated thickness (dash-dot) to measured thickness (solid line) along radar profiles, oriented West to East (Fig. 2.1). Track number is indicated in upper left corner of each pane. Difference between measured and calculated ice thickness is expressed as mean value ± one standard deviation, indicated in upper right corner of each panel.

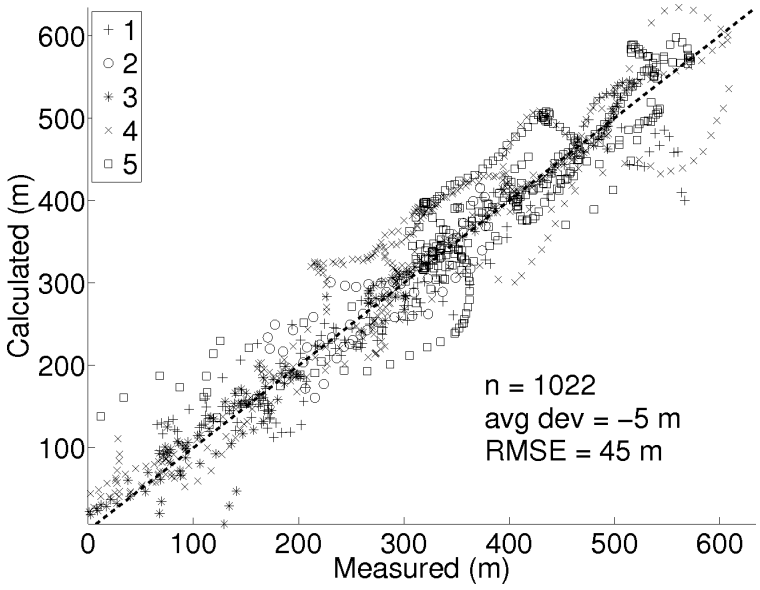

Figure 2.7. Comparison of calculated and measured ice thickness for all radar points (Fig. 2.1). Legend indicates to which radar track each point belongs. The statistics in the bottom right refer to the ensemble of points (n: number of points; avg dev: average deviation; RMSE: root mean square error)

in 2007. The median thickness of the glacier is also more than halved, from 225 m in 1957 to 100 m in 2007.

The maximum thickness of the ice, however, is nearly the same in the two years: 1040 m in 1957, and 1005 m in 2007. The location of thickest ice for both years is indicated in Figure 2.3, and is very high on the glacier, where very little thickness change has occurred.

The calculated bed topography, over the 1957 glacier extent, ranges from 525 m below sea level at its deepest point ($\xi \approx 52$ km, Fig. 2.1), to 3670 m above sea level at its highest point ($\xi \approx 0$ km). The deepest part of the bed covered by the current (2011) glacier extent is, by contrast, 280 m below sea level ($\xi \approx 41.5$). At the June 2011 location of the terminus ($\xi \approx 48.2$ km), the maximum calculated depth is 154 m below sea level.

The portions of the bedrock topography lying below sea level are 11%, 6%, and 4% for the glacier extents in 1957, 2007, and 2011, respectively. In the centerline coordinate system, the calculated bed rises above sea level at $\xi \approx 36.4$ km, which is in good agreement with previous estimates (Mayo and others, 1979). This is also 11.7 km from the current (2011) terminus.

We also compare calculated ice thicknesses to ice thicknesses derived from radar measurements. A comparison of individual radar tracks is shown in Figure 2.6, and comparison of all measured and calculated ice thicknesses is shown in Figure 2.7. Based on comparison to radar, the method appears to work best in areas with many overlapping velocity datasets, like the eastern trunk (radar tracks 3-5, Figs. 2.1 and 2.6). Only one radar track (Track 3, Figs. 2.1 and 2.6) is cross-flow, at least for part of its extent. For the part of the track that is cross-flow (distance along track 6-12 km, Track 3, Fig. 2.6), the difference between the calculated and measured ice thickness is as small as it is for the along-flow portion of the track, lending confidence that the method succeeds for both cross-flow and along-flow directions.

2.7.4 Volume Change

We calculate the total ice volume for Columbia Glacier in 1957 and 2007 using the ice thickness maps (Fig. 2.5). For 1957, we calculate a total ice volume of 294 km^3, and 134 km^3 for 2007. The calculated volume loss over the period 1957-2007 is then 160 km^3. The resulting percentage volume loss of 54% indicates that Columbia Glacier has lost over half of its volume since 1957, most of which occurred following the onset of retreat, ca. 1982. Assuming a density of 900 kg m^{-3}, the calculated mass loss is 144 Gt.

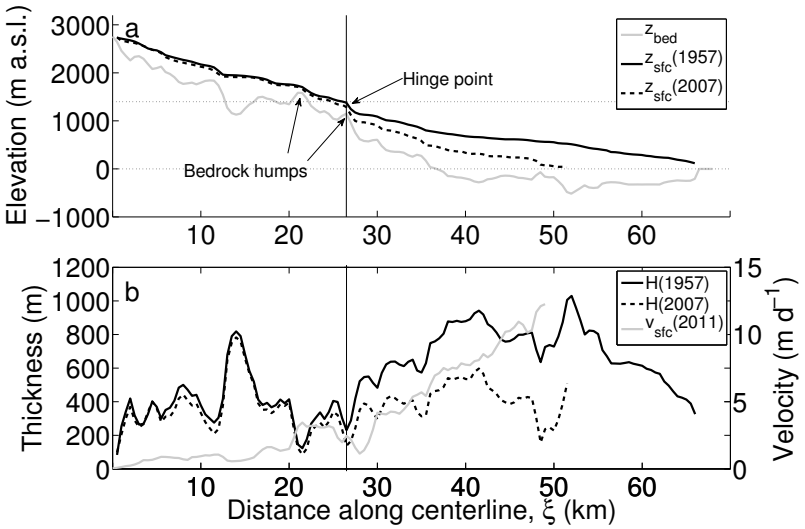

Figure 2.8. (a) Calculated centerline bed topography and surface elevation in 1957 and 2007, with location of apparent separation between upper and lower glacier regions indicated. (b) Calculated ice thickness along centerline in 1957 and 2007, along with 2011 centerline surface velocity, showing jump in velocity near location of apparent hinge point between upper and lower glacier regions.

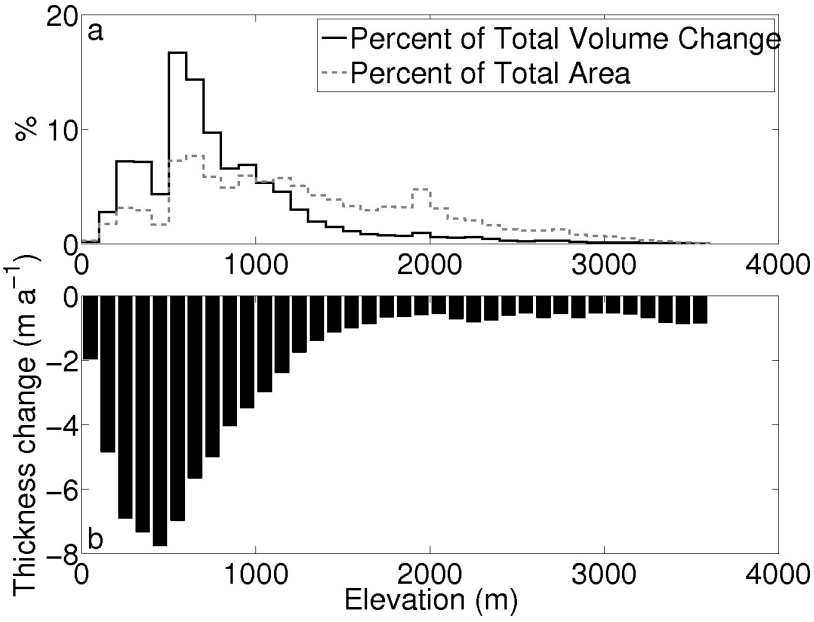

Figure 2.9. (a) Percent of total volume change 1957-2007, along with percent of total area (1957 hypsometry), and (b) thickness change 1957-2007 for each 100 m elevation band (from 0 m to 3700 m, 1957 hypsometry).

For the 1957 glacier extent, the calculated ice volume below sea level is 18 km^3 (6% of the total; cf. 11% of the glacier area below sea level), and for the 2007 glacier extent, the calculated ice volume below sea level was 7 km^3 (5%; cf. 6%).

Figure 2.8 illustrates the existence of a clear separation between the upper ($\xi < 26.5$ km) and lower ($\xi > 26.5$ km) glacier. This separation is also demonstrated in Figure 2.9a. A majority (91%) of the volume change over the period 1957-2007 has occurred at 1957 surface elevations below 1400 m a.s.l. Despite making up a substantial portion of the total 1957 area (34%), elevations above 1400 m contributed little (9%) to the total volume change over the period.

2.8 Discussion

Our method to compute spatially distributed glacier thickness is based on evaluation of the mass continuity equation between adjacent flowlines that are interpolated from surface velocity fields. The main advantage this method has compared with other methods for calculating ice thickness is its assimilation of available data, thereby giving sound constraints on the calculated ice thickness. Because the method does not calculate the ice thickness on the whole glacier domain at once, it is likely faster than other methods that solve the mass continuity equation on a grid.

The requirement of accurate and dense surface velocity fields is both an advantage, and a disadvantage, to this method. The method is only applicable in regions where ice is flowing and surface velocity fields are available. It is also limited in application to a single glacier at a time, and significant work is required to estimate the total ice volume of an entire region. For individual glacier applications, however, it is both accurate and easily implemented. At present, there are no tidewater glaciers in the world with the wealth of data available at Columbia Glacier, but increased availability and application of remote sensing data, such as TerraSAR-X and TanDEM-X imagery, will serve to reduce the input data barrier.

We tested sensitivity of calculated ice thickness to different components of Equation (2.6) in the early phase of Columbia Glacier's retreat (1984 and 1985). Because typical values of each component are small compared with typical values of ice flux at that time, we find that calculated ice thickness is not sensitive to relatively large changes in the value of each component. It should be stressed that this is most likely not typical for alpine glaciers. It is also likely not true for the upper region of the glacier, where dynamic thin-

Table 2.4. Comparison of new bed topography map (Fig. 2.3) and topography map produced by Engel (2008). The new map is evaluated only over the domain covered by the previous map (Fig. 2.1). % below s.l. indicates the percentage of the bed that is below sea level.

	New map	Engel (2008)
Min. z_{bed} (m)	-525	-760
Max. z_{bed} (m)	590	710
% Below s.l.	14.5	13.2
H_{max}(1957) (m)	1040	1420
$\overline{H}$(1957) (m)	555	660
H_{max}(2007) (m)	695	1160
$\overline{H}$(2007) (m)	300	505

ning has been largely non-existent, and so errors in the other inputs ($\dot{b}_{\text{sfc}}$, velocity) are large relative to the ice thickness. Despite this, the method performs well on the upper region of the glacier, indicating its ability to calculate ice thickness in both fast-flowing and slow-flowing regions of a glacier.

We have tested the sensitivity of the calculated ice thickness to uniform values of γ only, but the possibility remains that values of γ may not be uniform at the upstream and downstream boundaries of each cell: that is, Equation (2.6) can be reduced to (with γ_R, γ_P the values of γ at the upstream and downstream boundaries, respectively):

$$H_R = \frac{\gamma_P}{\gamma_R} H_P, \tag{2.9}$$

where H_R, H_P are the ice thicknesses at the upstream and downstream boundaries, respectively. If the ratio of γ_P to γ_R reaches 0.8, then, the error introduced by assuming a uniform γ could reach 20%. In practice, however, the existence of such a large change in the value of γ over such a small distance ($< 200 - 300$ m) seems unlikely. If larger cell sizes are used, however, it may become necessary to consider nonuniform values of γ.

A comparison between the newly presented bed topography map and the previous (Engel, 2008) bed map shows that the previous map has overestimated the ice thickness by as much as 70%, a fact that is acknowledged by the author. Results of this comparison are shown in Table 2.4. There may be several reasons for this discrepancy between the two calculated bed topographies. First, Engel (2008) noted that spurious overdeepenings in calculated bed topography may be introduced when flowlines originating near

the terminus are used. To avoid this problem, we do not calculate flowlines in the near terminus region (within ~ 3 km of the terminus for any particular velocity field). Second, we use many overlapping velocity fields that were unavailable at the time of the previous study. Third, the previous study made the assumption that surface mass balance rates were zero and used thinning rates calculated from centerline laser altimetry profiles in the mid-1990s to estimate thinning rates in both the 1980s and in 2004. This assumption would most likely result in an overestimation of ice thickness, but a quantification of the extent is not presently available.

We also compare the bed topography calculated using our method with the estimate by Rasmussen (1988). The estimate computed by Rasmussen covers only the lowest 15 km of the 1957 glacier extent, which is approximately the limit of the bathymetry measurements. Comparing Rasmussen's estimate with the measured bathymetry yields a mean difference of 42 ± 130 m, while the mean difference between our calculated bed topography and the measured bathymetry is 8 ± 43 m.

With the full bed topography map, we calculated total ice volume for the years when full-coverage surface DEMs are available. As far as we know, this is the first estimate of total ice volume for Columbia Glacier. It is not, however, the first estimate of volume change at Columbia Glacier. Using thinning rates derived from laser altimetry, Arendt and others (2006) calculate a total mass loss over the period 1957-2004 of 141 Gt (3.01 Gt a^{-1}). Arendt and others do not take into account ice below sea level. Over the period 1962-2006, Berthier and others (2010) estimated the rate of volume loss above sea level at Columbia Glacier to be 2.43 Gt a^{-1}. Our estimate of 144 Gt (2.88 Gt a^{-1}; 2.68 Gt a^{-1} above sea level) during the period 1957-2007 is in between both of these reported estimates.

Figures 2.8 and 2.9 illustrate a decoupling between the upper and lower regions of the glacier at $\xi \approx 26.5$; this separation is apparent in both the surface elevation and ice thickness profiles as a "hinge point". Above this hinge point, the glacier surface is largely the same as it was in 1957; below this hinge point, the glacier has thinned in excess of 500 m in places. The calculated bed topography in the region of the hinge point shows several prominent bedrock humps along the centerline, where the ice thickness drops from $300 - 400$ m to $100 - 200$ m, approximately a 50% reduction in ice thickness over a length scale of $1 - 2$ km. These rapid drops in ice thickness likely serve to impede stress transmission between the upper and lower regions of the glacier, and retard the drawdown of ice to the lower glacier region.

There are abundant studies that calculate glacier volume change over recent time periods, but very few that calculate initial volumes, and that therefore can report relative volume changes. In a study estimating the glacier ice volume in the entire Swiss Alps, Farinotti and others (2009a) found that the ice volume of the Swiss Alps decreased by 12% over the period 1999-2008. In a second, smaller study of 20 glaciers in the southeastern Swiss Alps, Huss and others (2010) find a regional decrease of 47% of ice volume over the period 1900-2008. The authors determine total ice volume using the method developed by Farinotti and others (2009b). For individual glaciers in the region, percentage volume loss ranged from 30 to 75%. For the largest glaciers in the region (with surface areas of $7-17$ km^2), volume loss ranged from 38 to 62%. These mostly land-terminating glaciers exhibit the same relative changes in volume as Columbia Glacier, but over a time period that is over twice as long. Considering that volume change at Columbia Glacier was very nearly zero over the period 1957-1981 (Meier and Post, 1987; Rasmussen and others, 2011), Columbia Glacier has lost a comparable percentage of volume in one quarter the time as these glaciers (26 years). This discrepancy is not surprising, given that most of the volume change from Columbia Glacier is due to dynamic causes such as calving, whereas volume loss from glaciers in the Swiss Alps is due to more negative surface mass balances alone.

Based on our findings at Columbia Glacier, we suggest that the potential for a rapid acceleration of glacier discharge does not require a large portion of the glacier to be grounded below sea level; indeed, Columbia Glacier lost 50% of its ice volume between 1957 and 2007, despite having only 11% of the bed topography over the 1957 glacier extent below sea level. The Greenland Ice Sheet has a relatively large portion of its ice grounded below sea level (e.g., Bamber and others, 2001) and is drained by many outlet glaciers, some of which have deep troughs that extend into the interior of the ice sheet (e.g., Pfeffer and others, 2008). Recent studies of the outlet glaciers of the Greenland Ice Sheet (e.g., Howat and others, 2005; Rignot, 2006; Moon and Joughin, 2008) have shown an increase in both ice velocity and ice discharge, in a relatively short period of time. In light of the larger portion of the Greenland Ice Sheet being grounded below sea level, we might expect the recent, rapid adjustments in outlet glacier geometry to continue.

In addition to the potential implications for the Greenland Ice Sheet, our finding of a large, rapid, tidewater response with a small portion of the glacier grounded below sea level has implications for other mountain glaciers and ice caps. Tidewater glaciers are prevalent in many mountain glacier and ice cap systems around the world, in particular in

the Canadian and Russian Arctic, Svalbard, and the periphery of Greenland and Antarctica. Despite their importance for sea level rise (e.g., Meier and others, 2007; Hock and others, 2009), relatively little is known about the dynamics and stability of these systems.

Pfeffer (2007) proposed a simple mechanism to initiate irreversible tidewater retreat. By examining how waves of thickening and thinning propagate through a glacier, he found that instability arises when changes in glacier geometry serve to reduce resistive stresses more than driving stresses, and that stabilization can occur where there is a ratio of ice thickness to water depth h/h_w above 1.49, a negative longitudinal flux gradient ($\partial q/\partial x$), and high rates of diffusive thickening D. Applying this analysis to the 2011 data for Columbia Glacier, and averaging values over the 2.5 km nearest the terminus, we find an average value of $h/h_w = 1.7$, $\partial q/\partial x$ that is positive but nearly zero, and a rate of diffusion ($D/W = 2.64 \times 10^8$ m^2 a^{-1}, expressed per unit width) in the same order of magnitude as Pfeffer's values for Columbia Glacier ($D/W = 8.33 \times 10^8$ m^2 a^{-1}). In addition, the nondiffusive propagation speed is positive, indicating that perturbations propagate downstream, which in turn indicates stability.

We can also examine the slope of the bedrock along the centerline at Columbia Glacier. Weertman (1974) calculated that an ice sheet whose bed slopes inward toward the center is unstable, a finding supported by numerical experiments of tidewater glacier evolution (Vieli and others, 2001). At present, the bed slope at the terminus of Columbia Glacier slopes inward; it stops sloping inward at $\xi = 41.5$ km, 6 km from the present terminus location. Based on this, and the application of Pfeffer's (2007) analysis, it is possible that the rapid part of Columbia Glacier's retreat is nearing an end; at the very least, it does not seem likely that the retreat rate will match that seen in the 1980s and 1990s.

Because of its high calving rates, thinning rates at Columbia Glacier are not presently representative of most glaciers in Alaska. However, the well-studied retreat of Columbia Glacier could serve as an analogue to the opening of both Icy Bay and Glacier Bay, Alaska. The glaciers of Icy Bay retreated approximately 40 km between the early 20th century and present (Barclay and others, 2006), while the glaciers of Glacier Bay retreated over 100 km between the late 18th and early 20th centuries (e.g., Larsen and others, 2005; Molnia, 2008; Barclay and others, 2009). Because Columbia Glacier has been studied since before its retreat, it can provide some insight into how the retreats of the glaciers of Icy Bay and Glacier Bay evolved. Because the glaciers of Icy Bay and and Glacier Bay have largely slowed or finished their retreats (e.g., Porter, 1989; Molnia, 2008; Barclay and others, 2009),

they can provide insight into how Columbia Glacier will continue to evolve, until its retreat eventually ends.

2.9 Conclusions

We have presented a method, based on conservation of mass, for estimating spatially distributed glacier ice thickness and bed topography. The method requires velocity data of sufficient density to ensure that over the grid spacing used, ice thickness and surface velocity can be accurately interpolated. The other data requirements (multiple full-coverage DEMs, and surface mass balance rates) are large, but not necessarily prohibitive. Increased availability of remote sensing data products, such as velocity fields from TerraSAR-X, and surface DEMs from TanDEM-X, will likely serve to further reduce this barrier. Because the method is applicable to both fast and slow-moving ice, it can potentially be applied to any glacier for which sufficient data are available.

Using this method, we have presented a high resolution bed topography map for Columbia Glacier. The new topography map covers the entire glacier extent, both current and former, and is in excellent agreement with radar ice thickness measurements, with a mean difference between measured and calculated ice thickness of -5 m, and RMSE of 44 m. The majority of this error is likely due to our approximation of the current (2011) glacier surface elevation using DEMs extrapolated from previous years (2007 and 2010).

With this bed topography map, we have calculated the total ice volume at Columbia Glacier in 1957 and 2007, finding that the glacier has lost over 50% of its volume during this period. The majority of the calculated volume change is from areas where the 1957 surface is below 1400 m a.s.l. This is most likely due to the difficulty of transferring stress across several prominent bedrock humps that occur along the centerline, approximately 26 km from the head of the glacier.

The small fraction of the 1957 bed extent that is below sea level shows that having a large percentage of the bed below sea level is not necessary to initiate a rapid tidewater response. Because little is known about the stability and dynamics of tidewater glacier systems around the world, the implications of this finding for these other systems is unknown. Application of an analysis of tidewater stability to the present state of Columbia Glacier, as well as examination of its bedrock slope, indicate that the rapid portion of Columbia Glacier's retreat is perhaps nearing an end.

2.10 Acknowledgements

This research was supported in part by NSF grant EAR-0943742, NASA grant NNX11AF41G, NASA grant NNX11A023G, AON grant 0732726, NSF grant ARC-0732739, USGS Climate and Land Use Change Research Program support, and a UAF Center for Global Change Student Research Grant with funds from the Cooperative Institute for Alaska Research. We also thank pilot Paul Claus and Ultima Thule Lodge for logistical support in gathering radar data. We obtained the SPOT DEM as part of the SPIRIT (Stereoscopic survey of Polar Ice: Reference Images and Topographies) Polar Dali Program (©CNES 2008). Part of the TerraSAR-X data used in this study was provided under DLR A0 LAN_0164. Our thanks to Mathieu Morlighem and Daniel Farinotti for their helpful and constructive reviews on improving the manuscript. We also thank Tim Bartholomaus for his helpful comments in improving the manuscript.

2.11 References

Ahn, Y. and I. Howat, 2011. Efficient, automated glacier surface velocity measurement from repeat images using Multi-Image/Multi-Chip (MIMC) and null exclusion feature tracking, *IEEE Trans. Geosci. Remote Sens.*, **49**(8), 2838–2846.

Arendt, A., K. Echelmeyer, W. Harrison, C. Lingle and B. Valentine, 2002. Rapid wastage of Alaska glaciers and their contribution to rising sea level, *Science*, **297**(5580), 382–386.

Arendt, A., K. Echelmeyer, W. Harrison, C. Lingle, S. Zirnheld, V. Valentine, B. Ritchie and M. Druckenmiller, 2006. Updated estimates of glacier volume changes in the western Chugach Mountains, Alaska, and a comparison of regional extrapolation methods, *J. Geophys. Res.*, **111**(F03019).

Bahr, D. B., M. F. Meier and S. D. Peckham, 1997. The physical basis of glacier volume-area scaling, *J. Geophys. Res.*, **102**(B9), 20355–20362.

Bamber, J. L., R. L. Layberry and S. P. Gogineni, 2001. A new ice thickness and bed data set for the Greenland ice sheet 1. Measurement, data reduction, and errors, *J. Geophys. Res.*, **106**(D24), 33773–33780.

Barclay, D., J. Barclay, P. Calkin and G. Wiles, 2006. A revised and extended Holocene Glacial history of Icy Bay, Southern Alaska, U.S.A., *Arctic, Antarctic, and Alpine Res.*, **38**(2), 153–162.

Barclay, D., G. Wiles and P. Calkin, 2009. Holocene glacier fluctuations in Alaska, *Quat. Sci. Rev.*, **28**, 2034–2048.

Berthier, E., E. Schiefer, G. K. C. Clarke, B. Menounos and F. Rémy, 2010. Contribution of Alaskan glaciers to sea-level rise derived from satellite imagery, *Nature Geosci.*, **3**, 92–95.

Bevington, P. R., 1969. Data reduction and error analysis for the physical sciences, McGraw-Hill, New York.

Calkin, P. E., G. C. Wiles and D. J. Barclary, 2001. Holocene coastal glaciation of Alaska, *Quat. Sci. Rev.*, **20**, 449–461.

Clarke, G. K. C., E. Berthier, C. G. Schoof and A. H. Jarosch, 2009. Neural Networks Applied to Estimating Sublacial Topography and Glacier Volume, *J. Clim.*, **22**, 2146–2160.

Cogley, J. G., R. Hock, L. A. Rasmussen, A. A. Arendt, A. Bauder, R. J. Braithwaite, P. Jansson, G. Kaser, M. Möller, L. Nicholson and M. Zemp, 2011. Glossary of glacier mass balance and related terms, vol. 86 of *IHP-VII Tech. Doc. in Hydrol.*, UNESCO-IHP, Paris, IACS Contribution No. 2.

Conway, H., B. Smith, P. Vaswani, K. Matsuoka, E. Rignot and P. Claus, 2009. A low-frequency ice-penetrating radar system adapted for use from an airplane: test results from Bering and Malaspina Glaciers, Alaska, USA, *Ann. Glaciol.*, **50**(51), 93–97.

Cuffey, K. M. and W. S. B. Paterson, 2010. The physics of glaciers, Butterworth-Heinemann, fourth ed.

Engel, C. S., 2008. Defining basal geometry and force balance at Columbia Glacier, Alaska, (Master's thesis, University of Colorado).

Farinotti, D., M. Huss, A. Bauder and M. Funk, 2009a. An estimate of the glacier ice volume in the Swiss Alps, *Global Planet. Change*, **68**, 235–231.

Farinotti, D., M. Huss, A. Bauder, M. Funk and M. Truffer, 2009b. A method to estimate the ice volume and ice-thickness distribution of alpine glaciers, *J. Glaciol.*, **55**(191), 422–430.

Fastook, J., H. Brecher and T. Hughes, 1995. Derived bedrock elevations, strain rates and stresses from measured surface elevations: Jakobshavns Isbræ, Greenland, *J. Glaciol.*, **41**(137), 161–173.

Hock, R., M. de Woul, V. Radić and M. Dyurgerov, 2009. Mountain glaciers and ice caps around Antarctica make a large sea-level rise contribution, *Geophys. Res. Lett.*, **36**(L07501), doi:10.1029/2008GL037020.

Howat, I. M., I. Joughin, S. Tulaczyk and S. Gogineni, 2005. Rapid retreat acceleration of Helheim Glacier, east Greenland, *Geophys. Res. Lett.*, **32**(L22502), doi:10.1029/2005GL024737.

Huss, M., S. Usselmann, D. Farinotti and A. Bauder, 2010. Glacier mass balance in the South-Eastern Swiss Alps since 1900 and perspectives for the future, *Erdkunde*, **64**(2), 119–140.

Joughin, I., 2002. Ice-sheet velocity mapping: A combined interferometric and speckle-tracking approach, *Ann. Glaciol.*, **34**, 195–201.

Joughin, I., R. Kwok and M. Fahnestock, 1996. Estimation of ice-sheet motion using satellite radar interferometry: method and error analysis with application to Humboldt Glacier, Greenland, *J. Glaciol.*, **42**(142), 564–575.

Kienholz, C., 2010. Shrinkage of selected South-Central Alaskan Glaciers AD 1900-2010, (Master's thesis, University of Bern).

Korona, J., E. Berthier, M. Bernard, F. Rémy and E. Thouvenot, 2009. SPIRIT. SPOT 5 stereoscopic survey of polar ice: Reference images and topographies during the fourth international polar year (2007-2009), *ISPRS J. of Photogrammetry and Remote Sensing*, **64**(2), 204âĂŞ212.

Krimmel, R. M., 2001. Photogrammetric data set, 1957-2000, and bathymetric measurements for Columbia Glacier, Alaska, *USGS Water Res. Invest. Rep.*, **014089**.

Larsen, C. F., R. J. Motyka, J. T. Freymueller, K. A. Echelmeyer and E. R. Ivins, 2005. Rapid viscoelastic uplift in southeast Alaska caused by post-Little Ice Age glacial retreat, *Earth and Planet. Sci. Lett.*, **237**, 548–560.

Larsen, C. F., R. J. Motyka, A. A. Arendt, K. A. Echelmeyer and P. E. Geissler, 2007. Glacier changes in southeast Alaska and northwest British Columbia and contribution to sea level rise, *J. Geophys. Res.*, **112**(F01007).

Li, H., Z. Li, M. Zhang and W. Li, 2011. An improved method based on shallow ice approximation to calculate ice thickness along flow-line and volume of mountain glaciers, *J. of Earth Sci.*, **22**(4), 441–448.

Mayo, L. R., D. C. Trabant, R. March and W. Haeberli, 1979. Columbia Glacier stake location, mass balance, glacier surface altitude, and ice radar data, 1978 measurement year, *USGS Open File Rep.*, **79-1168**.

Meier, M. F. and A. Post, 1987. Fast tidewater glaciers, *J. Geophys. Res.*, **92**(B9), 9051–9058.

Meier, M. F., L. A. Rasmussen, R. M. Krimmel, R. W. Olsen and D. Frank, 1985. Photogrammetric determination of surface altitude, terminus position, and ice velocity of Columbia Glacier, Alaska, *USGS Prof. Pap.*, **1258-F**.

Meier, M. F., M. B. Dyurgerov, U. K. Rick, S. O'Neel, W. T. Pfeffer, R. S. Anderson, S. P. Anderson and A. F. Glazovsky, 2007. Glaciers dominate eustatic sea-level rise in the 21st century, *Science*, **317**(1064), doi:10.1126/science.1143906.

Molnia, B. F., 2008. Glaciers of North America – Glaciers of Alaska, R. S. Williams, Jr. and J. G. Ferrigno, eds., Satellite image atlas of glaciers of the world, United States Geological Survey, K52–K83, USGS Prof. Pap. 1386-K.

Moon, T. and I. Joughin, 2008. Changes in ice front position on Greenland's outlet glaciers from 1992 to 2007, *J. Geophys. Res.*, **113**(F02022), doi:10.1029/2007JF000927.

Morlighem, M., E. Rignot, H. Seroussi, E. Larour, H. Ben Dhia and D. Aubry, 2011. A mass conservation approach for mapping glacier ice thickness, *Geophys. Res. Lett.*, **38**(L19503), doi:10.1029/2011GL048659.

Noll, G. T., 2005. Report of equipment and methods to accompany data from project OPR-P132-RA-05, Eastern Prince William Sound, AK, Columbia Bay hydrographic survey sheets H11493 & H11494, *Tech. rep.*, National Oceanographic and Atmospheric Administration.

O'Neel, S., 2012. Surface mass balance of Columbia Glacier, Alaska, USA, 1978 and 2010 balance years, *USGS Data Series*, **676**, 8 p.

O'Neel, S., W. T. Pfeffer, R. Krimmel and M. Meier, 2005. Evolving force balance at Columbia Glacier, Alaska, during its rapid retreat, *J. Geophys. Res.*, **110**(F03012), doi:10.1029/2005JF000292.

Paden, J., T. Akins, D. Dunson, C. Allen and P. Gogineni, 2010. Ice-sheet bed 3-D tomography, *J. Glaciol.*, **56**(195), 3–11.

Pfeffer, W. T., 2007. A simple mechanism for irreversible tidewater glacier retreat, *J. Geophys. Res.*, **112**(F03S2), doi:10.1029/2006JF000590.

Pfeffer, W. T., J. T. Harper and S. O'Neel, 2008. Kinematic Constraints on Glacier Contributions to 21st-Century Sea-Level Rise, *Science*, **321**, 1340–1343.

Porter, S. C., 1989. Late Holocene fluctuations of the fiord glacier system in Icy Bay, Alaska, U.S.A., *Arctic and Alpine Res.*, **21**(4), 364–379.

Radić, V. and R. Hock, 2010. Regional and global volumes of glaciers derived from statistical upscaling of glacier inventory data, *J. Geophys. Res.*, **115**(F01010), doi:10.1029/2009JF001373.

Radić, V., R. Hock and J. Oerlemans, 2008. Analysis of scaling methods in deriving future volume evolutions of valley glaciers, *J. Glaciol.*, **54**(187), 601–612.

Rasmussen, L. A., 1988. Bed topography and mass-balance distribution of Columbia Glacier, Alaska, U.S.A., determined from sequential aerial photography, *J. Glaciol.*, **34**(117), 208–216.

Rasmussen, L. A., H. Conway, R. M. Krimmel and R. Hock, 2011. Surface mass balance, thinning and iceberg production, Columbia Glacier, Alaska, 1948-2007, *J. Glaciol.*, **57**(203), 431–440.

Rignot, E., 2006. Changes in ice dynamics and mass balance of the Antarctic ice sheet, *Phil. Trans. R. Soc. A*, **364**, doi:10.1098/rsta.2006.1793.

Seroussi, H., M. Morlighem, E. Rignot, E. Larour, D. Aubry, H. Ben Dhia and S. S. Kristensen, 2011. Ice flux divergence anomalies on 79north Glacier, Greenland, *Geophys. Res. Lett.*, **38**(L09501), doi:10.1029/2011GL047338.

Strozzi, T., A. Luckman, T. Murray, U. Wegmüller and C. L. Werner, 2002. Glacier motion estimation using SAR offset-tracking procedures, *IEEE Trans. Geosci. Remote Sens.*, **40**, 2384–91.

University Corporation for Atmospheric Research, 2012. Advanced Cooperative Arctic Data and Information Service, `http://www.aoncadis.org/home.htm`.

Vieli, A., M. Funk and H. Blatter, 2001. Flow dynamics of tidewater glaciers: a numerical modelling approach, *J. Glaciol.*, **47**(159), 595–606.

Walter, F., S. O'Neel, D. MacNamara, W. T. Pfeffer, J. N. Bassis and H. A. Fricker, 2010. Iceberg calving during transition from grounded to floating ice: Columbia Glacier, Alaska, *Geophys. Res. Lett.*, **37**(L15501), doi:10.1029/2010GL043201.

Warner, R. and W. Budd, 2000. Derivation of ice thickness and bedrock topography in data-gap regions over Antarctica, *Ann. Glaciol.*, **31**, 191–197.

Weertman, J., 1974. Stability of the junction of an ice sheet and an ice shelf, *J. Glaciol.*, **13**(67), 3–11.

Wilson, F. H., J. H. Dover, D. C. Bradley, F. R. Weber, T. K. Bundtzen and P. J. Haeussler, 1998. Geologic map of Central (Interior) Alaska, *USGS Open File Rep.*, **98-133-A**, version 1.2.

Chapter 3

Alaska Tidewater Glacier Terminus Positions, 1948-2012[1]

3.1 Abstract

Despite their relative importance to sea level rise, much is still unknown about the recent evolution of tidewater glaciers and their response to recent climate change, which confounds efforts to accurately predict future sea level rise. In this study, we present a 64 year record of length change for 50 Alaska tidewater glaciers. Using all available cloud-free Landsat images, we manually digitize calving front outlines for each glacier between 1972 and 2012, resulting in a total of more than $10,000$ outlines, ranging between 119 and 327 outlines per glacier. We manually digitize terminus outlines from USGS topographic maps and aerial mapping photos to provide a base length for glaciers before 1970. We find that 31 glaciers retreated over the course of the study, with a mean retreat rate of 60 m a^{-1}. The remaining 19 glaciers had a mean advance rate of 10 m a^{-1}. Seasonal oscillations in glacier length are calculated by removing annual changes in length; we find a mean seasonal change in glacier length of 60 ± 85 m a^{-1}. We use these seasonal oscillations to determine the significance of interannual changes in glacier length. All 50 glaciers underwent at least one period of significant advance or retreat; 40 glaciers had at least one period of both significant advance and retreat. Despite this, three glaciers in the region did not change significantly over the full course of the study. Several glaciers in the region underwent rapid, short retreats over the course of few years; closer examination shows that these retreats come either during years of anomalously high summer sea surface temperature (SST), or after a period of several years of anomalously warm summer SST. Finally, we examine the length change record to see any regional coherence in glacier behavior, but find none; however, two subregions show a coherence similar to recent observations in Greenland.

3.2 Introduction

Tidewater glaciers are glaciers that terminate in the ocean at either a grounded calving front or floating ice tongue. Post (1975) describes the 'tidewater glacier cycle', wherein glaciers slowly advance over the course of centuries, until thinning near the calving front initiates a rapid retreat that completes within decades, stabilizing only when the glacier

[1]This chapter has been submitted for publication to J. Geophys. Res. as McNabb, R. and R. Hock. Alaska tidewater glacier terminus positions, 1948-2012.

has retreated into shallow water. In general, the retreat phase of a tidewater glacier can be triggered by changes in climate; however, once retreat is initiated, the glacier's behavior is only weakly influenced by climate (Meier and Post, 1987; Post and Motyka, 1995; Pfeffer, 2007; Post and others, 2011).

The ability of tidewater glaciers to discharge large amounts of ice in a short period of time highlights their potential hazard to shipping traffic in nearby waters, as well as their potential importance to sea level rise (Carson and others, 2003; IPCC, 2007; AMAP, 2011). Recently, much attention has been focused on tidewater glacier fluctuations in Greenland (Moon and Joughin, 2008; Howat and Eddy, 2012; Moon and others, 2012). These studies have unprecedented spatial coverage, with every outlet glacier of the Greenland Ice Sheet included, though the temporal coverage is somewhat coarse, with at most one or two measurements per year for most outlet glaciers. Many of these studies have indicated that regional tidewater glacier behavior can be a reflection of local climate on sub-decadal, and even annual, timescales.

Previous studies have highlighted the potential for large contribution of Alaska glaciers to sea level rise (Arendt and others, 2002; Meier and Dyurgerov, 2002; Arendt and others, 2006; Larsen and others, 2007; Meier and others, 2007; Berthier and others, 2010). In general, studies of Alaska tidewater glaciers have been limited to short-term studies on only a few glaciers (Brown and others, 1982; O'Neel and others, 2001; Motyka and others, 2003); one notable exception is Columbia Glacier, which has been monitored almost continuously since the early 1970s (Brown and others, 1982; Meier and Post, 1987; Meier and others, 1994; Krimmel, 2001; O'Neel and others, 2005, 2007; Walter and others, 2010; Post and others, 2011; McNabb and others, 2012). In contrast to Columbia Glacier, long-term studies on the regional scale tend to have relatively coarse temporal resolution (Arendt and others, 2002, 2006; Larsen and others, 2007; Berthier and others, 2010).

Here we present a new regional-scale study of tidewater glacier terminus position for 50 Alaska tidewater glaciers. We digitize terminus outlines on U.S. Geological Survey (USGS) topographic maps to find glacier lengths in the late 1940s and 1950s, providing a context for long-term glacier length change. Using a collection of Landsat images acquired between 1972 and 2012, we manually digitize calving fronts for each available, cloud-free image. We use this record of front changes to examine both spatial and temporal patterns of glacier length change, including both long-term (annual and decadal) and seasonal changes. We then use the record of seasonal variations to estimate the long-term signifi-

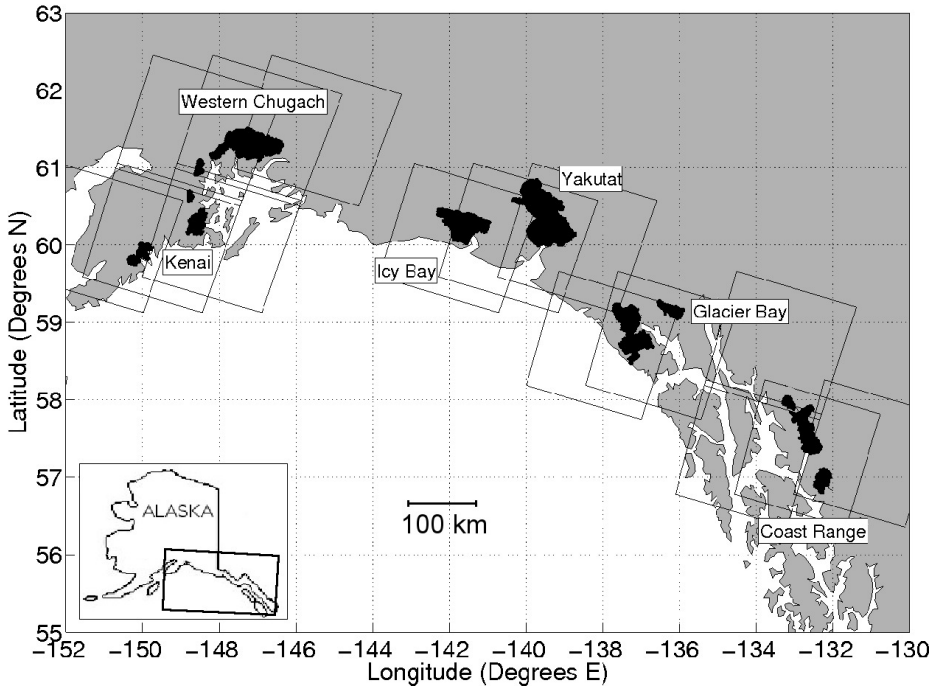

Figure 3.1. Location of the 50 studied tidewater glaciers and six subregions in Alaska. Approximate outlines of footprints of Landsat scenes are shown as black rectangles.

cance of the advance and retreat of each glacier, and track regional patterns. Finally, we examine similarities in patterns of length changes between different glaciers, and examine potential causes for those similarities.

3.3 Study Area

Alaska is a heavily glacierized region, with a total area of $87,100$ km^2 (including adjacent glaciers in the Yukon Territory and British Columbia, Canada; hereafter, “Alaska glaciers") covered by ice (Gardner and others, 2013). For the purpose of this study, we divide Alaska into six subregions, based on coverage by Landsat scenes (Fig. 3.1). Molnia (2008) identifies a total of 59 current and former tidewater glaciers in Alaska. For this study, we consider only those glaciers that Molnia identifies as “existing" tidewater glaciers, a total of 50 glaciers. Not all of these glaciers calved into tidewater for the duration of the study. These 50 glaciers represent a total area of $12,091$ km^2 (13.7% of the total Alaska glacier area) and range in size from a few square kilometers (Ogive Glacier, 2.8 km^2) to many thousands of square kilometers (Hubbard Glacier, 3400 km^2). Subregional information is detailed in

Table 3.1.

The Kenai peninsula has 11 tidewater glaciers (total area 1067 km^2), mainly divided between the Harding and Sargent Icefields. Two smaller glaciers (Beloit and Blackstone) are located in Blackstone Bay near Whittier. Several studies have examined trends in length fluctuation and rates of thinning (Wiles and Calkin, 1994; Wiles and others, 1995; Aðalgeirsdóttir and others, 1998; VanLooy and others, 2006), but they have mostly focused on the larger Harding Icefield, part of Kenai Fjords National Park.

The Western Chugach mountains are one of the largest contributors to sea level rise of all of the subregions in Alaska, losing almost 6 Gt a^{-1} over the period 1954-2006 (Berthier and others, 2010). The single largest contributor to sea level rise in this subregion is Columbia Glacier. It has lost over 130 km^3 of ice since 1957, corresponding to over 50% of its volume (Rasmussen and others, 2011; McNabb and others, 2012). There are 13 tidewater glaciers in this subregion (total area 2266 km^2), all of which calve into Prince William Sound; the majority of these glaciers are thinning and retreating, though none at the rates observed at Columbia (Berthier and others, 2010). A few glaciers, such as Harvard Glacier, are thickening and advancing (Arendt and others, 2006; Berthier and others, 2010).

The tidewater glaciers of Icy Bay have exhibited large scale changes in terminus position since the early 1900s, retreating over 40 km in that time (Porter, 1989; Barclay and others, 2006). Tyndall Glacier, located in Taan Fjord, shared a calving front with the other glaciers until the mid-20th century (Barclay and others, 2006), before retreating into Taan Fjord. As recently as 1960, the remaining five tidewater glaciers in this subregion shared a single calving front, but have since separated into independent calving fronts; we treat these as individual glaciers. At present, there are six tidewater glaciers in the subregion (total area 1694 km^2), the largest of which is Yahtse Glacier.

The Yakutat subregion has only two tidewater glaciers (total area 3580 km^2), Hubbard Glacier and Turner Glacier. Hubbard Glacier, at approximately 3400 km^2, is the largest temperate tidewater glacier in the world. Twice in the past few decades, Hubbard Glacier has advanced enough to block the entrance to the 60-km-long Russell Fjord (Trabant and others, 2003; Motyka and Truffer, 2007; Ritchie and others, 2008), only to retreat slightly and re-open the fjord entrance. The glacier is still advancing, in part driven by its extremely high accumulation area ratio (AAR) of 0.95 (Motyka and Truffer, 2007).

Between the end of the Little Ice Age and the present, the tidewater glaciers of Glacier Bay have retreated over 100 km (Barclay and others, 2009). The largest glacier in the sub-

Table 3.1. The six Alaska subregions defined in this study. Path/Row is the Landsat scene path and row number for each subregion, N_{glac} is the number of tidewater glaciers in each region (Molnia, 2008), N_{tw} is the number of glaciers that calve into tidewater during the course of this study, and A_{tw} is the total area of tidewater glaciers in the subregion.

Subregion	N_{glac}	N_{tw}	A_{tw} km^2	Largest Glacier	Landsat 4-7 Path/Row	Landsat 1-3 Path/Row
Kenai Peninsula	12	11	1067	Chenega	67/18, 68/18, 69/18	73/18, 74/18, 75/18
W. Chugach	14	13	2266	Columbia	66/18, 67/18, 68/18	72/17, 73/17 74/17
Icy Bay	8	6	1694	Yahtse	62/18, 63/18	67/18, 68/18
Yakutat	3	2	3580	Hubbard	61/18, 62/18	67/18
Glacier Bay	16	14	1866	Grand Pacific	59/19, 60/19	64/19, 65/19
Coast Range	6	4	1796	S. Sawyer	55/20, 56/20, 57/20, 57/19	60/20, 61/20, 62/20, 62/19

region is the Grand Pacific Glacier, which still calves into the Tarr Inlet. Most of these glaciers are still thinning and retreating; some, such as Johns Hopkins Glacier, are thickening and advancing (Larsen and others, 2007). In total, there are 14 tidewater glaciers in this subregion (total area 1866 km^2), though only six are tidewater for the entire period of this study.

The Coast Range has four current tidewater glaciers (total area 1796 km^2). Several studies have focused on LeConte Glacier, the southernmost tidewater glacier in the Northern Hemisphere, either on the short-term flow and calving dynamics (O'Neel and others, 2001, 2003), or on glacier-ocean interactions (Motyka and others, 2003). In general, these glaciers are all thinning and retreating, though none are currently in the midst of a rapid retreat.

3.4 Data

3.4.1 Topographic Maps

To estimate glacier lengths from before the beginning of the Landsat program, we use U.S. Geological Survey (USGS) 15-minute topographic maps. These maps are produced from aerial photographs acquired in the late 1940s to early 1970s, depending on location. The collection of aerial photographs used to create these maps is searchable online at `http://earthexplorer.usgs.gov`. Topographic maps produced by the USGS are dated to the year only; in order to determine the time of year for each map, we assign a date using the mean flight dates reported for each map.

In general, USGS topographic maps adhere to the National Map Accuracy Standards, which require that all maps produced by U.S. Federal Agencies be accurate to within 1/30th of an inch. For the $1:63{,}360$ scale maps that we use in this study, this means a nominal horizontal accuracy of 53.6 m. Several studies have indicated that errors in map topography can be much larger than the nominal error in Alaska (Aðalgeirsdóttir and others, 1998; Arendt and others, 2002), though most of these errors occur in areas of low contrast, such as the accumulation zone of glaciers. Because we do not have information about potential horizontal errors, however, we assume that the nominal error is correct.

3.4.2 Landsat Scenes

We compile a set of $1{,}963$ Landsat scenes acquired over Alaska between October 1972 and February 2012. Scenes are acquired with the Landsat 1-5 Multispectral Scanner (MSS)

sensor (1972-1994), the Landsat 4 and 5 Thematic Mapper (TM) sensor (1984-2011), and the Landsat 7 Enhanced Thematic Mapper Plus (ETM+) sensor (1999-2012). The MSS sensor has a ground resolution of $\sim$60 m in all bands, while the TM sensor has a ground resolution of 30 m in all bands. The ETM+ sensor has 30 m resolution in bands 1-5, 60 m in band 6, and 15 m in the panchromatic band 8. Each scene has been georeferenced and orthorectified by the USGS; where needed, we apply corrections to the georeferencing. From manually digitizing bedrock features in Landsat scenes, we estimate a horizontal accuracy of 60 m for each scene.

3.5 Methods

3.5.1 Digitization of Glacier Termini

Each topographic map is georeferenced. Terminus outlines of all tidewater glaciers are manually digitized for each scene using either a false-color composite of bands 5, 4, and 3 (Landsat 4, 5, and 7 TM/ETM+), a false-color composite of bands 4, 3, and 2 (Landsat 4 and 5 MSS), or a false-color composite of bands 6, 5, and 4 (Landsat 1-3 MSS). We find that this combination choice gives the greatest contrast between ice, surrounding rock, and sediment, as well as providing a good contrast between ice and water. The resulting dataset consists of 119 to 327 terminus outlines per glacier, with an average of 205 outlines per glacier, and a total number of over $10,000$ terminus outlines for the entire region.

3.5.2 Glacier Length

To calculate glacier lengths, a centerline coordinate system, ξ, for each glacier is manually defined, and is delineated from $\xi = 0$ km at the glacier head at vertices separated by 0.5 km through the most extended terminus position of the glacier. Length change is calculated using the so-called “Box Method" of Moon and Joughin (2008), with an example shown in Fig. 3.2. We first choose a gate, perpendicular to the centerline of the glacier. Wherever possible, we use the same gate for all terminus outlines; as glaciers do not always flow in straight lines on the map, we must sometimes choose new gates after the glacier has advanced or retreated around a corner. Once we have chosen a gate for each terminus outline, the average length between the terminus outline and this gate is then calculated. Finally, the total glacier length is calculated by adding this average length to the distance of the gate along the flowline.

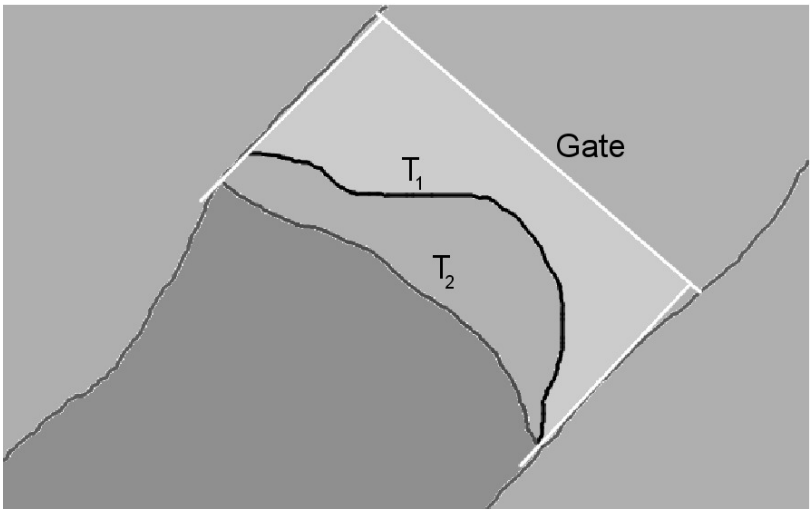

Figure 3.2. Example of the “Box method" for calculating glacier length change (Moon and Joughin, 2008). The mean distance from the gate to each terminus outline (T_1, T_2) is calculated. This is then added to the distance along the flowline of the gate to obtain the glacier length corresponding to each terminus position.

3.5.3 Seasonal Front Variations

Like all tidewater glaciers, Alaska tidewater glaciers undergo seasonal advance and retreat, in addition to interannual changes. To estimate the magnitude and timing of these seasonal changes, we remove a piecewise linear trend, calculated at annual intervals, from the length record between 1999-2012. Because of the sparsity of data, we use three-month averages of detrended lengths (December/January/February (DJF), March/April/May (MAM), June/July/August (JJA), September/October/November (SON)) to estimate this seasonal variation on an annual basis. We then average these seasonal values over the whole time period to estimate an average deviation from the trend in a given year.

Taking the seasonal amplitudes for each glacier in the study region, we can quantify the significance of interannual changes. For a single glacier, we set a threshold of significance $\varepsilon = 2A$, where A is the average amplitude of seasonal change calculated over the period 1999-2012. For a multiyear period of length t years, this becomes:

$$\varepsilon_{\text{mult}} = \frac{2A}{t}. \tag{3.1}$$

To estimate the significance of a given year for a glacier, we take the mean annual length for each glacier and differentiate this curve. These values are then grouped according

to continuous interannual advance or retreat, with the threshold for each year estimated according to Equation (3.1). Interannual length changes greater than this threshold are considered to be significantly greater than the mean interannual variation.

3.6 Results

3.6.1 Interannual Length Changes

Length changes are summarized in Fig. 3.3. Comparing front position at the end and beginning of the period, we find that in general, 31 glaciers (62% of the glaciers studied) retreated over the period 1948-2012. The percentage of retreating glaciers in a given decade, however, varied between 36% and 60% (Table 3.2). The mean length change over this time was negative (-35 ± 80 m a^{-1}). The mean rate of advance ($\pm$ one standard deviation; 19 glaciers total) over this time was 10 ± 15 m a^{-1}, while the mean retreat rate ($\pm$ one standard deviation) was 60 ± 90 m a^{-1}.

Table 3.2 summarizes decadal mean values of length change, retreat, and advance, as well as the maximum values of advance or retreat found for a given decade, over the four decades covered by the study. We do not include the start of the decade 2011-2020, nor decades before 1970, due to a lack of data. The mean rate of length change decreases throughout the study period, while the mean advance rate for all glaciers remains mostly similar through the study period (between $10 - 25$ m a^{-1}). In contrast, the mean retreat rate varied widely between the decades (-130 to -70 m a^{-1}), and the region as a whole experienced overall retreat in each decade. The median rate of length change for the whole period of the study, however, was nearly 0 m a^{-1}, suggesting that the regional length change signal is dominated by a few rapidly retreating glaciers.

Not all glaciers consistently advanced or retreated for the duration of the study, however, nor did they exhibit constant rates of advance or retreat. These changes varied widely on both annual and decadal timescales, as shown by the percentage of glaciers that retreated in each time period (Table 3.2). The mean variation in yearly length rates was 100 m a^{-1} for all glaciers (advancing or retreating), with 15 glaciers showing variation in rates of length change greater than 100 m a^{-1}, demonstrating that interannual length change can be highly variable.

As might be expected, the median and mean length changes for each region did not always agree with each other, as shown in Figure 3.4. For most regions in most decades, the regional median was somewhat larger than the mean, with perhaps the biggest exception

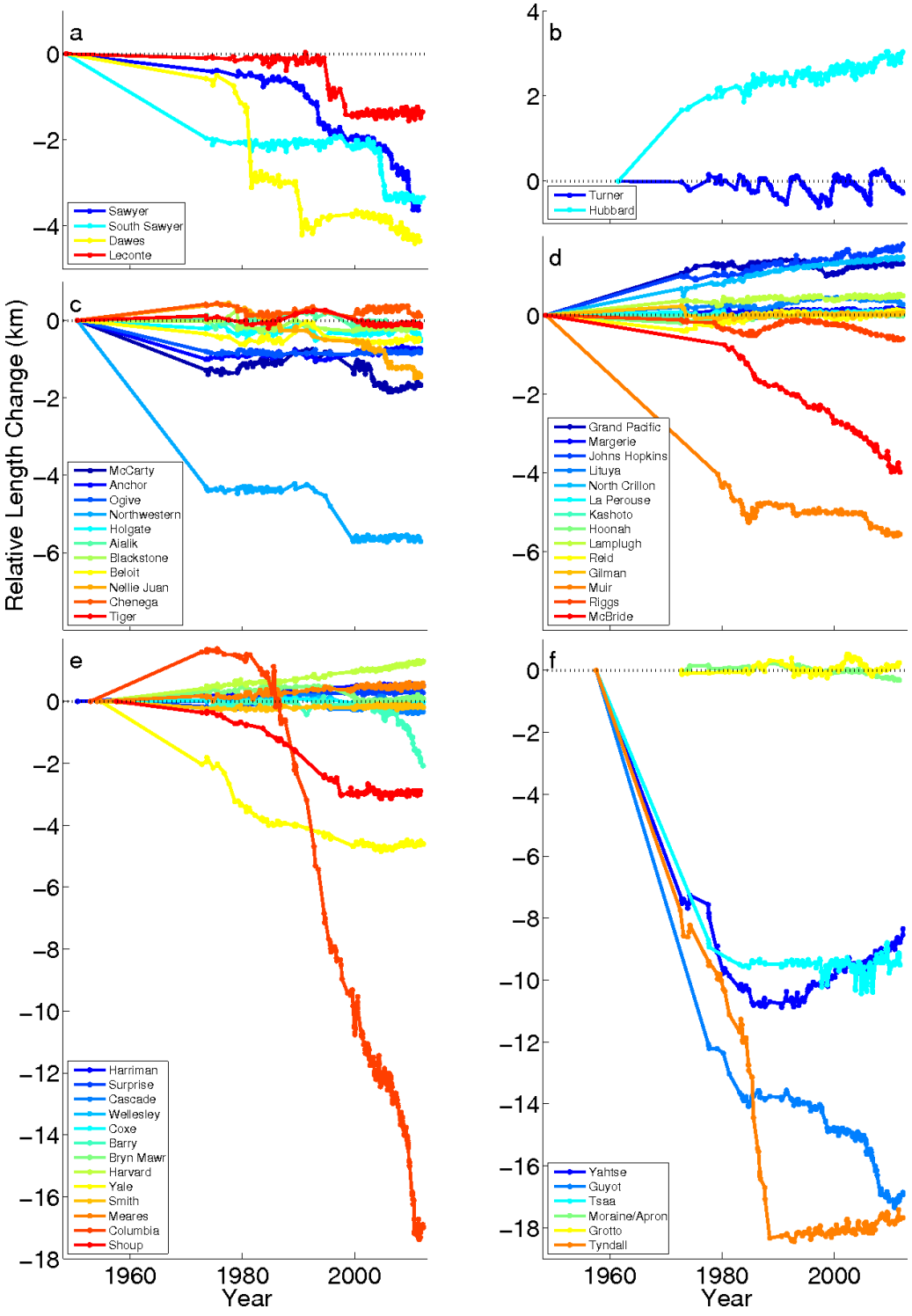

Figure 3.3. Time series of relative lengths for each glacier in the study area. (a) Coast Range subregion, (b) Yakutat subregion, (c) Kenai Peninsula subregion, (d) Glacier Bay subregion, (e) Western Chugach subregion, (f) Icy Bay subregion.

Table 3.2. General length change statistics, averaged for all 50 glaciers for the given time period; map date ranges between 1948 and 1961. Mean and Med. dL/dt are the mean and median length changes, respectively; mean and max. adv./ret. are the mean and maximum values of advance or retreat, respectively; % ret. is the percentage of glaciers that retreated over the given time period. All values are in m a^{-1}, except for % ret.

	dL/dt		Advance		Retreat		
Period	Mean	Median	Mean	Max	Mean	Max	% ret.
Map-1972	-50 ± 150	-5	25 ± 35	150	30 ± 180	-610	56
1973-1980	-40 ± 100	-10	15 ± 15	70	-75 ± 120	-440	60
1981-1990	-40 ± 150	5	20 ± 10	50	-130 ± 230	-960	36
1991-2000	-30 ± 110	0	20 ± 25	110	-65 ± 140	-740	54
2001-2010	-30 ± 100	0	10 ± 20	80	-75 ± 135	-640	48
Map-2012	-35 ± 80	-5	10 ± 15	60	-60 ± 90	-320	64

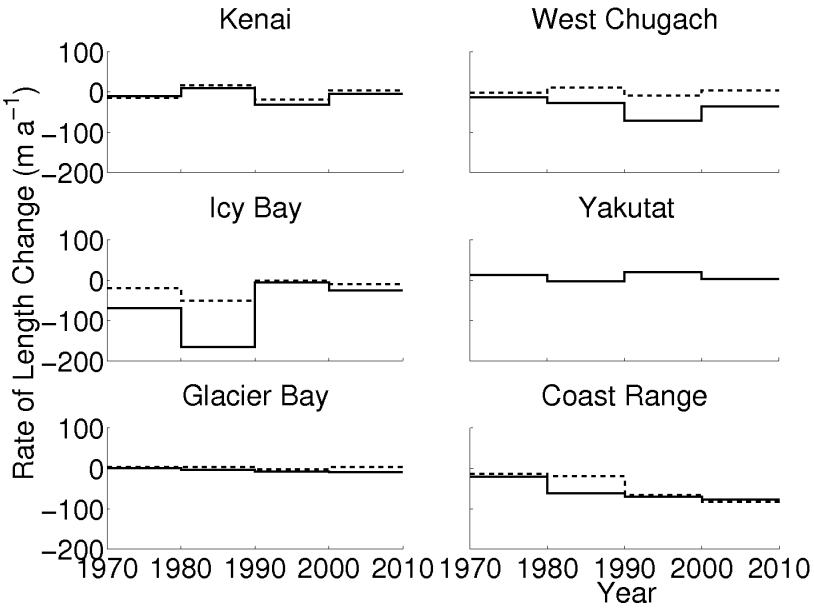

Figure 3.4. Decadal mean (solid) and median (dashed) rates of length change for each of the subregions defined in this study.

being Glacier Bay, whose mean and median length changes were very nearly the same throughout the study period. Surprisingly, the region with the largest discrepancy was not the Western Chugach with Columbia Glacier and its anomalous retreat, but Icy Bay ($\sim$ one km length change, or $\sim$100 m a^{-1}) during the 1980s.

3.6.2 Significance of Interannual Length Changes

Using the threshold given by Equation (3.1), we have calculated the significance of interannual length changes for each glacier in the region. Figure 3.5 shows the number of glaciers per year showing significant advance, significant retreat, and either significant advance or retreat for the period 1972-2012. The mean number of glaciers per year showing significant advance was quite similar to the mean number of glaciers per year showing significant retreat (11.3 ± 5.3 glaciers/year vs. 11.9 ± 4.9 glaciers/year), and no clear trends are present in either dataset.

Three glaciers (Coxe, Kashoto, and Chenega; Western Chugach, Glacier Bay, and Kenai subregions, respectively) did not significantly change over the full course of this study (1948-2012). Looking at smaller periods of advance or retreat, however, the picture changes somewhat. All 50 glaciers showed at least one period (period length $\geq$ one year) of signifi-

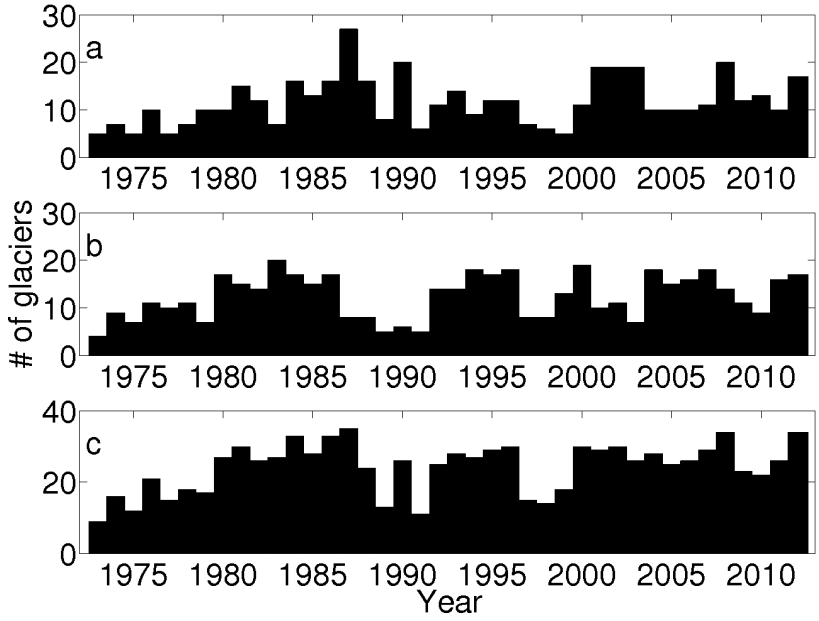

Figure 3.5. Number of glaciers showing (a) significant interannual advance, (b) significant interannual retreat, or (c) either significant interannual advance or retreat, for each year from 1972-2012.

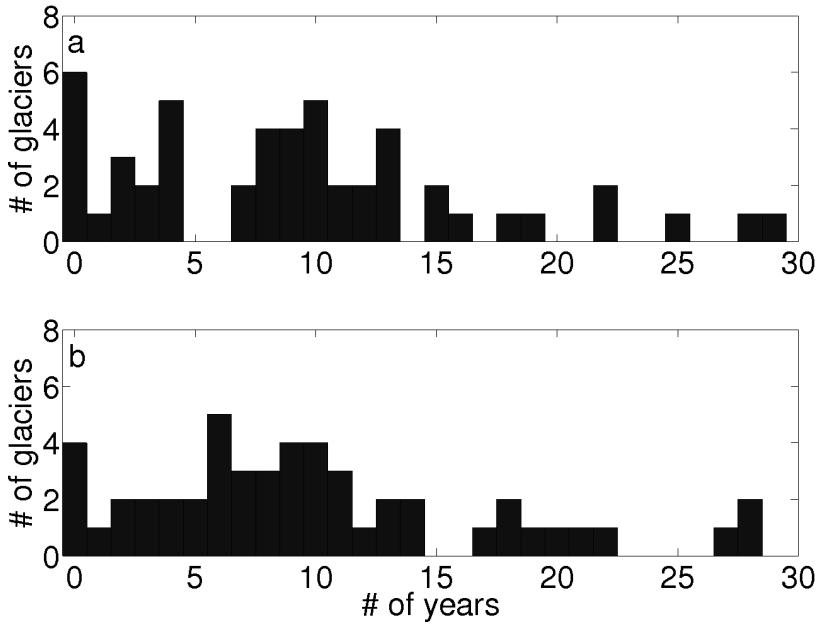

Figure 3.6. Number of glaciers showing a particular number of years of (a) advance, and (b) retreat, through the course of the study (1972-2012).

cant advance or retreat, with 40 glaciers having shown periods of both significant advance and significant retreat. Of the remaining ten glaciers, four glaciers showed only significant advance (Johns Hopkins, Kashoto, North Crillon, and Hubbard), while six glaciers (Sawyer, LeConte, McBride, Columbia, Nellie Juan, and Northwestern) showed only significant retreat.

Glacier retreats (and advances) tend to be highly variable in time. Figure 3.6 shows a histogram of the number of glaciers having a given number of years of significant advance or retreat. The mean number of years that glaciers significantly advanced over the time period 1972-2012 was 9.4 ± 7.4 (with a median of 9 years), while the mean number of years that glaciers significantly retreated over the same time period was 9.9 ± 7.2 (with a median of nine years). These periods of advance and retreat were rarely continuous, as the mean length of a period of significant advance was 2.2 ± 1.9 years (with a median of two years), and the mean length of a significant retreat was 2.2 ± 2.6 years (with a median of one year). Even the maximum length of periods of significant advance or retreat were similar, with the maximum period of advance being 22 years (North Crillon Glacier, Glacier Bay subregion), and the maximum period of retreat being 28 years (Columbia Glacier, Western Chugach subregion).

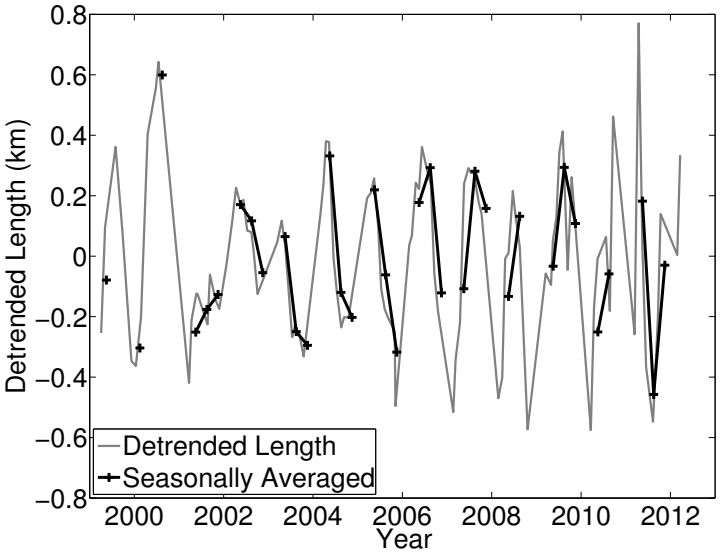

Figure 3.7. Columbia Glacier length record, 1999-2012, with a yearly piecewise-linear trend removed (gray line). Seasonally-averaged values are shown in black.

3.6.3 Seasonal Length Changes

Figure 3.3 shows that many glaciers in the region show pronounced seasonal changes in length, in addition to long-term trends. An example of the detrended 1999-2012 length changes is shown using the record from Columbia Glacier (Western Chugach subregion) in Fig. 3.7. Figure 3.8 shows the seasonally-averaged detrended lengths for each glacier. Figure 3.9 shows the timing of these seasonal cycles for all 50 glaciers, and Fig. 3.10 shows the timing divided by subregion. Not every glacier shows the same seasonality as others, and we discuss some potential reasons for this later. In general, however, most glaciers reach their maximum seasonal length in spring/summer (40 glaciers), and their minimum seasonal length in fall/winter (41 glaciers).

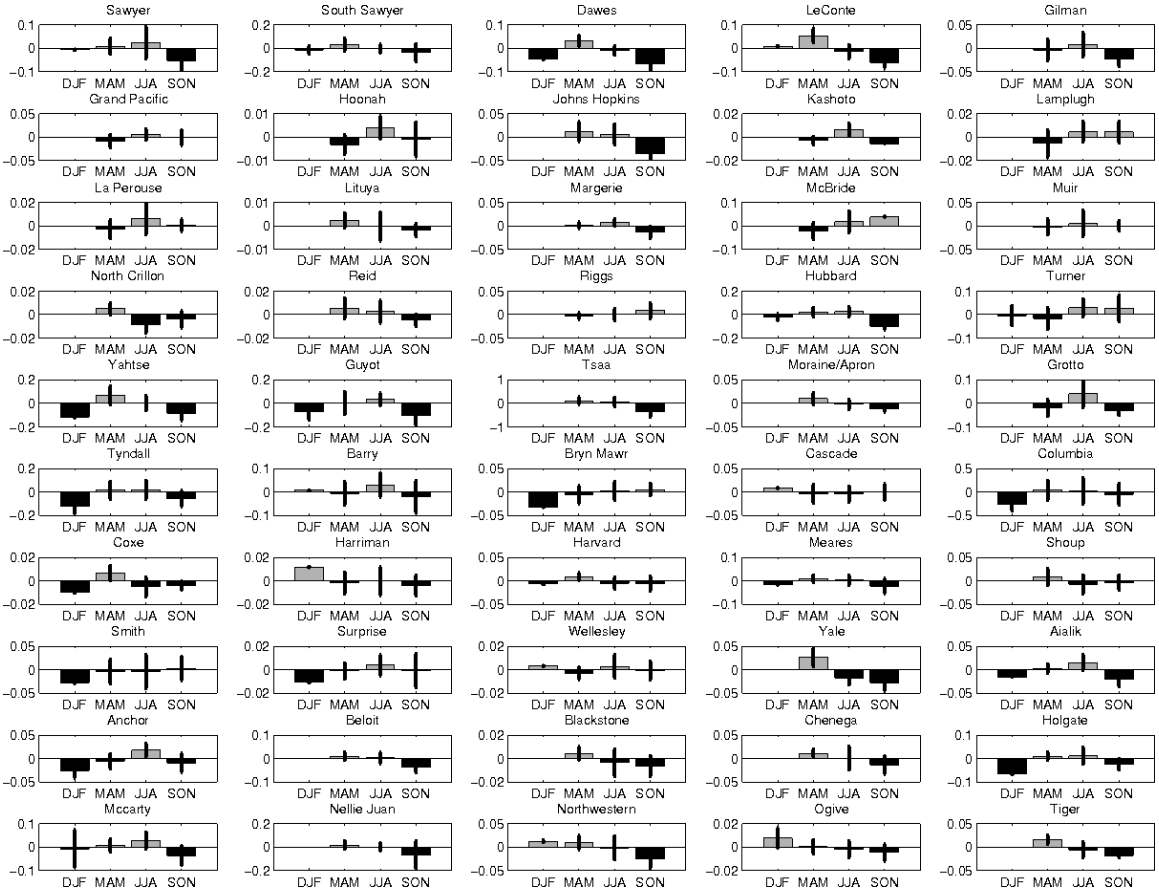

Figure 3.8. Mean seasonal deviation from trend for all 50 glaciers in this study, 1999-2012. Units for all panels are km a^{-1}. Error bars indicate standard deviation from mean for each three-month period.

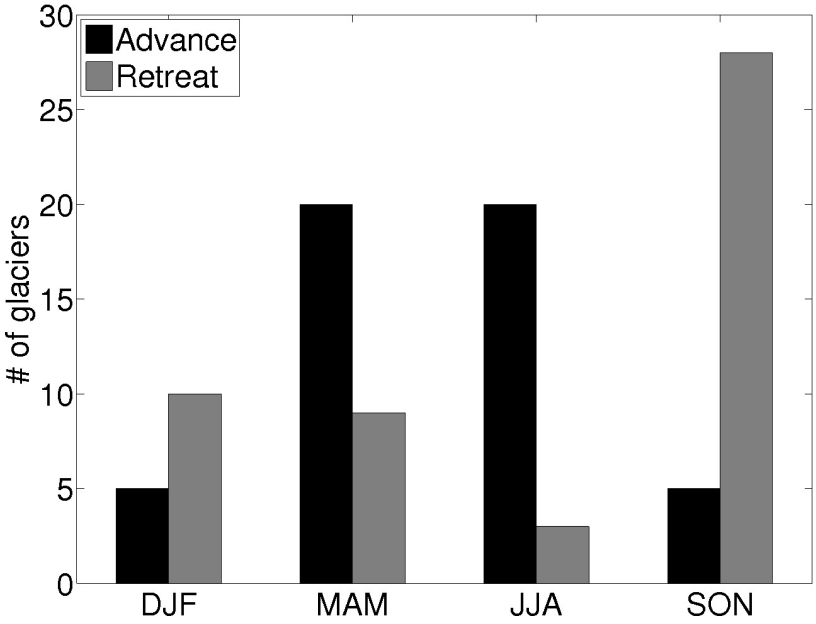

Figure 3.9. Timing of maximum advance from trend (black), and maximum retreat from trend (gray), for all 50 glaciers in this study. Note that most glaciers reach their maximum advance in spring/summer, and maximum retreat in fall/winter.

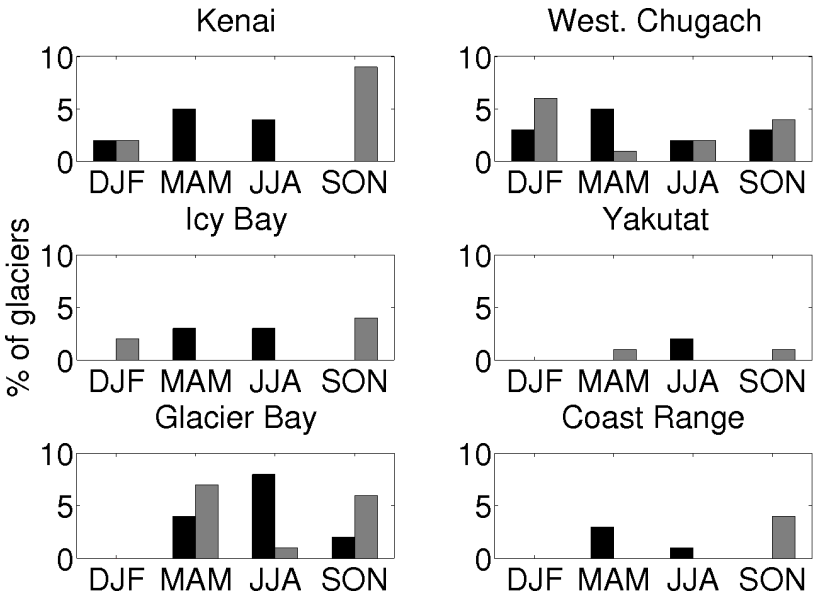

Figure 3.10. Timing of maximum advance (black) and retreat (gray) from trend for the 50 glaciers in this study, divided by subregion.

Taking the results for each glacier in the region, we find a mean ($\pm$ one standard deviation) amplitude of seasonal advance and retreat for the entire region of 60 ± 85 m a^{-1}, and a median value of 35 m a^{-1}. If we consider outliers to be more than two standard deviations above the mean value (seasonal amplitude >230 m a^{-1}), only Tsaa Glacier (Icy Bay subregion; 440 m a^{-1}) and Columbia Glacier (Western Chugach subregion; 385 m a^{-1}) register as outliers.

In addition to seasonal patterns of length change, some glaciers also showed multiyear patterns of advance and retreat, or other behavior that persisted for more than a single year. Turner Glacier (Yakutat Subregion, Fig. 3.3) shows a multiyear cycle, with a period of approximately six years, superimposed on a mean length change of very nearly zero. Turner Glacier is the only tidewater glacier in Alaska known to surge (Meier and Post, 1969; M. Truffer, personal communication, 2012), a fact reflected in this periodicity. During the late 1990s and early 2000s, Tsaa Glacier (Icy Bay subregion, Fig. 3.3) underwent drastic fluctuations in terminus position, with changes on the order of one km in less than a year. These rapid changes were only present during those time periods, however, with changes during other time periods being generally smaller. This may influence Tsaa's anomalously high amplitude of seasonal change.

3.7 Discussion

3.7.1 Tidewater Glacier Cycle

Post (1975) first described the tidewater glacier cycle, wherein tidewater glaciers undergo slow advance over the course of centuries, followed by a rapid retreat that completes over the course of decades. This framework has since been expanded (Meier and Post, 1987; Post and Motyka, 1995), but the basic tenets remain the same. Our length change record captures examples of glaciers in each of these phases of the cycle. Columbia Glacier has retreated over 18 km from its position at the entrance of Columbia Bay, where it had remained since ca. AD 1100 (Calkin and others, 2001). This retreat began ca. 1980, and has only about 10 km to go before the glacier has fully retreated from tidewater (McNabb and others, 2012), something that will likely happen within the next several decades (Colgan and others, 2012). While a detailed investigation of the future evolution of Columbia Glacier is beyond the scope of this dissertation, it seems likely that Columbia Glacier will stabilize and begin readvancing within the coming decades. As shown in Figure 3.3, most of the glaciers of Icy Bay have halted their retreats. Two of these glaciers (Yahtse and Tyn-

dall) have begun to readvance, embarking on the advance portion of the tidewater cycle.

It has been noted (Post, 1975; Calkin and others, 2001) that Columbia Glacier is the last major Alaska tidewater glacier to retreat from its Little Ice Age maximum extent. Glacier Bay began its retreat shortly after the conclusion of the Little Ice Age, Icy Bay began its retreat ca. 1900, and Hubbard Glacier concluded its retreat during the Little Ice Age (Porter, 1989; Barclay and others, 2001; Calkin and others, 2001; Trabant and others, 2003; Barclay and others, 2006, 2009). Figure 3.3 indicates that currently, many glaciers in Icy Bay and Glacier Bay have begun to advance, concluding their retreats in the 1970s (Icy Bay), or sometime before map date (Glacier Bay).

3.7.2 Step Change Retreats

Over the course of this study, 13 glaciers retreated more than three kilometers (an average rate of > 50 m a^{-1}): Sawyer, South Sawyer, and Dawes Glaciers in the Coast Range subregion; Northwestern Glacier in the Kenai subregion; Yale, Columbia, and Shoup Glaciers in the Western Chugach subregion; McBride and Muir Glaciers in the Glacier Bay subregion; and Guyot, Tsaa, Yahtse, and Tyndall Glaciers in the Icy Bay subregion. As previously mentioned, these rates of retreat were not constant through time. Several of these glaciers (Sawyer, South Sawyer, Dawes, LeConte, Northwestern, Nellie Juan, Yale, and Guyot) exhibited step changes in length, where the glacier stabilized, or at least slowed its retreat, for several years, before beginning a rapid retreat over the course of a few years.

Closer examination of these “step change" retreats, or at least those that occurred after 1999 when measurement density was sufficient to capture seasonal changes in length, shows that almost all of these retreats began in a year when the glacier did not undergo a seasonal advance (Figure 3.3). This observation agrees with observations of Greenland tidewater glaciers (Howat and others, 2010), where the authors attributed the triggering of multiyear, rapid retreats to anomalously high May sea surface temperature (SST), as well as an anomalously early clearing of ice melange from proglacial fjords. In each case, these glaciers stabilized for some period of time at a constriction in the fjord (e.g., Fig. 3.11, showing terminus position over time for Columbia Glacier, with topographic pinning points highlighted). While bedrock geometry helps explain why these glaciers stabilized where they did, it does not adequately explain the timing of these retreats.

To investigate one potential cause of these step change retreats, we use MODIS-derived SST products (downloaded from `http://oceancolor.gsfc.nasa.gov`). We average

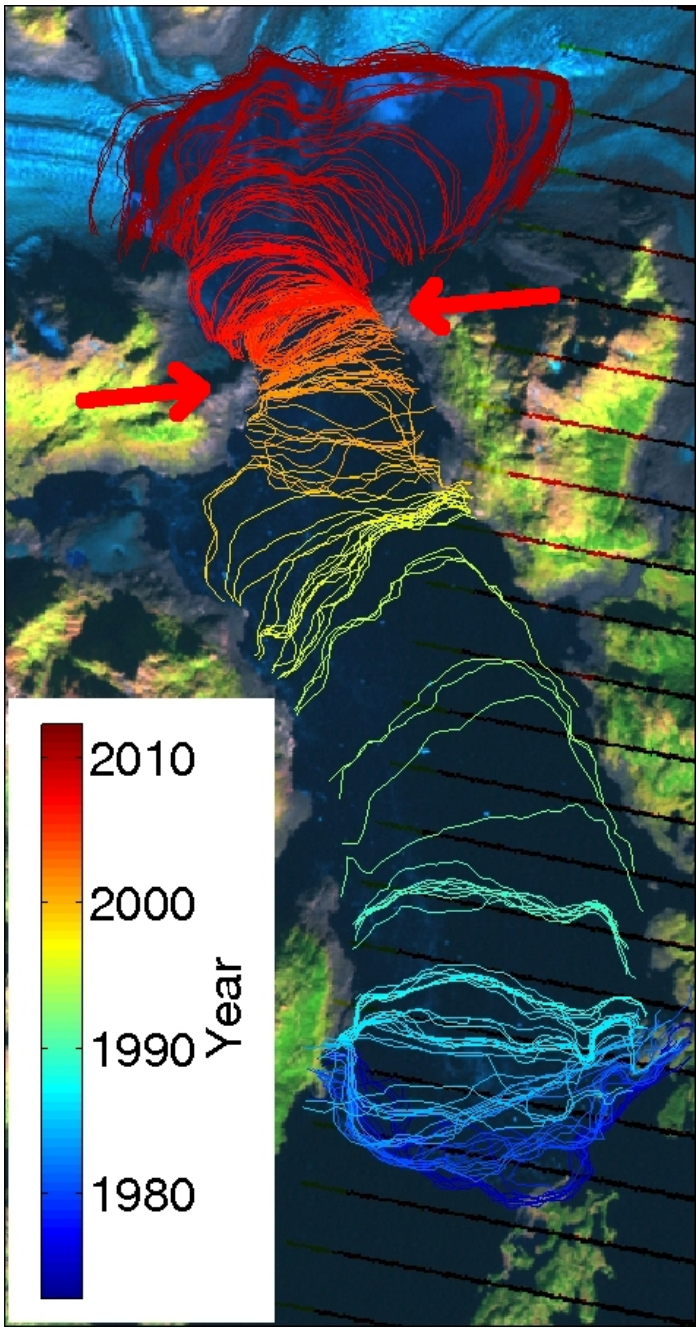

Figure 3.11. Terminus positions over time for Columbia Glacier. Color of terminus outline indicates the year from which the scene was acquired. Red arrows indicate location of topographic pinning points, where the glacier's retreat slowed dramatically during the period 2000-2004.

SST values over the area of interest (in this case, Tracy Arm and Icy Bay), and take the seasonal average of the resulting time series. Figure 3.12a shows both MODIS-derived summer (June/July/August) SST anomaly and glacier length for Tracy Arm since 2000, the fjord containing both Sawyer and South Sawyer Glaciers. Figure 3.12b shows both glacier length and summer SST anomaly for Icy Bay and Guyot Glacier since 2000. These three glaciers underwent step change retreats beginning in 2004, 2004, and 2006, respectively. Sawyer Glacier stabilized briefly, before again undergoing a step change retreat beginning in 2010. For Tracy Arm, the 2004 summer SST was $\sim$1.5°C warmer than the 2000-2012 average summer SST, while in Icy Bay, 2004-2006 summer SSTs were $0.5-1.5$°C warmer than the 2000-2012 average. For Tracy Arm, 2008 was an anomalously cool ($\sim$1.5°C cooler than 2000-2012), while 2009 was more normal. In each case, then, the step change retreat began either in a year with an anomalously warm summer SSTs (Sawyer, South Sawyer), or after several years of anomalously warm summer SSTs (Guyot).

Compared to the other glaciers in Icy Bay (Yahtse, Tsaa, Moraine/Apron, Grotto, and Tyndall), Guyot glacier is relatively unprotected at its terminus. Moraine/Apron and

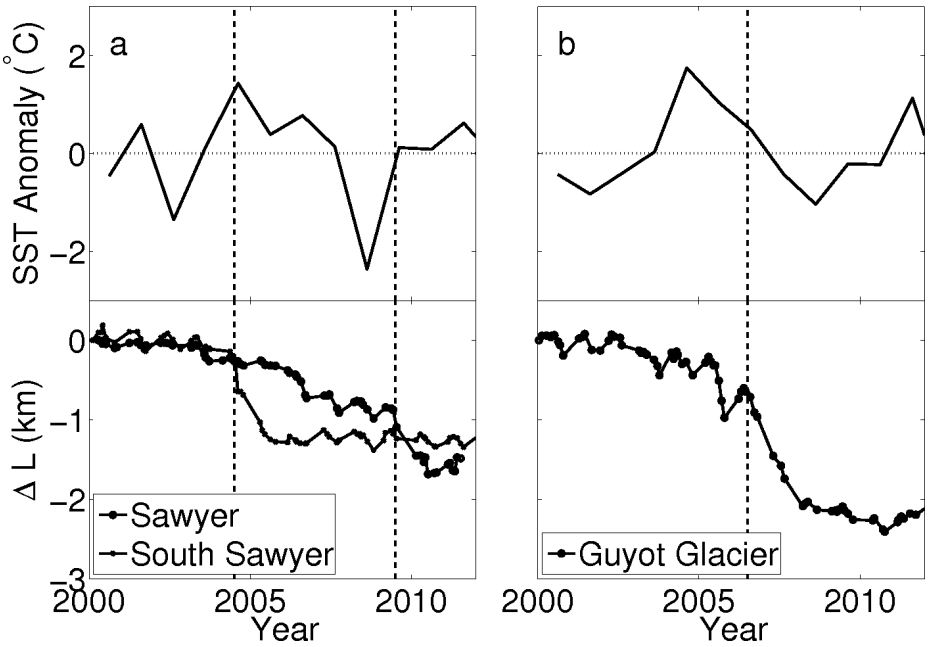

Figure 3.12. (a) Summer SST anomalies (relative to the 2000-2012 summer mean) for Tracy Arm and relative length change for Sawyer and South Sawyer Glaciers. (b) as (a), but for Icy Bay and Guyot Glacier. Vertical lines indicate timing of step change retreats, coincident with large changes in SST anomaly.

Grotto glaciers are almost completely retracted from tidewater, Tyndall and Yahtse Glaciers have been advancing since the mid-1980s (and therefore are protected by a moraine shoal that exposes far less ice to warm ocean water), and Tsaa Fjord is much more shallow than Guyot Fjord. Anomalously warm summer SSTs, such as those observed in Icy Bay from 2004-2006 (Fig. 3.12b), would then likely have a greater effect on Guyot than other glaciers in the same fjord system. Sawyer and South Sawyer Glaciers share a fjord, so the simultaneous triggering of a retreat is consistent with warming ocean waters; both glaciers stabilized after the step change retreat, but Sawyer began to retreat again after 2009. This, again, illustrates the stabilizing effect (and potential limits thereof) of bedrock geometry: Sawyer retreated into a relatively wider constriction than South Sawyer, and was again vulnerable to the warming observed 2009-2010 (Fig. 3.12a).

Despite this correlation with anomalously warm SST and the triggering of step change retreats, further study is needed in order to definitively demonstrate the cause of the triggering of these retreats. In general, irreversible tidewater retreat occurs when critical thinning near the terminus increases ice velocity, which in turn increases ice drawdown and thinning in a positive feedback loop (Pfeffer, 2007). Bedrock constrictions and the development of a moraine shoal are two possible causes for the stabilization of tidewater termini; an increase in positive mass balance is another potential cause, but given current trends in Alaska and the globe (Radić and Hock, 2011), this seems less likely. Increased submarine melt from an influx of warm ocean water is only one potential cause for the triggering of tidewater retreat (of many), but these observations suggest that further study of these processes and the retreats of these glaciers is warranted, to further our understanding of tidewater glacier behavior.

3.7.3 Seasonal Length Changes

In general, tidewater glaciers are thought to advance in the winter, reaching a maximum annual length in early summer, and retreat during the summer, reaching a minimum annual length in late summer/early winter (Krimmel, 2001; Moon and Joughin, 2008; Ritchie and others, 2008). Figures 3.9 and 3.10 show that on average, this is true for the 50 glaciers in this study. 40 glaciers show their maximum advance in the spring (March/April/May) or summer (June/July/August), and 41 glaciers show their maximum retreat in the fall (September/October/November) or winter (December/January/February). Of the ten individual glaciers that do not fit into this 'typical' behavior, most have small seasonal ampli-

tudes (mean $\pm$ standard deviation of 18 ± 17 m a^{-1}) much lower than the error associated with individual length measurements. One of these glaciers, Turner Glacier, is a surging glacier, and its behavior is more likely dominated by different mechanisms than the other glaciers in this set.

Recently, a few studies have investigated potential causes for seasonal fluctuations in tidewater glacier length (Ritchie and others, 2008; Howat and others, 2010). Ritchie and others (2008) attributed seasonal changes in length primarily to changes in ice velocity, although location of the moraine shoal and changes in seawater temperature were found to play a role. Howat and others (2010) found that seasonal formation (and subsequent disappearance) of an ice melange may explain the onset of seasonal retreat.

It is possible that the atypical seasonal behavior exhibited by these ten glaciers is a result of measurement error; however, several of these glaciers have retreated from tidewater since the beginning of the study period. Glaciers that do not terminate in tidewater typically have surface velocities that decrease toward the terminus. We might expect, then, that seasonal advance (and retreat) for these glaciers would occur at different times of year than marine-terminating glaciers that have surface velocities increasing towards the terminus and that are influenced by ocean water.

In addition to more normally-timed seasonal length changes, Tsaa Glacier (Icy Bay subregion) shows a pronounced, rapid cycle of advance and retreat, on the order of one km in the span of one year, from about 1995 though 2005 (Fig. 3.3d). While a detailed investigation into the causes of this behavior is beyond the scope of this study, it should be noted that Tsaa Fjord is one of few in southern Alaska that forms a thick sea ice cover (Fig. 3.13), of the type usually observed in Greenland tidewater fjords (e.g., Amundson and others, 2010). This cover does not form every year, perhaps explaining why this pattern of rapid advance and retreat is observed only intermittently (T. Bartholomaus, personal communication, 2012).

3.7.4 Regional Behavior

Howat and Eddy (2012) present a record of outlet glacier length change for Greenland over the period 1972-2010. They find that over the period 2000-2010, over 90% of these glaciers retreated, with some areas having all glaciers in retreat. At no point during our study do we see this level of coherence between glaciers in the region; the decade with the highest percentage of retreating glaciers is 1991-2000, with 60%. During the period 2001-

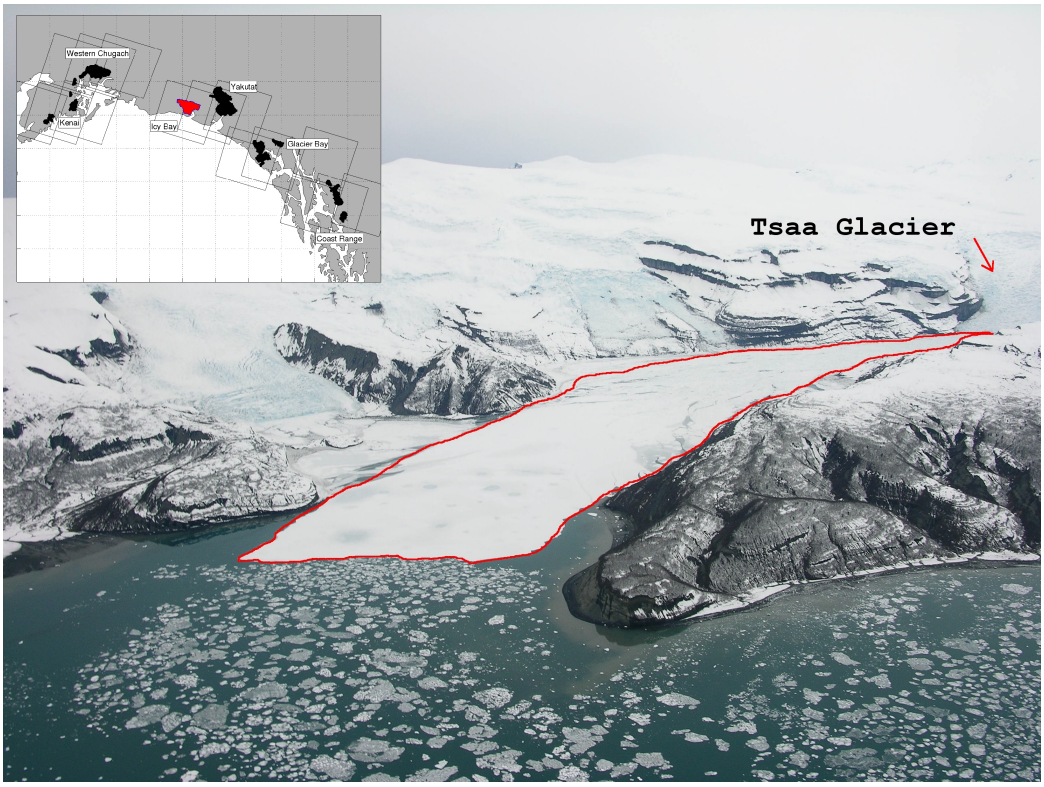

Figure 3.13. Tsaa Fjord (Icy Bay subregion), taken 11 April 2010. Note the large, rigid "plug" of sea ice in the fjord (red outline), suggesting that local sea ice conditions have a strong effect on the seasonal advance and retreat of Tsaa Glacier, as observed at tidewater glaciers in Greenland. Photo courtesy Tim Bartholomaus.

2010, we see only 46% of glaciers in the study region retreating. This is most likely due to the number of glaciers in Alaska that have been undergoing retreat for the majority of the 20th century. In contrast, many tidewater glaciers in Greenland were stable or advancing during that time period (Howat and Eddy, 2012).

On a subregional basis, however, glacier behavior is more coherent than throughout the region as a whole. Both the Glacier Bay and Kenai subregions have decadal mean and median rates of length change that are nearly identical (Fig. 3.4). In Glacier Bay, this is likely due to the low rates of length change observed (less than ten m a^{-1} on average), but the Kenai is much different. Not only are the regional mean rates of length change higher than in Glacier Bay ($20-30$ m a^{-1} on average), but there is a clear alternation between decadal retreat and advance reflected in both the mean and median rates of length change for the subregion.

Unlike the other subregions, which consist mainly of individual glaciers that do not share a common ice source, the Kenai subregion glaciers are primarily divided amongst the Harding and Sargent Icefields. The two glaciers in the subregion that are not part of either of these icefields, Beloit and Blackstone, share a common ice source. In this respect, the glaciers of the Kenai peninsula are more similar to the tidewater glaciers studied in Greenland, which share a common ice source in the Greenland Ice Sheet, and may be more susceptible to common factors that would influence synchronous behavior.

3.7.5 Patterns of Significant Length Changes

Patterns of significant advance and retreat over the course of the study are very similar to each other. The mean number of years that glaciers significantly advanced or retreated over the course of the study are nearly identical, as is the mean number of glaciers per year that significantly advanced or retreated. Even the length of typical periods of significant advance or retreat are nearly identical. Because of the rapid and unstable nature of tidewater glacier retreat, as well as the generally retracted lengths of most Alaska tidewater glaciers (Viens, 1995), we would expect most tidewater retreats to be relatively short over the period of this study: glaciers that are in a retracted position are most likely unable to sustain long-term retreat. A typical period of mean significant retreat lasts fewer than two years, with the only exceptions being glaciers that are retreating from their Little Ice Age maximum lengths.

3.8 Conclusions

We have presented a detailed record of glacier length changes for 50 Alaska tidewater glaciers over the period 1948-2012, with over $10,000$ individual glacier fronts digitized from nearly 2000 Landsat scenes. Examination of this record shows that over 60% of glaciers significantly retreated over the course of the study period. Yearly rates of length change can be quite large, with several glaciers advancing or retreating more than one hundred meters per year. These rates are not constant, with many glaciers having changes in retreat rate exceeding hundreds of meters per year. Seasonal variations can also be rather large, with some glaciers showing seasonal amplitudes of several hundred meters per year.

For many glaciers in the region, we observe “step change" retreats, where glaciers quickly retreat from a stable position, usually located at a topographic constriction, and stabilize again at another topographic constriction. These retreats do not begin at the same

time, and are not consistent throughout subregions. Examination of three such retreats, including two glaciers that share a fjord, indicates that these retreats are triggered after several years of abnormally warm summer sea surface temperatures (SSTs) in their fjords, a finding consistent with observations of tidewater glaciers in West Greenland. Further study to determine whether these retreats are triggered solely by anomalously warm summer SSTs, or by a combination of factors, is warranted based on these findings.

Recent studies have suggested that on regional scales, tidewater glacier retreat can be quite coherent. While we do not find any such evidence indicating regional-scale coherence for all glaciers in Alaska, several subregions do show similar patterns of behavior to those observed in Greenland. One subregion in particular, the Kenai subregion, shows consistent patterns of oscillation between retreat and advance on a decadal scale. This subregion contains many glaciers that share a common ice source, much like tidewater glaciers in Greenland, which may provide one explanation for their general coherence.

On long-term time scales, tidewater glaciers are shown to undergo periods of long, slow advance over the course of centuries, and rapid retreats that complete on the scale of decades. We find glaciers in the region in each stage of the tidewater glacier cycle. Glacier retreats are typically short-lived and come in bursts; the average glacier undergoes continuous retreat for only a year or two before stabilizing for a year or more. This is most likely due to the retracted nature of most Alaska tidewater glaciers, as glaciers that continuously retreat for more than a few years at a time are transitioning from a stable extended position towards a stable retracted position.

3.9 References

Aðalgeirsdóttir, G., K. A. Echelmeyer and W. D. Harrison, 1998. Elevation and volume changes on the Harding Icefield, Alaska, *J. Glaciol.*, **44**(148), 570–582.

AMAP, 2011. Snow, Water, Ice and Permafrost in the Arctic (SWIPA): Climate Change and the Cryosphere, Arctic Monitoring and Assessment Programme (AMAP), Oslo, Norway.

Amundson, J. M., M. Fahnestock, M. Truffer, J. Brown, M. P. Lüthi and R. J. Motyka, 2010. Ice mélange dynamics and implications for terminus stability, Jakobshavn Isbræ, Greenland, *J. Geophys. Res.*, **115**(F01005), doi:10.1029/2009JF001405.

Arendt, A., K. Echelmeyer, W. Harrison, C. Lingle and B. Valentine, 2002. Rapid wastage of Alaska glaciers and their contribution to rising sea level, *Science*, **297**(5580), 382–386.

Arendt, A., K. Echelmeyer, W. Harrison, C. Lingle, S. Zirnheld, V. Valentine, B. Ritchie and M. Druckenmiller, 2006. Updated estimates of glacier volume changes in the western Chugach Mountains, Alaska, and a comparison of regional extrapolation methods, *J. Geophys. Res.*, **111**(F03019).

Barclay, D., P. Calkin and G. Wiles, 2001. Holocene history of Hubbard Glacier in Yakutat Bay and Russell Fiord, southern Alaska, *Geol. Soc. of Am. Bull.*, **113**, 388–402.

Barclay, D., J. Barclay, P. Calkin and G. Wiles, 2006. A revised and extended Holocene Glacial history of Icy Bay, Southern Alaska, U.S.A., *Arctic, Antarctic, and Alpine Res.*, **38**(2), 153–162.

Barclay, D., G. Wiles and P. Calkin, 2009. Holocene glacier fluctuations in Alaska, *Quat. Sci. Rev.*, **28**, 2034–2048.

Berthier, E., E. Schiefer, G. K. C. Clarke, B. Menounos and F. Rémy, 2010. Contribution of Alaskan glaciers to sea-level rise derived from satellite imagery, *Nature Geosci.*, **3**, 92–95.

Brown, C. S., M.F. Meier and A. Post, 1982. Calving speed of Alaska tidewater glaciers, with application to Columbia Glacier, *USGS Prof. Pap.*, **1258-C**.

Calkin, P. E., G. C. Wiles and D. J. Barclary, 2001. Holocene coastal glaciation of Alaska, *Quat. Sci. Rev.*, **20**, 449–461.

Carson, R.T., R. C. Mitchell, M. Hanemann, R. J. Kopp, S. Presser and P. A. Ruud, 2003. Contingent Valuation and Lost Passive Use: Damages from the Exxon Valdez Oil Spill, *Env. and Res. Econ.*, **25**(3), 257–286.

Colgan, W., W. T. Pfeffer, H. Rajaram, W. Abdalati and J. Balog, 2012. Monte Carlo ice flow modeling projects a new stable configuration for Columbia Glacier, Alaska, c. 2020, *The Cryosphere*, **6**, 1395–1409, doi:10.5194/tc-6-1395-2012.

Gardner, A. S., G. Moholdt, J. G. Cogley, A. A. Arendt, J. Wahr, E. Berthier, R. Hock, W. T. Pfeffer, G. Kaser, S. R. M. Ligtenberg, T. Bolch, M. J. Sharp, J. O. Hagen, M. van den Broeke and F. Paul, 2013. A consensus estimate of glacier contributions to sea level rise: 2003-2009, *Science*, **340**, doi:10.1126/science1234532.

Howat, I. and A. Eddy, 2012. Multi-decadal retreat of Greenland's marine-terminating glaciers, *J. Glaciol.*, **57**(203), 389–396.

Howat, I. M., J. E. Box, Y. Ahn, A. Herrington and E. M. McFadden, 2010. Seasonal variability in the dynamics of marine-terminating outlet glaciers in Greenland, *J. Glaciol.*, **56**(198), 601–613.

IPCC, 2007. Climate Change 2007: The Physical Science Basis: Contribution of Working Group I to the Fourth Assessment Report of the Intergovernmental Panel on Climate Change, Cambridge University Press, [S. Solomon and D. Qin and M. Manning and Z. Chen and M. Marquis and K. B. Averyt and M. Tignor and H. L. Miller (eds.)].

Krimmel, R. M., 2001. Photogrammetric data set, 1957-2000, and bathymetric measurements for Columbia Glacier, Alaska, *USGS Water Res. Invest. Rep.*, **014089**.

Larsen, C. F., R. J. Motyka, A. A. Arendt, K. A. Echelmeyer and P. E. Geissler, 2007. Glacier changes in southeast Alaska and northwest British Columbia and contribution to sea level rise, *J. Geophys. Res.*, **112**(F01007).

McNabb, R., R. Hock, S. O'Neel, L. A. Rasmussen, Y. Ahn, M. Braun, H. Conway, S. Herreid, I. Joughin, W. T. Pfeffer, B. E. Smith and M. Truffer, 2012. Using Surface Velocities to Calculate Ice Thickness and Bed Topography: A Case Study at Columbia Glacier, Alaska, *J. Glaciol.*, **58**(212).

Meier, M. and M. Dyurgerov, 2002. How Alaska affects the world, *Science*, **297**, 350–351.

Meier, M. F. and A. Post, 1969. What are glacier surges?, *Can. J. of Earth Sci.*, **6**(4).

Meier, M. F. and A. Post, 1987. Fast tidewater glaciers, *J. Geophys. Res.*, **92**(B9), 9051–9058.

Meier, M., S. Lundstrom, D. Stone, B. Kamb, H. Engelhardt, N. Humphrey, W. Dunlap, M. Fahnestock, R. Krimmel and R. Walters, 1994. Mechanical and hydrologic basis for the rapid motion of a large tidewater glacier, 1. Observations, *J. Geophys. Res.*, **99**(B8), 15219–15229.

Meier, M. F., M. B. Dyurgerov, U. K. Rick, S. O'Neel, W. T. Pfeffer, R. S. Anderson, S. P. Anderson and A. F. Glazovsky, 2007. Glaciers dominate eustatic sea-level rise in the 21st century, *Science*, **317**(1064), doi:10.1126/science.1143906.

Molnia, B. F., 2008. Glaciers of North America – Glaciers of Alaska, R. S. Williams, Jr. and J. G. Ferrigno, eds., Satellite image atlas of glaciers of the world, United States Geological Survey, K52–K83, USGS Prof. Pap. 1386-K.

Moon, T. and I. Joughin, 2008. Changes in ice front position on Greenland's outlet glaciers from 1992 to 2007, *J. Geophys. Res.*, **113**(F02022), doi:10.1029/2007JF000927.

Moon, T., I. Joughin, B. Smith and I. Howat, 2012. 21st-century evolution of Greenland outlet glacier velocities, *Science*, **336**, 576–578, 10.1126/science.1219985.

Motyka, R. J. and M. Truffer, 2007. Hubbard Glacier, Alaska: 2002 closure of Russell Fjord and implications for future dams, *J. Geophys. Res.*, **112**(F2), F02004, doi:10.1029/2006JF000475.

Motyka, R. J., L. Hunter, K. Echelmeyer and C. Connor, 2003. Submarine melting at the terminus of a temperate tidewater glacier, Leconte Glacier, Alaska, *Ann. Glaciol.*, **36**, 57–65.

O'Neel, S., K. A. Echelmeyer and R. J. Motyka, 2001. Short-term flow dynamics of a retreating tidewater glacier: LeConte Glacier, Alaska U.S.A., *J. Glaciol.*, **47**(159).

O'Neel, S., K. A. Echelmeyer and R. J. Motyka, 2003. Short-term variations in calving of a tidewater glacier: LeConte Glacier, Alaska, U.S.A., *J. Glaciol.*, **49**(167), 587–598.

O'Neel, S., W. T. Pfeffer, R. Krimmel and M. Meier, 2005. Evolving force balance at Columbia Glacier, Alaska, during its rapid retreat, *J. Geophys. Res.*, **110**(F03012), doi:10.1029/2005JF000292.

O'Neel, S., H. P. Marshall, D. E. McNamara and W. T. Pfeffer, 2007. Seismic detection and analysis of icequakes at Columbia Glacier, Alaska, *J. Geophys. Res.*, **112**(F03S23), doi:10.1029/2006JF000595.

Pfeffer, W. T., 2007. A simple mechanism for irreversible tidewater glacier retreat, *J. Geophys. Res.*, **112**(F03S2), doi:10.1029/2006JF000590.

Porter, S. C., 1989. Late Holocene fluctuations of the fiord glacier system in Icy Bay, Alaska, U.S.A., *Arctic and Alpine Res.*, **21**(4), 364–379.

Post, A., 1975. Preliminary hydrography and historical terminal changes of Columbia Glacier, Alaska, *U.S. Geol. Surv. Hyrdolog. Invest. Atlas*, **HA-559**.

Post, A. and R. J. Motyka, 1995. Taku and Le Conte glaciers, Alaska: calving-speed control of late Holocene asynchronous advances and retreats, *Phys. Geog.*, **16**, 59–82.

Post, A., S. O'Neel, R. J. Motyka and G. Streveler, 2011. A complex relationship between calving glaciers and climate, *EOS Trans.*, **92**(37), 305–306.

Radić, V. and R. Hock, 2011. Regionally differentiated contribution of mountain glaciers and ice caps to future sea-level rise, *Nat. Geosci.*, **4**, 91–94, doi:10.1038/NGEO1052.

Rasmussen, L. A., H. Conway, R. M. Krimmel and R. Hock, 2011. Surface mass balance, thinning and iceberg production, Columbia Glacier, Alaska, 1948-2007, *J. Glaciol.*, **57**(203), 431–440.

Ritchie, J., C. Lingle, R. Motyka and M. Truffer, 2008. Seasonal fluctuations in the advance of a tidewater glacier and potential causes: Hubbard Glacier, Alaska, USA, *J. Glaciol.*, **54**(186), 401–411.

Trabant, D., R. Krimmel, K. Echelmeyer, S. Zirnheld and D. Elsberg, 2003. The slow advance of a calving glacier: Hubbard Glacier, Alaska, U.S.A., *Ann. Glaciol.*, **36**, 45–50.

VanLooy, J., R. Forster and A. Ford, 2006. Accelerating thinning of Kenai Peninsula glaciers, Alaska, *Geophys. Res. Lett.*, **33**(L21307), doi:10.1029/2006GL028060.

Viens, R. J., 1995. Dynamics and Mass Balance of Temperate Tidewater Calving Glaciers of Southern Alaska, (Master's thesis, Univ. of Washington).

Walter, F., S. O'Neel, D. MacNamara, W. T. Pfeffer, J. N. Bassis and H. A. Fricker, 2010. Iceberg calving during transition from grounded to floating ice: Columbia Glacier, Alaska, *Geophys. Res. Lett.*, **37**(L15501), doi:10.1029/2010GL043201.

Wiles, G. C. and P. E. Calkin, 1994. Late Holocene, high-resolution glacial chronologies and climate, Kenai Mountains, Alaska, *Geol. Soc. of Am. Bull.*, **106**, 281–303.

Wiles, G. C., P. E. Calkin and A. Post, 1995. Glacier fluctuations in the Kenai Fjords, Alaska, U.S.A.: an evaluation of controls on iceberg-calving glaciers, *Arctic and Alpine Res.*, **27**(3), 234–245.

Chapter 4

Alaska Tidewater Glacier Velocities and Frontal Ablation, 1985-2012[1]

4.1 Abstract

Despite their potential importance to sea level rise, little is known about the proportion of mass loss due to frontal ablation (the sum of ice loss through calving and submarine melt) from tidewater glaciers outside of the Greenland and Antarctic ice sheets. Frontal ablation contributes about half of the mass loss from the ice sheets, and lack of both understanding of and data on these important processes has been cited as a major hindrance to accurate predictions of global sea level rise. We present a 27 year record of surface velocity and frontal ablation for 20 Alaska tidewater glaciers (representing 80% of the total tidewater glacier area in the region), derived using a feature tracking algorithm, all available cloud-free Landsat 5 and 7 scenes, and estimates of glacier ice thickness derived from an inversion of surface topography. We find that total mean rate of frontal ablation for these 20 glaciers over the period 1985-2012 is 16.2 ± 6.5 Gt a^{-1}; scaling this result by area to the remaining 30 tidewater glaciers in Alaska, we estimate a mean rate of frontal ablation of 18.3 ± 7.3 Gt a^{-1} over the period 1985-2012. Two glaciers in particular, Hubbard and Columbia, account for over 50% of the frontal ablation signal of the set of 20 glaciers. Seasonal changes in surface velocity match well with seasonal changes in length, indicating that rates of frontal ablation do not remain constant throughout the year. Despite coming from $\sim 15\%$ of the glacierized area in the region, frontal ablation is a significant contributor to the regional mass budget. We estimate a specific mass loss through frontal ablation for all Alaska glaciers of 0.21 m water equivalent (w.e.) a^{-1}, equivalent to estimates from Svalbard, and over three times the rate for Greenland.

4.2 Introduction

Much attention has been paid to the current status and future evolution of the Greenland and Antarctic ice sheets, and especially their potential contribution to eustatic sea level rise (Rignot and Kanagaratnam, 2006; Truffer and Fahnestock, 2007; Rignot and others, 2008a,b; Shepherd and others, 2012). In spite of this attention, the fourth Intergovernmental Panel on Climate Change (IPCC) report cites the lack of understanding of frontal ablation (the sum of mass lost through calving and mass lost through submarine melt) as

[1] A version of this chapter is being prepared for submission to Nat. Geoscience as McNabb, R. and R. Hock. Alaska Tidewater Glacier Velocities and Frontal Ablation, 1985-2012

the single largest factor hindering attempts to accurately assess and predict global glacier mass change, and hence, the cryospheric contribution to sea level rise (IPCC, 2007). Recent studies have indicated that frontal ablation is responsible for 40-60% of the mass loss from the Greenland Ice Sheet (Rignot and Kanagaratnam, 2006; Rignot and others, 2008b; van den Broeke and others, 2009) and a majority of the mass loss from the Antarctic ice sheets (Rignot, 2006; Rignot and others, 2008a). Owing to the complicated nature of the mechanisms behind both calving and submarine melt, however, accurate models and predictions of frontal ablation do not exist.

Many studies have attempted to define an overarching “calving law," to allow modeling of calving rates. Due to the complexities present at the ice-ocean interface, no such law presently exists (Amundson and Truffer, 2010). The earliest attempts at a calving law focused on the water depth at the calving front (Brown and others, 1982; Pelto and Warren, 1991), though these relationships were shown to break down for glaciers in rapid retreat (Van der Veen, 1996). The next group of studies focused on the height of the calving front above flotation (Van der Veen, 1996; Vieli and others, 2001), though this formulation failed to provide for floating ice shelves and tongues. More recently, crevasse depth (Benn and others, 2007) and strain rate near the calving front (Alley and others, 2008; Amundson and Truffer, 2010) have been proposed as controlling mechanisms. Statistical studies of the calving face have also been employed (Bassis, 2011), and approaches using damage mechanics have been developed (Borstad and others, 2012).

Because it is assumed that calving is the dominant process of frontal ablation, many studies neglect submarine melting at the calving face (Vieli and others, 2002). Recently, however, studies have begun to focus on the role that submarine melt plays in terms of frontal ablation. For example, in a study at LeConte Glacier, Alaska, Motyka and others (2003) found that melt below the waterline was roughly equal to the calving velocity, reaching levels of 10 m d^{-1}. Another study found that an influx of warm ocean water likely led to the disintegration of the floating tongue at Jakobshavn Isbrae, Greenland, leading to that outlet glacier’s speed-up and retreat (Holland and others, 2008; Motyka and others, 2011). Efforts at quantifying submarine melt at other outlet glaciers in Greenland (Rignot and others, 2010, 2012) have continued to implicate the ocean as a major factor in tidewater glacier mass balance, with levels of submarine melt between 0.7 and 3.9 m d^{-1}. Rignot and others (2013) estimate that over half of the frontal ablation from Antarctic ice shelves comes from submarine melt.

Despite comprising less than one percent of all glacier ice on earth, mountain glaciers and ice caps (those bodies of ice separate from the main Greenland and Antarctic ice sheets) are responsible for over half of the total cryospheric contribution to sea level rise (Meier and others, 2007; Gardner and others, 2013). Even less is known of the relative contribution of frontal ablation to the mass balance of these glaciers than is known of that for the ice sheets. Estimates of frontal ablation on a regional level are scarce, though some do exist. Studies of Svalbard tidewater glaciers estimate that frontal ablation is approximately 30% of the total net mass loss from the archipelago (Błaszczyk and others, 2009), 30% of the total ablation from individual ice caps (Dowdeswell and others, 2002, 2008), and nearly 100% of the net mass loss from individual ice caps and glaciers (Moholdt and others, 2012; Nuth and others, 2012). Studies from Arctic Canada estimate that frontal ablation is approximately 30% of the mass loss from individual ice caps, and approximately 10% of the net mass loss from the region as a whole (Burgess and others, 2005; Gardner and others, 2011).

Recent studies, employing a variety of techniques, have shown Alaska glaciers to be significant contributors to global sea level rise (Arendt and others, 2002; Meier and Dyurgerov, 2002; Arendt and others, 2006; Meier and others, 2007; Luthcke and others, 2008; Hock and others, 2009; Berthier and others, 2010; Dyurgerov, 2010; Radić and Hock, 2011; Gardner and others, 2013; Radić and others, 2013), though the fraction of that contribution that is due to frontal ablation is unknown. Since achieving their Little Ice Age maxima between AD 1750 and 1900, most glaciers in the region have been retreating, though several have been thickening and advancing in recent decades (Calkin and others, 2001; Larsen and others, 2007). Present estimates of mass loss from Alaska glaciers are approximately 50-90 Gt a^{-1} (Luthcke and others, 2008; Jacob and others, 2012; Gardner and others, 2013; Luthcke and others, 2013), though the overall partitioning of this mass loss is unknown.

In order to learn about the importance of frontal ablation to Alaska tidewater glaciers, this study estimates surface velocities and rates of frontal ablation at 20 Alaska tidewater glaciers over the period 1985-2012. Using a collection of Landsat images acquired between 1985 and 2012, we apply a feature tracking algorithm to calculate fields of surface velocity for each glacier. We then use these surface velocities, along with ice thicknesses to estimate rates of frontal ablation over this time period. We adjust for surface mass balance by assuming a constant rate of surface ablation between the flux gate and the terminus. Ice thickness for each glacier is calculated using a physically-based method to invert surface

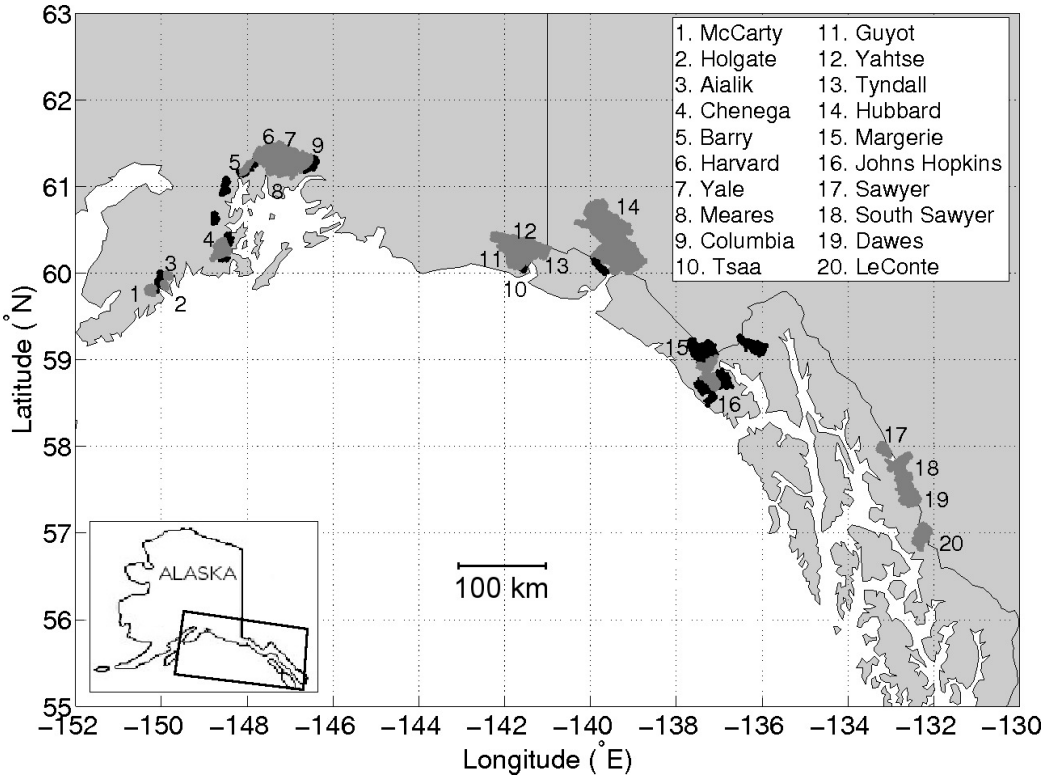

Figure 4.1. Location of the 20 studied tidewater glaciers in Alaska. Glaciers used in this study are outlined in gray and labeled as shown in the legend; black outlines indicate other tidewater glaciers.

topography to determine bed elevation (Huss and Farinotti, 2012). We compare seasonality of velocities to seasonality of length changes, which enables us to discuss the seasonality of frontal ablation. Finally, we use estimates of regional mass loss to compare regional rates of frontal ablation with approximate regional climatic balances.

4.3 Study Area

Glaciers in Alaska (including adjacent glaciers in the Yukon and British Columbia; hereafter "Alaska glaciers") cover a total area of $87,100$ km^2 (Gardner and others, 2013). A total of 59 glaciers, representing approximately 14% of the total glacier area, have been identified as either currently or formerly tidewater (Viens, 1995; Molnia, 2008); for this study we consider a subset of 20 glaciers that have large, active calving fronts and most likely represent the vast majority of loss due to frontal ablation in the region. These 20 glaciers cover approximately 9800 km^2 (representing 80% of the total tidewater glacier area, or 11%

Table 4.1. General statistics for glaciers studied, ordered by their area. Here, # pairs is the number of Landsat scene pairs used to derive the velocity record for the glacier, dL/dt is the mean rate of change of glacier length over the period 1985-2012 (data from Chapter 3), $\bar{v}$ is the mean surface ice velocity through the flux gate, F is the mean rate of frontal ablation through the study period in both Gt a^{-1} and m a^{-1} (divided by glacier area), Flux is the mean ice flux through each gate in Gt a^{-1}, and % is the percentage contribution of that glaciers frontal ablation to the regional total.

Name	Area	# pairs	dL/dt	$\bar{v}$	F	F	Flux	Reg. Pct.
	km^2		m a^{-1}	m a^{-1}	Gt a^{-1}	m a^{-1}	Gt a^{-1}	
Hubbard	3402	59	27	3.7	6.5 ± 2.6	1.91	7.0	40.2
Yahtse	1084	44	102	5.1	1.1 ± 0.4	1.00	1.2	6.7
Columbia	944	52	-483	3.8	2.8 ± 1.1	2.93	2.4	17.1
Dawes	604	33	-23	2.0	0.4 ± 0.2	0.63	0.4	2.4
S. Sawyer	565	46	-123	1.7	0.3 ± 0.1	0.50	0.3	1.8
Harvard	527	42	23	1.6	0.9 ± 0.4	1.73	1.0	5.6
Leconte	482	31	-9	3.3	0.9 ± 0.3	1.81	0.9	5.4
Chenega	392	34	2	2.2	0.3 ± 0.1	0.84	0.4	2.0
J. Hopkins	254	44	15	2.6	0.3 ± 0.1	1.03	0.3	1.6
Guyot	220	44	-186	4.7	0.6 ± 0.3	2.95	0.6	4.0
Tsaa	203	44	-23	3.7	0.2 ± 0.1	1.07	0.2	1.3
Margerie	182	39	7	1.0	0.1 ± 0.0	0.37	0.1	0.4
Yale	165	39	-13	2.9	0.5 ± 0.2	2.73	0.5	2.8
Meares	149	30	12	1.8	0.4 ± 0.2	2.83	0.4	2.6
Tyndall	145	29	2	2.0	0.2 ± 0.1	1.10	0.2	1.0
Sawyer	145	28	-92	0.5	0.2 ± 0.1	1.06	0.1	0.9
Mccarty	119	35	-45	1.4	0.2 ± 0.1	1.41	0.2	1.0
Barry	106	51	-147	1.7	0.2 ± 0.1	1.65	0.2	1.1
Aialik	74	62	3	2.4	0.3 ± 0.1	3.88	0.3	1.8
Holgate	56	25	24	0.8	0.0 ± 0.0	0.55	0.0	0.2
All Glaciers	9819				16.2 ± 6.5	1.65		100.00

of the total glacier area), and range in size from 55 km^2 (Holgate Glacier) to over 3400 km^2 (Hubbard Glacier). Information about individual glaciers is given in Table 4.1, and a map of the study region is shown in Fig. 4.1.

On average, the 20 glaciers in this study have retreated 45 ± 156 m a^{-1} over the period 1985-2012 (Chapter 3). The mean value is heavily influenced by several glaciers with rapid retreats, however, as the median length change over this same period is -6 m a^{-1}. Of the 13 glaciers in the study that have retreated over the period 1985-2012, Columbia Glacier has retreated the most (17.3 km of retreat). Columbia Glacier began a rapid retreat ca. 1980 (Meier and Post, 1987; Meier and others, 1994), with over 50% of its volume lost since 1957 (Rasmussen and others, 2011; McNabb and others, 2012). Only one other glacier in this study, Guyot Glacier, has retreated more than three kilometers since 1985 (3.2 km, Chapter 3). The 13 retreating tidewater glaciers considered in this study have undergone a mean retreat of 2.4 ± 4.6 km since 1985, compared to the mean retreat of 2.4 ± 4 km shown by the 31 retreating tidewater glaciers studied in Chapter 3.

The largest advancing tidewater glacier in this study, Hubbard Glacier, is also the largest temperate tidewater glacier in the world (Trabant and others, 2003). Since 1985, Hubbard Glacier has advanced 0.9 km, blocking the entrance to Russell Fjord twice, in 1986 and 2002 (Trabant and others, 2003; Motyka and Truffer, 2007; Ritchie and others, 2008). The glacier with the largest advance since 1985, however, is Yahtse Glacier, having advanced 2.5 km in that time. The seven advancing tidewater glaciers in this study have undergone a mean advance of 0.7 ± 0.9 km since 1985, compared to the mean advance of 0.4 ± 0.4 km shown by the 19 advancing tidewater glaciers studied in Chapter 3.

4.4 Data

4.4.1 Landsat Imagery

Landsat images are used to derive glacier lengths (Chapter 3) and derive surface ice velocities through feature tracking. The Landsat program, first launched in 1972, provides a record of images encompassing over 40 years. Since the 1982 launch of the Landsat 4 mission, images are available with 30 m ground resolution, and with the 1999 launch of the Landsat 7 mission, images are available with 15 m ground resolution. We compiled a set of 1,683 Landsat scenes acquired over Alaska between April 1984 and December 2012; scenes separated by 35 days or fewer were unavailable until 1985. Scenes were acquired with the Landsat 5 Thematic Mapper (TM) sensor (1984-2011) and the Landsat 7 Enhanced The-

matic Mapper Plus (ETM+) sensor (1999-2012). Each scene has been georeferenced and orthorectified by the Landsat program; where needed, we manually applied corrections to the georeferencing using manually selected ground control points. This correction was needed for fewer than one percent of the images used. Analysis of georeferencing has been performed by manually digitizing static ground features in each image, with accuracy of $\sim$30 m (Chapter 3).

4.4.2 Ice Thicknesses

Ice thickness measurements of Alaska tidewater glaciers are sparse, with only one glacier in our study set, Columbia Glacier, having sufficient measurements to use for this study. McNabb and others (2012) present ice thickness and inferred bed topography for Columbia Glacier, using a method based on mass continuity. The method takes surface velocity fields, surface topography, rates of change of surface elevation, and rates of surface mass balance. The resulting ice thickness is then compared to radar data, with a resulting root mean square error (RMSE) between modeled and measured ice thickness of 45 m. To estimate ice thickness for Columbia Glacier flux gates, we use the bed topography inferred by McNabb and others (2012), as well as surface DEMs derived from aerial photogrammetry. Because DEMs are not available for every year where we have Landsat imagery, we estimate the ice surface in a given year by assuming linear rates of surface change between successive DEMs.

For the remaining 19 glaciers, ice thicknesses are taken from an inventory compiled by Huss and Farinotti (2012). Using glacier outlines from the Randolph Glacier Inventory (RGI, Gardner and others, 2013), as well as digital elevation models (DEMs) derived from Shuttle Radar Topography Mission (SRTM) and Advanced Spaceborne Thermal Emission and Reflection Radiometer (ASTER) data, Huss and Farinotti applied a method based on mass conservation and principles of ice flow dynamics to invert surface topography for ice thickness. This method begins by calculating the so-called “apparent mass balance", or the difference between the rate of surface mass balance and the rate of change of the glacier surface. In order to account for the effect of calving on the apparent mass balance of tidewater glaciers, the authors prescribed an adjustment to the equilibrium line altitude (ELA), $\Delta \mathrm{ELA}_{\mathrm{calv}}$, in their model, which has the effect of reducing the apparent mass balance in a manner that imitates calving. Values of $\Delta \mathrm{ELA}_{\mathrm{calv}}$ were defined for an RGI region, but not individual glaciers; comparison of the resulting estimated calving fluxes to published

values yielded agreement to within 50% (Huss and Farinotti, 2012).

Huss and Farinotti (2012) do not estimate the accuracy of ice thickness for every individual glacier in their inventory, and instead report estimates for the accuracy of regional ice volume. Comparison of measured ice thicknesses for Columbia Glacier with those calculated by Huss and Farinotti yields an average difference of -140 ± 190 m and an RMSE of 240, or approximately $45 - 50\%$ of measured values, within the agreement asserted by Huss and Farinotti. We assume that this RMSE is representative of glaciers in the region and use it to estimate the uncertainty in frontal ablation arising from using these ice thicknesses; this does not cover the uncertainty arising from assuming that these ice thicknesses remain constant throughout the study period, which we address in Section 4.6.3.

4.5 Methods

4.5.1 Surface Velocities

Surface velocities are estimated using Landsat scenes as input to a feature tracking algorithm. Each Landsat scene is cropped to fit a window showing the terminus region of the glacier. These windows are chosen once for a glacier and are not resized, which means that they are large enough to account for glacier retreat and advance. For each glacier, images are sorted by date within sets of path/row pairs, and image pairs are chosen from images separated by between 16 and 35 days.

The feature tracking algorithm used here was developed by Mark Fahnestock (personal communication, 2012), and is based on principles first described by Scambos and others (1992). It is a MATLAB (©1984-2013 Mathworks, Inc.) script that takes a small subset (chip) of the first (source) image, then searches for a similar looking feature by taking progressive subsets (chips) within a larger search window in the second (destination) image. The correlation between each chip (source and destination) is recorded into a larger matrix of correlations. Matches are chosen by looking for peaks in the correlation matrix. The final, accepted match is chosen based on both the strength of the correlation ($r > 0.7$), as well as the direction of the flow; that is, we discard matches found upstream of the source feature.

Not all of the image pairs used are completely free of cloud or shadows; even a difference in snow cover from one scene to the next is enough to cause false correlations with the feature tracking algorithm. In order to interpolate values of surface velocity at such locations, it is necessary to introduce a filter. Since we are interested in the surface velocities across a cross-section of the glacier ("flux gate"), this significantly enhances our ability to

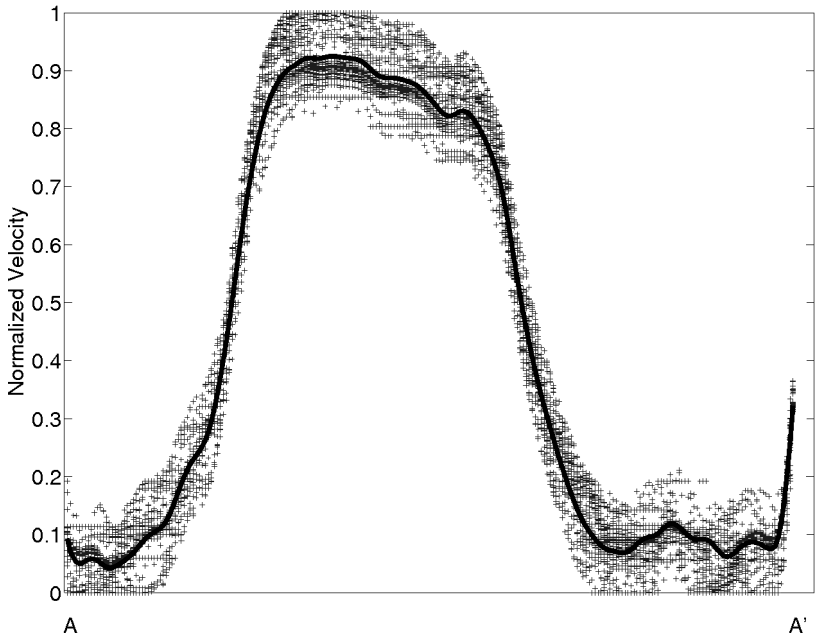

Figure 4.2. Standard surface velocity curve for Hubbard Glacier along flux gate A-A′ (Fig. 4.3). Individual measurements between 1985-2012 are shown as crosses, and the black line is the running mean.

remove false correlations.

First, we choose velocity fields that are free of cloud or shadow effects and calculate the dot product of the velocity field with the flux gate normal in each image. While the magnitudes of the velocities across this flux gate vary through time, the spatial pattern of the normalized velocity curves remains relatively constant (Fig. 4.2). We normalize these cross-sections to their individual maximum values and find the mean normalized velocity curve taken from the set of cross-sections. We take this curve of mean values to be the standard velocity curve for each glacier and use it to fill in holes found in other image pairs.

For each image that has cloud or shadowing effects, we apply the following technique. First, any values along the flux gate that indicate sharp transitions or spikes in velocity are discarded. Next, we discard values that are more than five standard deviations from the mean value along the flux gate. We then normalize this individual velocity curve to the maximum value along this curve, and exclude values that differ from the standard velocity curve by more than 0.1 (10%). Finally, we fill in the holes in this curve using the standard velocity curve found earlier, and the maximum cross-sectional velocity from this profile,

and smooth the final cross-sectional velocity curve with a moving average filter.

4.5.2 Frontal Ablation

We define the rate of frontal ablation u_f (the sum of the calving rate u_c and the melt rate at the terminus $\dot{m}$) as the difference between the ice velocity at the terminus u_t and the rate of change of the terminus position $\partial L/\partial t$ (cf. O'Neel and others, 2003; Amundson and Truffer, 2010):

$$u_f(t,x,y,z) = u_c(t,x,y,z) + \dot{m}(t,x,y,z) \cdot \hat{n} = u_t(t,x,y,z) - \frac{\partial L}{\partial t}(t,x,y,z) \cdot \hat{n}, \tag{4.1}$$

where $\hat{n}$ is the normal vector to the plane of the terminus. We choose the notation u_f because we are explicitly focusing on the mass loss at the terminus (frontal ablation), rather than only the mass lost through calving (Cogley and others, 2011). In this study, we choose to report frontal ablation as having a positive sign.

The total rate of frontal ablation F, is then u_f integrated over the terminus; because this surface is constantly changing, we instead integrate over a cross-section ("flux gate") of the glacier, Ω, located some distance upstream of the terminus. In so doing, we are introducing uncertainty into our estimates by assuming that no mass is lost to surface ablation after passing the flux gate, and we adjust our rates of frontal ablation accordingly (Section 4.5.3).

Here, we assign the coordinate y to be along the flux gate. Because $\partial L/\partial t$ is not defined at Ω, we use the width-averaged value, which we label dL/dt, and multiply it by the area of the flux gate, A. This has the same effect as integrating $\partial L/\partial t$ over the terminus:

$$F = \iint u_f \cdot \hat{n}\, dy\, dz = \iint u_t \cdot \hat{n}\, dy\, dz - A\frac{dL}{dt}, \tag{4.2}$$

where we have suppressed the notation (t,y,z) for ease of reading.

The depth-averaged velocity at a given location is the integral of the vertical ice velocity profile $u(z)$ over the ice thickness H at that location. At the glacier terminus, then, the depth-averaged velocity is:

$$\frac{1}{H}\int_H u(z)\, dz = \gamma u_s, \tag{4.3}$$

where u_s is the surface velocity, and $\gamma \in [0.8, 1]$ is a factor relating u_s to u (Cuffey and Paterson, 2010). Because the ice flow near the terminus of most tidewater glaciers is primarily driven by sliding, we assume that $\gamma = 0.9$ for all glaciers in this study (Rasmussen, 1988; Pfeffer, 2007; McNabb and others, 2012).

With this, our expression for F becomes (with the dependence of F on t and the dependences of H and u_s again made explicit):

$$F(t) = \gamma \int_0^W H(t,y)\, u_s(t,y) \cdot \hat{n}\, dy - A\frac{dL}{dt}, \tag{4.4}$$

where W is the width of the flux gate.

From Chapter 3, we have already calculated rates of change of terminus position by manually outlining terminus position for all 50 Alaska tidewater glaciers, giving us a time series of values of dL/dt for each glacier. For each glacier, we choose a flux gate (Ω) well upstream of the furthest retreated terminus position, and use this same flux gate for each velocity field.

4.5.3 Surface Mass Balance

Because our chosen flux gates are located some distance upstream of the terminus, we must adjust our rates of frontal ablation to account for mass lost through surface ablation between the flux gate and the terminus. The surface mass balance B of the area S between the flux gate and the terminus is the integral of the rate of surface mass balance $\dot{b}$ over that area. We assume that $\dot{b}$ is constant in both space and time, and equal to -10 m a^{-1}. This may well be a slight overestimation for most glaciers, but is approximately equal to maximum rates of both modeled and measured near-terminus surface mass balances in the region (Rasmussen and others, 2011; Johnson and others, 2013). B is then:

$$B = \int_S \dot{b}\, dS = \dot{b}S. \tag{4.5}$$

We calculate S for each velocity measurement, so for retreating glaciers B decreases with time (and increases with time for advancing glaciers).

4.6 Results

4.6.1 Surface Velocities

Mean values of surface velocity for each glacier's flux gate are given in Table 4.1. In general, velocities averaged along flux gates range from 0.5 m d^{-1} to 5.1 m d^{-1} throughout the study period. An example of a surface velocity field is shown in Fig. 4.3 for Hubbard Glacier; note areas of rapid apparent motion in both the fjord and over bedrock, while a much smoother field is shown over the glacier itself. This is due to iceberg motion in the

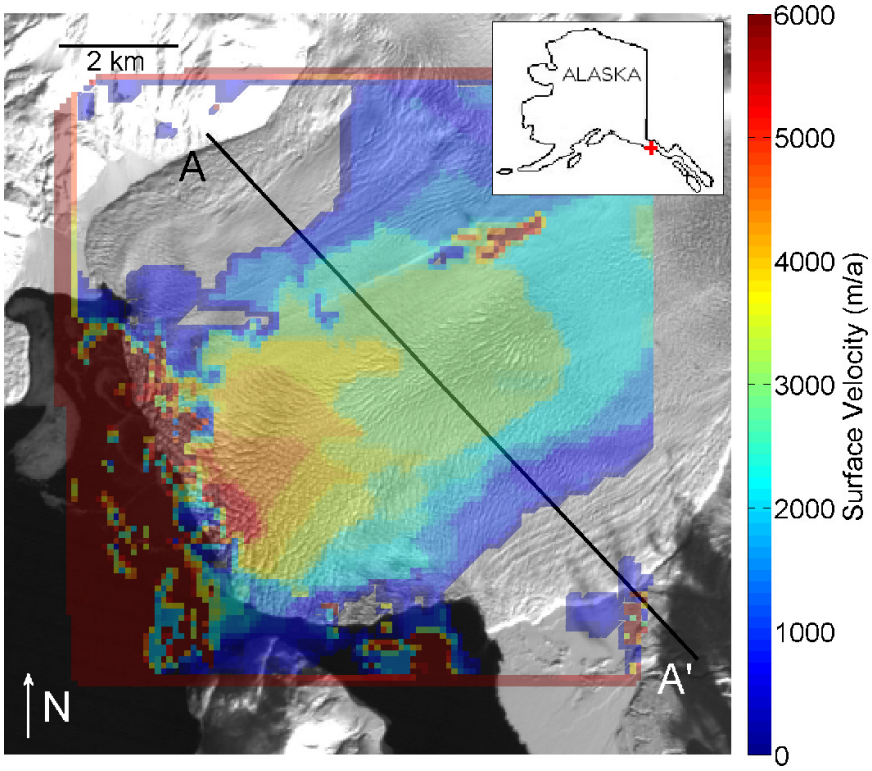

Figure 4.3. Surface velocity field for Hubbard Glacier, overlain with a Landsat 5 scene acquired 21 March 1995. Terminus positions from each scene (21 March 1995, 6 April 1995) are shown as red and white lines, respectively. Line A-A′ (black line) indicates the flux gate used for Hubbard Glacier.

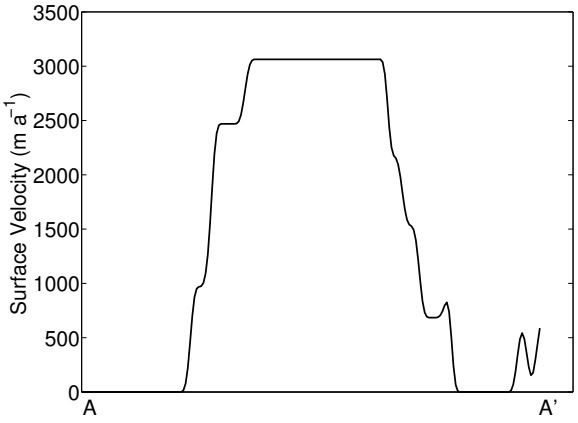

Figure 4.4. Cross-section of surface velocity field of Hubbard Glacier, taken along the line A-A′ (Fig. 4.4). Increase in velocity near A′ is most likely due to approaching the edge of the cropped images, and not any actual surface motion.

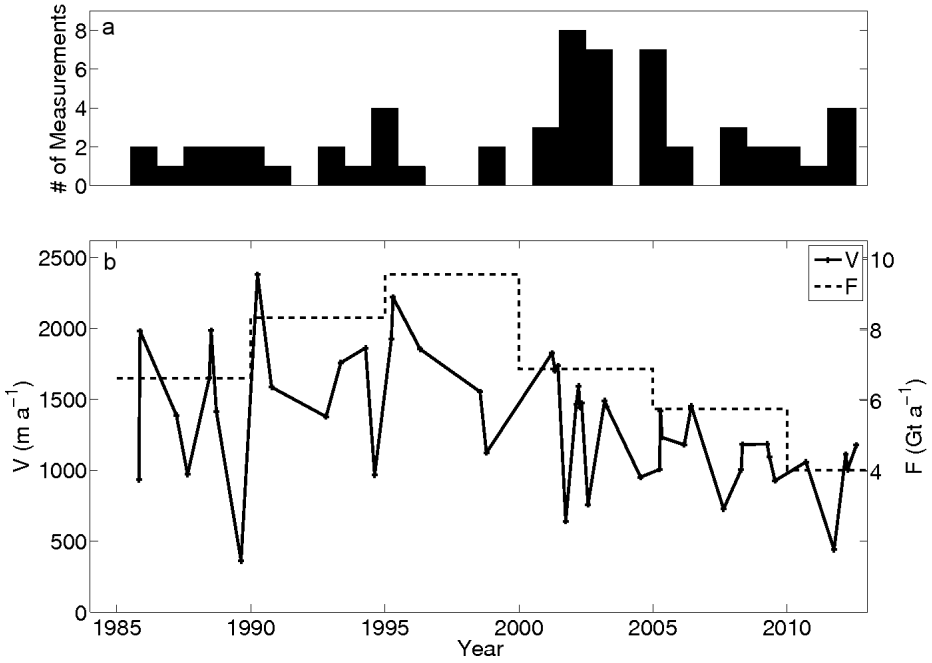

Figure 4.5. (a) Number of measurements (image pairs) per year for Hubbard Glacier used in this study. (b) Time series of mean cross-sectional velocity for Hubbard Glacier (solid line), and frontal ablation (F) time series integrated over five-year segments (dashed line).

fjord and changing snow cover and shadow, respectively. Images where these errors dominate the area around the flux gate are discarded; otherwise, these errors are masked and the velocity field filled in using the filtering procedure described earlier. Figure 4.4 shows a cross-section of this velocity field along the line A-A', while the whole time series for Hubbard Glacier is shown in Fig. 4.5.

For many glaciers, there is a clear, persistent, seasonal variation in the velocity record (Fig. 4.6). For each glacier, we estimate the seasonal amplitude, as well as the timing of the seasonal cycle, by taking three-month averages of velocities (December-January-February (DJF), March-April-May (MAM), June-July-August (JJA), September-October-November (SON)). We then average these seasonal values over the whole time period to estimate an average deviation from the trend in a given year. In general, the seasonal cycle amplitude is approximately 50% of the peak velocity, varying between approximately 20 and 80% of the peak velocities. Most peak velocities occur in spring/early summer, with the slowest velocities coming in late summer/early autumn (Fig. 4.7).

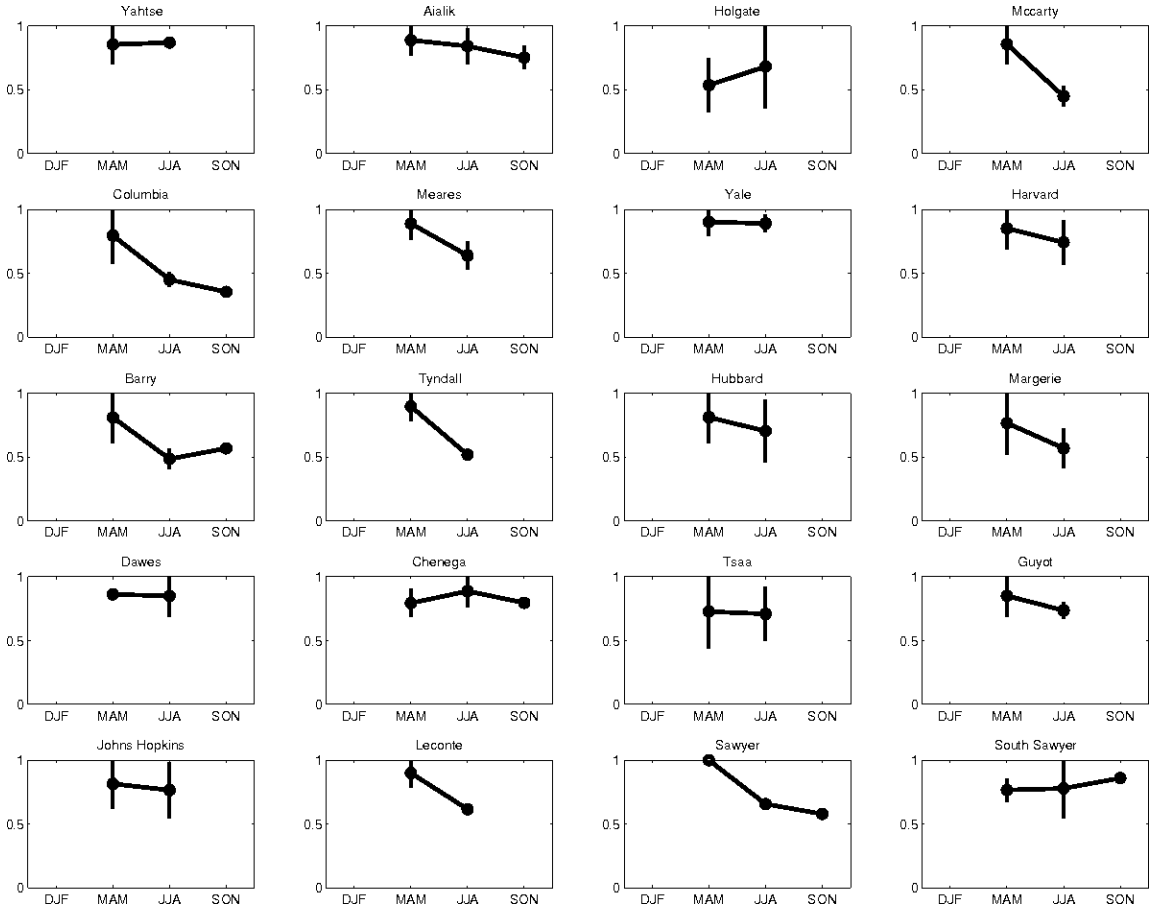

Figure 4.6. Mean seasonal surface velocity for each of the 20 glaciers in this study, normalized to the maximum observed velocity. Error bars indicate standard deviation from mean for each three-month period.

4.6.2 Frontal Ablation

Because our timeseries of frontal ablation values are not constantly spaced in time, we integrate the time series for each glacier and divide by the total timespan in order to compare rates between glaciers. These values are reported in Table 4.1. We also integrate over pentades between 1985 and 2009, and over the three year period 2010-2012, to construct a time series for the region (Fig. 4.8). These pentades give us an estimate of how frontal ablation changes over time; they also help to reduce the reliance on a single measurement in a given year, which may not be representative of the annual frontal ablation.

The glacier with the highest rate of frontal ablation over the study period is Hubbard Glacier, with a mean rate of 6.5 ± 2.6 Gt a^{-1}, followed by Columbia Glacier, with a mean

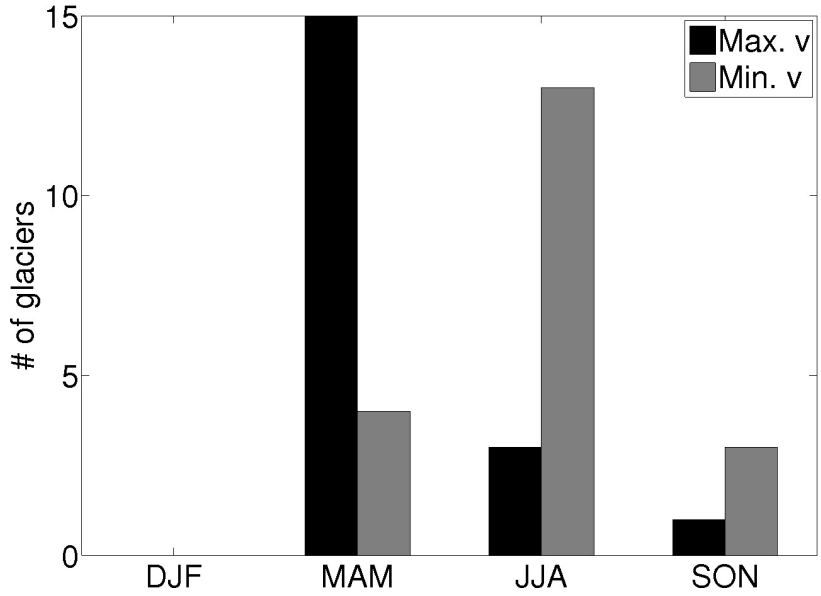

Figure 4.7. Timing of maximum and minimum surface velocity for each of the 20 glaciers in this study.

rate of 2.8 ± 1.1 Gt a^{-1}. Hence, two glaciers represent approximately 57% of the frontal ablation over the time period of this study. Another three glaciers (Yahtse, Harvard, and LeConte) have rates of frontal ablation of approximately 0.9 Gt a^{-1} or greater; these five glaciers represent over 75% of the loss through frontal ablation for the 20 glaciers studied.

If we look at specific rates of frontal ablation (frontal ablation normalized by the glacier area), several glaciers stand out. First, Aialik Glacier has a relatively low rate of frontal ablation (0.3 ± 0.1 Gt a^{-1}), but by far the highest specific rate of frontal ablation (3.88 m water equivalent (w.e.) a^{-1}). The next three glaciers with the largest rate of specific frontal ablation are Guyot Glacier, Columbia Glacier, and Meares Glacier (2.95 m w.e. a^{-1}, 2.93 m w.e. a^{-1}, and 2.83 m w.e. a^{-1}, respectively); of these, only Columbia Glacier ranks higher than fifth in terms of total loss through frontal ablation for the region.

4.6.3 Uncertainty Analysis

Uncertainty in values of frontal ablation arises primarily from uncertainty in values of surface velocity, and uncertainty in values of ice thickness. Uncertainties in surface velocities arise from point identification in images and interpolation of irregularly spaced data to grid nodes, as well as the error in georeferencing. We use the following equation to esti-

mate the uncertainty (in m a^{-1}) in velocities derived from aerial photographs (cf. McNabb and others, 2012):

$$E_{\text{vel}} = 365\frac{C\Delta x}{\Delta t}, \tag{4.6}$$

where C is uncertainty in image registration and feature tracking in pixels (p), Δx is the image resolution in m p^{-1}, and Δt is the time separation between successive images in days. Using typical values of one pixel for C, 30 m p^{-1} for Δx, and 32 d for Δt, we estimate an uncertainty of 345 m a^{-1} in velocity values derived from Landsat 5 scenes, and 171 m a^{-1} in velocity values derived from Landsat 7 scenes (Δx = 15 m p^{-1}). Given typical values of surface velocity averaged over cross-sectional profiles, this corresponds to a ∼20% uncertainty in velocity.

Uncertainties in ice thickness arise primarily from errors in the thickness modeling, the glacier outlines and DEM used, and field data (Huss and Farinotti, 2012). Based on comparison of modeled and measured ice thicknesses, Huss and Farinotti (2012) estimate that the root-mean-square of the relative single-glacier error is approximately 30%, which

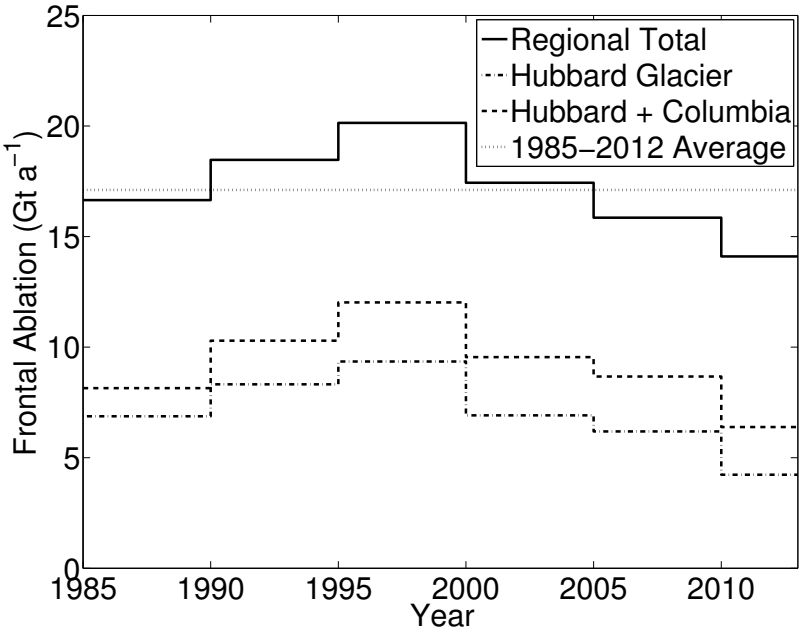

Figure 4.8. Pentadally-averaged values of frontal ablation for the 20 glaciers used in this study (solid line), Hubbard Glacier alone (dash-dot line), Hubbard and Columbia Glaciers (dashed line), and the 1985-2012 average for the 20 glaciers.

we adopt here. This estimate is slightly lower than our comparison with Columbia Glacier data (Section 4.4.2), which covered the whole glacier. Comparison in the lower part of the glacier yields a lower error than the glacier as a whole, so we adopt 30% as a reasonable estimate for the region as a whole.

Uncertainties can also arise when assuming that ice thickness H is constant in time. At this time, we only have information about how ice thickness at Columbia Glacier has changed over the course of the study period, and we analyze the effect of this assumption on rates of frontal ablation by using a single year's ice thickness for Columbia Glacier. For this analysis, we use the 2007 SPOT DEM (Korona and others, 2009), as Huss and Farinotti (2012) calculate ice thickness and bed topography using DEMs that are primarily from 2000 onward. The resulting mean rate of frontal ablation for Columbia Glacier, using only the 2007 ice thickness, is 2.0 ± 0.8 Gt a^{-1} (cf. 2.8 ± 1.1 Gt a^{-1} using the evolving ice thicknesses), or an uncertainty of $\sim$30%. Because of the high rates of thinning observed at Columbia Glacier over the course of its retreat, we would expect the actual uncertainties introduced at other glaciers to be much lower. In addition, several glaciers (e.g., Hubbard and Harvard Glaciers) have been thickening and advancing over the course of this study; using evolving ice thicknesses for these glaciers would result in lower estimates of frontal ablation. Because we are unable to quantify these uncertainties for other glaciers, we do not include this term in estimating the final uncertainties in our results.

Finally, uncertainties in rates of glacier length change arise primarily from errors in manual digitization of terminus outlines and errors in georeferencing of images (Chapter 3). Based on this, we estimate that the uncertainty in annual rates of glacier length change are approximately 10%. Assuming that each of these uncertainties (surface velocities, ice thicknesses, and glacier length change) are uncorrelated, we arrive at a final estimate for uncertainty in rates of frontal ablation of 40%.

4.6.4 Scaling to Entire Region

Figure 4.9 shows that, in general, glaciers with a larger area lose more mass through frontal ablation. In itself, this is not especially surprising - glaciers with more area are generally thicker, have larger calving fronts, and have higher surface velocities. We can use this relationship to scale our rates of frontal ablation to estimate the value for all Alaska tidewater glaciers. The scaled values (along with the glacier areas) are shown in Table 4.2; summing the scaled estimates for the other 30 glaciers yields an additional 2.1 ± 0.8 Gt a^{-1}, for a total

Table 4.2. Frontal ablation for the remaining Alaska tidewater glaciers not included in this study, derived from applying the scaling relationship shown in Fig. 4.9.

Name	Area km^2	F Gt a^{-1}	Name	Area km^2	F Gt a^{-1}
Grand Pacific	565	0.5	Blackstone	68	0.1
Turner	177	0.2	Tiger	59	0.1
Northwestern	161	0.1	Moraine/Apron	30	0.0
Lamplugh	142	0.1	Bryn Mawr	26	0.0
Shoup	131	0.1	Gilman	26	0.0
La Perouse	124	0.1	Beloit	23	0.0
McBride	119	0.1	Coxe	20	0.0
Riggs	116	0.1	Smith	19	0.0
Nellie Juan	98	0.1	Cascade	17	0.0
North Crillon	90	0.1	Wellesley	15	0.0
Lituya	84	0.1	Anchor	14	0.0
Muir	78	0.1	Grotto	11	0.0
Surprise	77	0.1	Hoonah	11	0.0
Reid	70	0.1	Kashoto	5	0.0
Harriman	69	0.1	Ogive	3	0.0
All glaciers	2450	2.1			

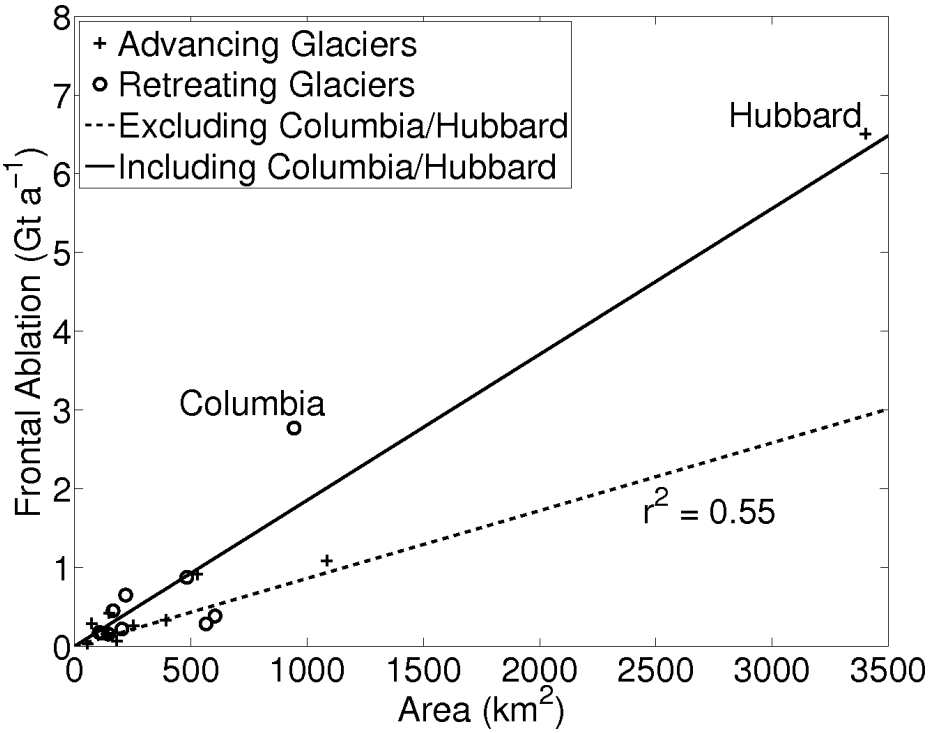

Figure 4.9. Frontal Ablation as a function of Area for the 20 glaciers used in this study. Glaciers that advanced over the period 1985-2012 are shown as crosses, glaciers that retreated over the same time period are shown as circles. Dashed line indicates linear fit to all data, with coefficient of determination (r^2) as indicated.

for the region of 18.3 ± 7.3 Gt a^{-1}. The 20 glaciers that we use in this study, then, represent $\sim$89% of the total frontal ablation from the region.

4.7 Discussion

4.7.1 Surface Velocities

Our velocity record shows a seasonal variation in velocity for most glaciers in the region, reflecting the seasonal variation of different factors that affect flow velocity, such as glacier hydrology, surface mass balance, and fjord conditions. The amplitude of these variations can be quite large, even when averaged over a cross-sectional profile of the glacier. On average, the amplitude of the seasonal variation in surface velocity is 55 ± 25% of the peak annual velocity, with the lowest velocity values coming in the summer months (JJA). If estimates of frontal ablation are made using only one velocity measurement, or using velocity measurements from only one time of year, they may severely overestimate or underesti-

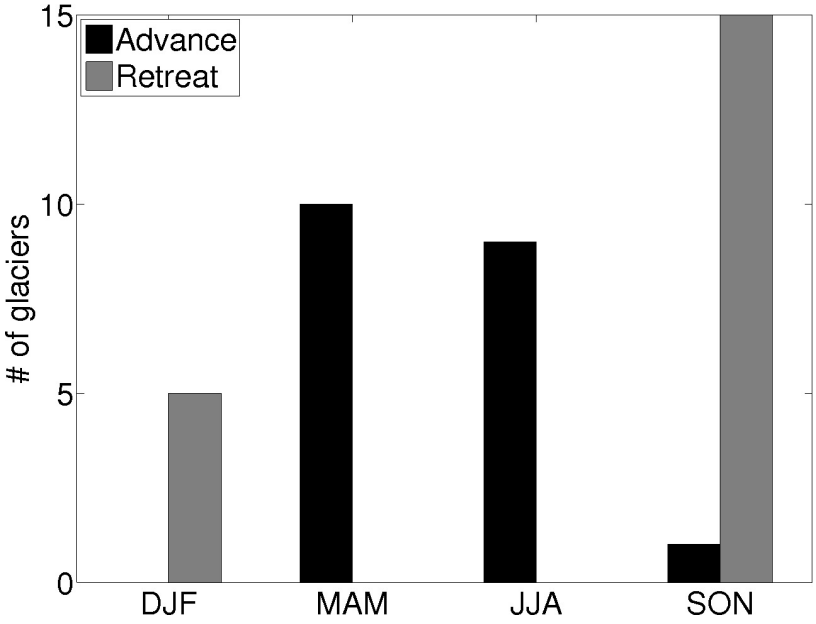

Figure 4.10. Timing of maximum advance and retreat for each of the 20 glaciers in this study.

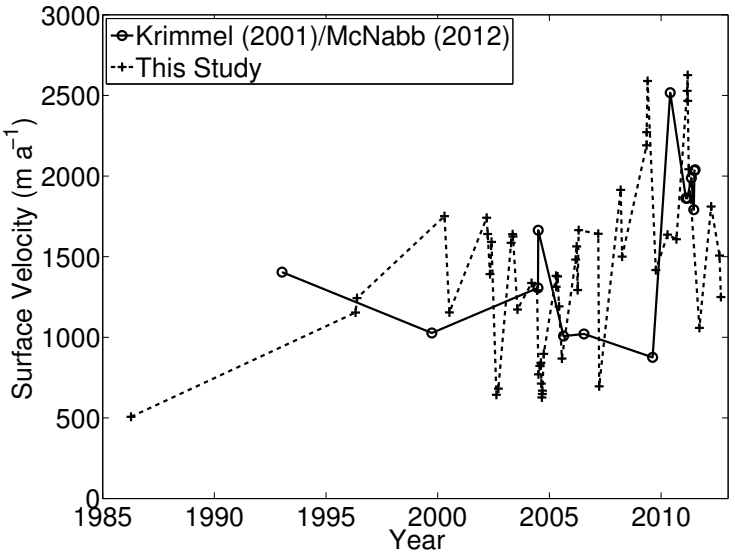

Figure 4.11. Surface velocities for Columbia Glacier from Krimmel (2001) and McNabb and others (2012) (circles), compared to surface velocities derived in this study from Landsat feature tracking (crosses).

mate the actual frontal ablation, possibly by as much as 80%.

In general, seasonality of velocities matches with seasonality of length changes for the 20 glaciers in this study (Fig. 4.10). Most glaciers are at their peak velocity in the spring/summer months (19 of 20 glaciers), and most glaciers are at their maximum seasonal lengths in those months (19 of 20). Most glaciers are at their minimum surface velocities in the summer months (13 of 20 glaciers) while most glaciers reach their minimum seasonal length in the fall (15 glaciers) or winter (five glaciers). Because the rate of length change is generally defined as the difference between ice velocity and the rate of frontal ablation at the terminus (e.g., Ritchie and others, 2008), this indicates that rates of frontal ablation are not constant throughout the year. This poses another issue with using measurements from one time of the year.

This seasonal variation in rates of frontal ablation allows us to consider potential mechanisms driving frontal ablation throughout the year. As surface velocities decrease after a spring speedup, rates of frontal ablation increase as both air and fjord water temperatures increase. Penetration of meltwater into crevasses has been hypothesized as one mechanism to increase calving (Benn and others, 2007), and submarine melting is increased by both increased ocean water temperatures and convection driven by mixing of fjord water with meltwater at the terminus (Motyka and others, 2003). As air and fjord water temperatures decrease into the fall and winter, frontal ablation slows, and the glacier begins to readvance.

Several glaciers in the region have records of ice velocity that we can compare to our values. Trabant and others (2003) give centerline values of ice velocity for Hubbard Glacier of approximately $5-9$ m d^{-1} at a location near our flux gate over the period 1980-2000, matching our values for the centerline velocity of Hubbard Glacier. Krimmel (2001) and McNabb and others (2012) publish a record of ice velocity for Columbia Glacier from 1983-2012, overlapping with the time period of our Landsat scenes; a comparison of these records is shown in Fig. 4.11. In general, these records agree well with each other, indicating that our reported uncertainty in ice velocity of 345 m a^{-1} may be an upper bound.

4.7.2 Frontal Ablation

Brown and others (1982) present estimates of calving rate and calving flux for 12 Alaska tidewater glaciers, several of which we study here. A comparison of our estimates with theirs is shown in Table 4.3. The time periods of these two studies do not overlap, which

Table 4.3. Comparison of estimates of frontal ablation from Brown and others (1982) and this study. Period of estimates for Brown and others (1982) are given (MM/DD/YY); all estimates for this study are for the period 1985-2012.

Name	Period	Brown and others (1982)	This study (1985-2012)
		Gt a^{-1}	Gt a^{-1}
McCarty	8/64-8/65	< 0.1	0.2
Harvard	6/21/78-9/1/78	0.2	0.9
Yale	7/15/77-9/3/77	0.9	0.5
Meares	7/15/77-9/3/77	0.1	0.4
Columbia	10/1/77-9/31/78	1.3	2.8
Tyndall	8/64-8/65	0.5	0.2
Hubbard	8/20/77-10/1/77	2.2	6.5
Margerie	7/17/77-9/1/77	0.1	0.1
Johns Hopkins	7/17/77-9/1/77	0.4	0.3
South Sawyer	7/12/77-8/30/77	0.8	0.3

may account for several of the discrepancies we find. For example, their estimate for Columbia Glacier is based on surface velocities and ice thickness measurements from 1977, before Columbia Glacier began its rapid retreat. Yale Glacier was in the midst of a rapid retreat in 1977, and it has since largely stabilized. Brown and others' ice velocity values also come from late in the summer (July-September), when many of these glaciers are reaching their slowest speeds. Thus, many of their values are likely underestimations of the true annual value of frontal ablation, a fact that is reflected by our apparent overestimation of their values. O'Neel and others (2003) estimated a rate of frontal ablation of 1.0 Gt a^{-1} for LeConte Glacier over the period 2 May - 4 June 1999, in line with our estimate of 0.9 ± 0.4 Gt a^{-1}.

O'Neel and others (2003) also estimated that the near-terminus surface mass balance (B) of LeConte Glacier amounted to ~ -0.07 Gt a^{-1}, or $\sim$10% of the rate of frontal ablation. This compares well with our estimate for LeConte Glacier ($B \approx -0.04$ Gt a^{-1}). It also compares well overall with our estimates for the region as a whole, where the mean value ($\pm$ one standard deviation) of B for all 20 glaciers is -0.06 ± 0.09 Gt a^{-1}, and the regional value of B is $\sim$8% of F. While one might expect that our implicit assumption that $\dot{b}$ does not change seasonally would have an effect on the seasonality observed in rates of

F, the overall low percentage of B compared to F suggests that this would not be much of a concern.

Our estimate of 2.8 ± 1.1 Gt a^{-1} of frontal ablation for Columbia Glacier, 1985-2012, is somewhat lower than both the estimate from Rasmussen and others (2011) of 5.5 Gt a^{-1} for the period 1982-2007, and ice flux estimate for 1983-2001 from O'Neel and others (2005) of 3.3 Gt a^{-1}. Rasmussen and others (2011) estimate "calving" as the difference between surface mass balance and volume change, while O'Neel and others (2005) estimate ice discharge using the same flux gate approach that we use. Both Rasmussen and others (2011) and this study indicate an uptick in frontal ablation after 2001 for Columbia Glacier.

4.7.3 Total Mass Loss

Here, we use the "best estimate" for regional mass loss over the period 2003-2009 of 50 ± 17 Gt a^{-1} from Gardner and others (2013); this estimate results from other studies whose estimates range between ~ 40 and ~ 85 Gt a^{-1}, albeit over different time periods (Luthcke and others, 2008; Berthier and others, 2010; Jacob and others, 2012; Luthcke and others, 2013). The change in mass ΔM for the region can be written:

$$\Delta M = B_{\text{clim}} - F, \tag{4.7}$$

where B_{clim} is the climatic mass balance of the region (i.e. the sum of the surface and internal mass balances; Cogley and others, 2011).

Given the value of 50 ± 17 of ΔM and our estimate for F, the climatic mass balance for the region over the period 2003-2009 must be extremely negative (approximately -15 to 50 Gt a^{-1}). Without frontal ablation, then, the mass loss from Alaska glaciers would be significantly lower, at around 30 Gt a^{-1}. Frontal ablation, then, is a significant and non-negligible component of the regional mass budget for Alaska glaciers, despite coming from only $\sim 15\%$ of the glacierized area in the region. This agrees with the range of contributions observed in Svalbard, Patagonia, and the Greenland and Antarctic ice sheets, where frontal ablation is a significant portion of the regional mass budget (Błaszczyk and others, 2009; van den Broeke and others, 2009; Gardner and others, 2011; Shepherd and others, 2012; Gardner and others, 2013; Rignot and others, 2013).

Hagen and others (2003) estimate a value for frontal ablation from all Svalbard tide-water glaciers of 4 ± 1 Gt a^{-1}, amounting to nearly 90% of the net mass loss from the archipelago. Using ASTER imagery to estimate ice velocities, Błaszczyk and others (2009)

estimate a value of 6.75 ± 1.7 Gt a^{-1} frontal ablation for the period 2000-2006. Svalbard glaciers cover an area of about $36,600$ km^2, meaning a range in specific mass loss of $0.11 - 0.27$ m w.e. a^{-1}. Rignot and Kanagaratnam (2006) estimate loss due to frontal ablation from the Greenland ice sheet of 150 Gt a^{-1}, for a specific mass loss of 0.09 m w.e. a^{-1}. Taking an area of $89,000$ km^2 for all Alaska glaciers, we estimate a specific mass loss of 0.21 m w.e. a^{-1} from frontal ablation for all Alaska glaciers. This value is near the upper end of the estimate for Svalbard, and is over three times the estimate for Greenland, indicating the importance of frontal ablation in the mass budget of regions with tidewater glaciers.

4.8 Conclusion

Using Landsat scenes and a feature tracking algorithm, we have presented a long-term record of ice velocity for 20 Alaska glaciers over the period 1985-2012. Using these surface velocities, estimates of ice thickness, derived rates of length change, and a first-order estimate of surface mass balance between the flux gate and the terminus, we present a record of frontal ablation for these 20 glaciers; to our knowledge, this is the first detailed, regional-scale, long-term study of frontal ablation for Alaska tidewater glaciers.

For the entire set of glaciers studied, we estimate a mean rate of frontal ablation of 16.2 ± 6.5 Gt a^{-1} over the period 1985-2012; assuming a linear relationship between glacier area and frontal ablation rate, we extend this estimate to 30 other tidewater glaciers in Alaska, giving a final result of 18.3 ± 7.3 Gt a^{-1} lost through frontal ablation for Alaska tidewater glaciers. Comparison of our estimates for individual glaciers with estimates from other studies yields general agreement; we find that large discrepancies are likely a result of differences in measurement period or extension of measurements from a single time of year to annual averages.

We find that surface velocities for Alaska tidewater glaciers are highly seasonal, with the seasonal amplitude averaging approximately 50% of the peak velocity, peak values occurring early in the summer, and the lowest values occurring late in the summer. Any estimates of frontal ablation made using surface velocities should take this seasonal variability into consideration.

These seasonal cycles agree with observed seasonal cycles of glacier length, though there is a clear lag between the lowest surface velocities and the most retreated seasonal terminus position, indicating that rates of frontal ablation are not constant throughout the year. This seasonality, in turn, indicates that changes in ice flux from up glacier alone do

not account for the seasonal length change, and suggests that other processes (increased submarine melt, increased calving driven by meltwater-induced fractures) assume control later in the year when ice flux decreases.

Our regional estimate of frontal ablation indicates the overall importance of frontal ablation in the mass budget of all Alaska glaciers. Without frontal ablation, the mass loss from Alaska Glaciers would be significantly reduced, from ~ 50 Gt a^{-1} to ~ 30 Gt a^{-1}, despite only coming for approximately 15% of the total glacier area; this fact serves to highlight the overall importance of frontal ablation in the mass budget of regions with tidewater glaciers, a finding echoed by other studies. We do not, however, suggest that frontal ablation is the primary driver of the mass budget of tidewater glacier regions, as do some other studies; such an attribution requires knowledge of the total ablation from the region, information that we do not possess. The regional total of frontal ablation is heavily dominated by two glaciers in particular (Hubbard and Columbia), suggesting that regional rates of frontal ablation can be well approximated by studying only a few glaciers.

4.9 References

Alley, R. B., H. J. Horgan, I. Joughin, K. M. Cuffey, T. K. Dupont, B. R. Parizek, S. Anandakrishnan and J. Bassis, 2008. A simple law for ice-shelf calving, *Science*, **322**(5906), 1344, doi:10.1126/science.1162543.

Amundson, J. M. and M. Truffer, 2010. A unifying framework for iceberg calving models, *J. Glaciol.*, **56**(199), 822–830.

Arendt, A., K. Echelmeyer, W. Harrison, C. Lingle and B. Valentine, 2002. Rapid wastage of Alaska glaciers and their contribution to rising sea level, *Science*, **297**(5580), 382–386.

Arendt, A., K. Echelmeyer, W. Harrison, C. Lingle, S. Zirnheld, V. Valentine, B. Ritchie and M. Druckenmiller, 2006. Updated estimates of glacier volume changes in the western Chugach Mountains, Alaska, and a comparison of regional extrapolation methods, *J. Geophys. Res.*, **111**(F03019).

Bassis, J. N., 2011. The statistical physics of iceberg calving and the emergence of universal calving laws, *J. Glaciol.*, **57**(201), 3–16.

Benn, D. I., N. R.J. Hulton and R. H. Mottram, 2007. 'Calving laws', 'sliding laws' and the stability of tidewater glaciers, *Ann. Glaciol.*, **46**, 123–130.

Berthier, E., E. Schiefer, G. K. C. Clarke, B. Menounos and F. Rémy, 2010. Contribution of Alaskan glaciers to sea-level rise derived from satellite imagery, *Nature Geosci.*, **3**, 92–95.

Błaszczyk, M., J. A. Jania and J. O. Hagen, 2009. Tidewater Glaciers of Svalbard: Recent changes and estimates of calving fluxes, *Polish Polar Res.*, **30**(2), 85–142.

Borstad, C. P., A. Khazendar, E. Larour, M. Morlighem, E. Rignot, M. P. Schodlok and H. Seroussi, 2012. A damage mechanics assessment of the Larsen B ice shelf prior to collapse: Toward a physically-based calving law, *Geophys. Res. Lett.*, **39**(L18502), doi:10.1029/2012GL053317.

van den Broeke, M., J. Bamber, J. Ettema, E. Rignot, E. Schrama, W. J. van de Berg, E. van Meijgaard, I. Velicogna and B. Wouters, 2009. Partitioning recent Greenland mass loss, *Science*, **326**, doi:10.1126/science.1178176.

Brown, C. S., M.F. Meier and A. Post, 1982. Calving speed of Alaska tidewater glaciers, with application to Columbia Glacier, *USGS Prof. Pap.*, **1258-C**.

Burgess, D., M. J. Sharp, D. W. F. Mair, J. Dowdeswell and T. J. Benham, 2005. Flow dynamics and iceberg calving rates of Devon Ice Cap, Nunavut, Canada, *J. Glaciol*, **51**(173), 219–230.

Calkin, P. E., G. C. Wiles and D. J. Barclary, 2001. Holocene coastal glaciation of Alaska, *Quat. Sci. Rev.*, **20**, 449–461.

Cogley, J. G., R. Hock, L. A. Rasmussen, A. A. Arendt, A. Bauder, R. J. Braithwaite, P. Jansson, G. Kaser, M. Möller, L. Nicholson and M. Zemp, 2011. Glossary of glacier mass balance and related terms, vol. 86 of *IHP-VII Tech. Doc. in Hydrol.*, UNESCO-IHP, Paris, IACS Contribution No. 2.

Cuffey, K. M. and W. S. B. Paterson, 2010. The physics of glaciers, Butterworth-Heinemann, fourth ed.

Dowdeswell, J. A., R. Bassford, M. Gorman, M. Williams, A. Glazovsky, Y. Macheret, A. Shepherd, Y. Vasilenko, L. Savatyuguin and H. Hubberten, 2002. Form and flow of the Academy of Sciences Ice Cap, Severnaya Zemlya, Russian High Arctic, *J. Geophys. Res.*, **107**(B4), doi 10.1029/2000JB000129.

Dowdeswell, J., J. Benham, T. Strozzi and J. O. Hagen, 2008. Iceberg calving flux and mass balance of the Austfonna ice cap on Nordaustlandet, Svalbard, *J. Geophys. Res.*, **113**(F03022), doi:10.1029/2007JF000905.

Dyurgerov, M. B., 2010. Reanalysis of Glacier Changes: From the IGY to the IPY, 1960-2008, *Data of Glaciol. Studies*, **108**, 1–116.

Gardner, A. S., G. Moholdt, B. Wouters, G. J. Wolken, D. O. Burgess, M. J. Sharp, J. G. Cogley, C. Braun and C. Labine, 2011. Sharply increased mass loss from glaciers and ice caps in the Canadian Arctic Archipelago, *Nature*, **473**, 357–360.

Gardner, A. S., G. Moholdt, J. G. Cogley, A. A. Arendt, J. Wahr, E. Berthier, R. Hock, W. T. Pfeffer, G. Kaser, S. R. M. Ligtenberg, T. Bolch, M. J. Sharp, J. O. Hagen, M. van den Broeke and F. Paul, 2013. A consensus estimate of glacier contributions to sea level rise: 2003-2009, *Science*, **340**, doi:10.1126/science1234532.

Hagen, J. O., K. Melvold, F. Pinglot and J. A. Dowdeswell, 2003. On the net mass balance of the glaciers and ice caps in Svalbard, Norwegian Arctic, *Arct., Antarct., and Alp. Res.*, **35**(2), 264–270.

Hock, R., M. de Woul, V. Radić and M. Dyurgerov, 2009. Mountain glaciers and ice caps around Antarctica make a large sea-level rise contribution, *Geophys. Res. Lett.*, **36**(L07501), doi:10.1029/2008GL037020.

Holland, D. M., R. H. Thomas, B. De Young, M. H. Ribergaard and B. Lyberth, 2008. Acceleration of Jakobshavn Isbræ triggered by warm subsurface ocean waters, *Nature Geosci.*, **1**, 659–664, doi:10.1038/ngeo316.

Huss, M. and D. Farinotti, 2012. Distributed ice thickness and volume of all glaciers around the globe, *J. Geophys. Res.*.

IPCC, 2007. Climate Change 2007: The Physical Science Basis: Contribution of Working Group I to the Fourth Assessment Report of the Intergovernmental Panel on Climate Change, Cambridge University Press, [S. Solomon and D. Qin and M. Manning and Z. Chen and M. Marquis and K. B. Averyt and M. Tignor and H. L. Miller (eds.)].

Jacob, T., J. Wahr, W. T. Pfeffer and S. Swenson, 2012. Recent contributions of glaciers and ice caps to sea level rise, *Nature*, **482**, 514–518, doi:10.1038/nature10847.

Johnson, A. J., C. F. Larsen, N. Murphy, A. A. Arendt and S. L. Zirnheld, 2013. Mass balance in the Glacier Bay area of Alaska, USA, and British Columbia, Canada, 1995-2011, using airborne laser altimetry, *J. Glaciol.*, **59**(216), doi:10.3189/2013JoG12J101.

Korona, J., E. Berthier, M. Bernard, F. Rémy and E. Thouvenot, 2009. SPIRIT. SPOT 5 stereoscopic survey of polar ice: Reference images and topographies during the fourth international polar year (2007-2009), *ISPRS J. of Photogrammetry and Remote Sensing*, **64**(2), 204âĂŞ212.

Krimmel, R. M., 2001. Photogrammetric data set, 1957-2000, and bathymetric measurements for Columbia Glacier, Alaska, *USGS Water Res. Invest. Rep.*, **014089**.

Larsen, C. F., R. J. Motyka, A. A. Arendt, K. A. Echelmeyer and P. E. Geissler, 2007. Glacier changes in southeast Alaska and northwest British Columbia and contribution to sea level rise, *J. Geophys. Res.*, **112**(F01007).

Luthcke, S. B., A. A. Arendt, D. D. Rowlands, J. J. McCarthy and C. F. Larsen, 2008. Recent glacier mass changes in the Gulf of Alaska region from GRACE mascon solutions, *J. Glaciol.*, **54**(188), 767–777.

Luthcke, S. B., T. Sabaka, B. Loomis, A. Arendt, J. McCarthy and J. Camp, 2013. Antarctica, Greenland and Gulf of Alaska land ice evolution from an iterated GRACE global mascon solution, *J. Glaciol.*, **59**(216), doi:10.3189/2013JoG12J147.

McNabb, R., R. Hock, S. O'Neel, L. A. Rasmussen, Y. Ahn, M. Braun, H. Conway, S. Herreid, I. Joughin, W. T. Pfeffer, B. E. Smith and M. Truffer, 2012. Using Surface Velocities to Calculate Ice Thickness and Bed Topography: A Case Study at Columbia Glacier, Alaska, *J. Glaciol.*, **58**(212).

Meier, M. and M. Dyurgerov, 2002. How Alaska affects the world, *Science*, **297**, 350–351.

Meier, M. F. and A. Post, 1987. Fast tidewater glaciers, *J. Geophys. Res.*, **92**(B9), 9051–9058.

Meier, M., S. Lundstrom, D. Stone, B. Kamb, H. Engelhardt, N. Humphrey, W. Dunlap, M. Fahnestock, R. Krimmel and R. Walters, 1994. Mechanical and hydrologic basis for the rapid motion of a large tidewater glacier, 1. Observations, *J. Geophys. Res.*, **99**(B8), 15219–15229.

Meier, M. F., M. B. Dyurgerov, U. K. Rick, S. O'Neel, W. T. Pfeffer, R. S. Anderson, S. P. Anderson and A. F. Glazovsky, 2007. Glaciers dominate eustatic sea-level rise in the 21st century, *Science*, **317**(1064), doi:10.1126/science.1143906.

Moholdt, G., J. O. Hagen, T. Eiken and T. V. Schuler, 2012. Geometric changes and mass balance of the Austfonna ice cap, Svalbard, *The Cryosphere*, **4**, 21–34.

Molnia, B. F., 2008. Glaciers of North America – Glaciers of Alaska, R. S. Williams, Jr. and J. G. Ferrigno, eds., Satellite image atlas of glaciers of the world, United States Geological Survey, K52–K83, USGS Prof. Pap. 1386-K.

Motyka, R. J. and M. Truffer, 2007. Hubbard Glacier, Alaska: 2002 closure of Russell Fjord and implications for future dams, *J. Geophys. Res.*, **112**(F2), F02004, doi:10.1029/2006JF000475.

Motyka, R. J., L. Hunter, K. Echelmeyer and C. Connor, 2003. Submarine melting at the terminus of a temperate tidewater glacier, Leconte Glacier, Alaska, *Ann. Glaciol.*, **36**, 57–65.

Motyka, R. J., M. Fahnestock, M. Truffer, J. Mortensen and S. Rysgaard, 2011. Submarine melting of the 1985 Jakobshavn Isbræ floating tongue and the triggering of the current retreat, *J. Geophys. Res.*, **116**(F1), doi:10.1029/2009JF001632.

Nuth, C., T. V. Schuler, J. Kohler, B. Altna and J. O. Hagen, 2012. Estimating the long-term calving flux of Kronebreen, Svalbard, from geodetic elevation changes and mass-balance modelling, *J. Glaciol.*, **58**(207), 119–133.

O'Neel, S., K. A. Echelmeyer and R. J. Motyka, 2003. Short-term variations in calving of a tidewater glacier: LeConte Glacier, Alaska, U.S.A., *J. Glaciol.*, **49**(167), 587–598.

O'Neel, S., W. T. Pfeffer, R. Krimmel and M. Meier, 2005. Evolving force balance at Columbia Glacier, Alaska, during its rapid retreat, *J. Geophys. Res.*, **110**(F03012), doi:10.1029/2005JF000292.

Pelto, M. S. and C.R. Warren, 1991. Relationship between tidewater glacier calving velocity and water depth at the calving front, *Ann. Glaciol.*, **15**, 115–118.

Pfeffer, W. T., 2007. A simple mechanism for irreversible tidewater glacier retreat, *J. Geophys. Res.*, **112**(F03S2), doi:10.1029/2006JF000590.

Radić, V. and R. Hock, 2011. Regionally differentiated contribution of mountain glaciers and ice caps to future sea-level rise, *Nat. Geosci.*, **4**, 91–94, doi:10.1038/NGEO1052.

Radić, V., A. Bliss, A. C. Beedlow, R. Hock, E. Miles and J. G. Cogley, 2013. Regional and global projections of twenty-first century glacier mass changes in responce to climate scenarios from global climate models, *Clim. Dyn.*, doi:10.1007/s00382-013-1719-7.

Rasmussen, L. A., 1988. Bed topography and mass-balance distribution of Columbia Glacier, Alaska, U.S.A., determined from sequential aerial photography, *J. Glaciol.*, **34**(117), 208–216.

Rasmussen, L. A., H. Conway, R. M. Krimmel and R. Hock, 2011. Surface mass balance, thinning and iceberg production, Columbia Glacier, Alaska, 1948-2007, *J. Glaciol.*, **57**(203), 431–440.

Rignot, E., 2006. Changes in ice dynamics and mass balance of the Antarctic ice sheet, *Phil. Trans. R. Soc. A*, **364**, doi:10.1098/rsta.2006.1793.

Rignot, E. and P. Kanagaratnam, 2006. Changes in the velocity structure of the Greenland Ice Sheet, *Science*, **314**, 986–990.

Rignot, E., J. L. Bamber, M. R. van den Broeke, C. Davis, Y. Li, W. J. van de Berg and E. van Meijgaard, 2008a. Recent Antarctic ice mass loss from radar interferometry and regional climate modelling, *Nat. Geosci.*, **1**, doi:10.1038/ngeo102.

Rignot, E., J. E. Box, E. Burgess and E. Hanna, 2008b. Mass balance of the Greenland ice sheet from 1958 to 2007, *Geophys. Res. Lett.*, **35**(L20502), doi:10.1029/2008GL035417.

Rignot, E., M. Koppes and I. Velicogna, 2010. Rapid submarine melting of the calving faces of West Greenland glaciers, *Nature Geosci.*, **3**, 187–191.

Rignot, E., I. Fenty, D. Menemenlis and Y. Xu, 2012. Spreading of warm ocean waters around Greenland as a possible cause for glacier acceleration, *Ann. Glaciol.*, **53**(60), 257–266.

Rignot, E., S. Jacobs, J. Mouginot and B. Scheuchl, 2013. Ice shelf melting around Antarctica, *Science*, 10.1126/science.1235798.

Ritchie, J., C. Lingle, R. Motyka and M. Truffer, 2008. Seasonal fluctuations in the advance of a tidewater glacier and potential causes: Hubbard Glacier, Alaska, USA, *J. Glaciol.*, **54**(186), 401–411.

Scambos, T. A., M. J. Dutkiewicz, J. C. Wilson and R. A. Bindschadler, 1992. Application of image cross-correlation to the measurement of glacier velocity using satellite image data, *Rem. Sens. of Env.*, **42**, 177–186.

Shepherd, A. and 46 others, 2012. A reconciled estimate of ice-sheet mass balance, *Science*, **338**, 1183–1189, doi:10.1126/science.1228102.

Trabant, D., R. Krimmel, K. Echelmeyer, S. Zirnheld and D. Elsberg, 2003. The slow advance of a calving glacier: Hubbard Glacier, Alaska, U.S.A., *Ann. Glaciol.*, **36**, 45–50.

Truffer, M. and M. Fahnestock, 2007. Rethinking Ice Sheet Time Scales, *Science*, **315**(1508), doi:10.1126/science.1140469.

Van der Veen, C. J., 1996. Tidewater calving, *J. Glaciol.*, **42**(141), 375–385.

Vieli, A., M. Funk and H. Blatter, 2001. Flow dynamics of tidewater glaciers: a numerical modelling approach, *J. Glaciol.*, **47**(159), 595–606.

Vieli, A., J. Jania and L. Kolondra, 2002. The retreat of a tidewater glacier: observations and model calculations on Hansbreen, Spitsbergen, *J. Glaciol.*, **48**(163), 592–600.

Viens, R. J., 1995. Dynamics and Mass Balance of Temperate Tidewater Calving Glaciers of Southern Alaska, (Master's thesis, Univ. of Washington).

Chapter 5
Conclusions

In this thesis, we have presented a method to estimate ice thickness and bed topography from surface data and applied that method to estimate ice thickness and bed topography at Columbia Glacier; presented a 50+ year record of glacier length change for 50 Alaska tidewater glaciers from terminus outlines digitized using USGS topographic maps and Landsat scenes; and, using surface velocities derived from Landsat scenes and modeled ice thicknesses, presented a 27 year record of frontal ablation for 20 Alaska tidewater glaciers.

Frontal ablation is a huge part of the mass loss of Alaska glaciers, amounting to between 25 and 60% of the total surface mass balance from the entire region (despite only representing 15% of the total glacierized area). The total frontal ablation from the region, here estimated to be 18.3 ± 7.3 Gt a^{-1}, is dominated by only a few glaciers. A mere 5 glaciers are responsible for approximately 75% of the 20 glacier total of 16.2 ± 6.5 Gt a^{-1}, despite representing only 65% of the area of those 20 glaciers. After scaling our results to include another 30 glaciers, these 5 glaciers still account for approximately 67% of the regional total, despite only representing 52% of the 50 glacier total area.

Both surface velocities and glacier lengths vary greatly on a seasonal basis, with both tending to peak in late spring/early summer and tending to reach their minima in late summer/early autumn. In general, glaciers are at their maximum retreat when they reach their minimum surface velocities, indicating that rates of frontal ablation vary throughout the year. On average, seasonal amplitudes are approximately 50% of the annual peak velocity, but they can be as much as 80% of the peak values, indicating that estimates of frontal ablation using velocity measurements from a single measurement, or from a single time of year, may be severe underestimations (or overestimations) of the true annual value.

Using our method to estimate ice thickness, and its application to Columbia Glacier, we have shown that Columbia Glacier has lost over 50% of its volume over its 30+ year retreat. The majority of that volume loss is from the lower reaches of the glacier, which is not particularly surprising; what is surprising is how little the upper reaches of the glacier have changed in that same time. This may be due to two bedrock humps located approximately 26.5 km from the head of the glacier along the current flowline, where ice thickness decreases by half over approximately 1-2 km.

A simple analysis of tidewater glacier stability to investigate the potential of the glacier for future instability and rapid retreat shows that Columbia Glacier appears to be at or near

stabilization and may be ending its retreat within a decade or so. The current location of the terminus is approximately 13 km from where the bed rises above sea level; at its current rate of retreat, the glacier will reach this point within about 25 years. The current location of the terminus is also only 6 km from where the bed slope is no longer positive downglacier, another potential stabilizing point, and one that would be reached much sooner.

While recent studies from Greenland have highlighted the potential for regional-scale coherence of tidewater glacier behavior, we find no such coherence for all glaciers in Alaska. Dividing the region into smaller subregions, however, we do see consistent patterns of behavior in some subregions. One in particular, the Kenai subregion, shows a consistent oscillation between advance and retreat on a decadal scale. Unlike the other regions, and much like Greenland, the glaciers in the Kenai subregion generally share a common ice source. This may make them more susceptible to similar behavior between glaciers, though a detailed investigation of this coherence is beyond the scope of this study.

Outlook

The first, and perhaps most obvious, extension of this work would be to predict future rates of frontal ablation. Given the time series of frontal ablation produced, it may be possible to constrain future rates of frontal ablation by considering various scenarios for the future. For example, we could constrain future rates of frontal ablation with the assumption that surface velocities will not increase by more than a factor of two over the coming century; we could also make use of the fact that many Alaska tidewater glaciers are nearly fully retreated from tidewater and are unlikely to increase rates of frontal ablation much at all. These methods could potentially be crude, but would provide first-order constraints on future rates of frontal ablation.

The time series of Alaska tidewater glacier frontal ablation can also be extended back in time, using aerial mapping photographs from ca. 1948-1975. Properly georeferenced and orthorectified, these photographs can be used in much the same way as we have used Landsat scenes - applying feature tracking to obtain apparent ice motion and using derived bed topographies with surface elevations to estimate ice thicknesses. Such an effort would be an excellent extension of this current work, and provide a much longer-term context to our estimates of frontal ablation.

It may also be useful to use the methods outlined in this thesis to estimate frontal ablation from other regions of the world that have tidewater glaciers: Svalbard, Arctic Canada,

and Patagonia. Such a comparison would provide a longer time series of frontal ablation than is currently available for any of these regions, and for those regions that currently have estimates of frontal ablation such as Svalbard and Arctic Canada, they can give us an idea of both changes in frontal ablation over time and a good comparison of these methods (Landsat-based) with other methods used to estimate frontal ablation on a regional basis. Comparison of Sea Surface Temperature records in Alaska, as well as other locations, may provide insight into trends in frontal ablation on a regional basis.

Finally, the datasets we have produced over the course of this work should be utilized in modeling efforts, either as input, as calibration, or to test various models. For example, the bed topography we have produced for Columbia Glacier can be used as input to ice flow models in order to predict the future evolution of that glacier, as well as to test various calving criteria as input to those models. The record of glacier length change could be used in further investigation of regional-scale glacier change. The frontal ablation record could potentially be used in the calibration of a regional-scale model of frontal ablation. In any event, more data will hopefully serve to clarify, and not confound, efforts to predict future rates of frontal ablation, and of sea level rise.